An Investigation of Nitinol and Titanium Alloys for the Correction of Spinal Scoliosis

Elena Lukina

Submitted for the degree of Doctor of Philosophy

Faculty of Science, Engineering and Computing

Kingston University London

February 2014

BEST COPY AVAILABLE.

VARIABLE PRINT QUALITY

I, Elena Lukina, confirm that the work presented in this Thesis is my own. Where information has been derived from other sources, I confirm that this has been indicated in the Thesis

ABSTRACT

Surgery for early onset scoliosis (EOS) often requires instrumentation which enables the pediatric patient's spine to grow. The drawback of growing rods (Ellipse Technologies, USA) is the requirement of periodical extension (at least twice a year). In contrast, in growth-guidance sliding devices such as the Shilla (Medtronic, USA) or LSZ-4D (Conmet, Russia) the extension procedure is not necessary since only one or few fixtures are locked whilst other fixtures make it possible for rods to slide allowing growth of the spine. However, due to the absence of fusion in sliding devices increased rate of fractures of rods is possible. Additionally, movement of rods against fixtures may result in the generation of wear debris. Among traditional metallic materials used for such instrumentation titanium alloys are the most biocompatible and are widely used as fixtures material, while Nitinol, an alloy with Shape memory effect, is a promising material for rods due to having potential for more gradual and sustained correction associated with its shape memory effect and potentially reducing adjacent segment degeneration due to its super-elastic properties.

The aim of this thesis was to investigate complications associated with implantation of growth-guidance sliding LSZ-4D in pediatric patients and to investigate the use of Nitinol and titanium alloy (Ti6Al4V) for this application.

Analysis of retrieved components of LSZ growth-guidance sliding device (LSZ-4D) made from titanium alloy (Ti6Al4V) implanted in paediatric patients together with associated tissues showed metallosis which in some cases led to the development of complications including seromas and fistula formation. These complications occurred in 5 out of the 25 patients investigated. Another 4 patients encountered fatigue fracture of rods.The volume wear rate measured for the retrieved components of LSZ-4D was found to be 12.5 mm^3 per year. In these 25 patients with implanted LSZ-4D devices there was a statistically significant increase in titanium and vanadium ions in the whole blood.

With a view to replacing titanium alloy rods with Nitinol an investigation on the fatigue behaviour of Nitinol revealed that creating a microstructure which increased deformation due to a martensitic phase transformation improved high strain amplitude fatigue resistance of Nitinol, whereas precipitation of nanosize Ni-rich particles and decreasing of $Ti_4Ni_2O_x$ inclusions resulted in an increase in low strain fatigue resistance.

The wear behaviour of Nitinol in comparison to titanium alloy was also investigated and showed that the wear resistance of Nitinol tested against titanium alloy (Ti6Al4V) in the

simulated body environment is approximately 100 fold greater compared to titanium alloy (Ti6Al4V) and is similar to that of CoCr alloy. Nevertheless, Nitinol – Ti6Al4V combination still generates high volumetric wear associated with debris release from the Ti6Al4V component.

Coating and treating the surface with TiN (titanium nitride), DLC (diamond like carbon) coatings and ion implantation of nitrogen ions in some instances reduced the wear. The deposition of a TiN coating only on the titanium component in a Nitinol – Ti6Al4V combination significantly improved the wear performance and this was associated with the protection of titanium component whereas the application of DLC improved the wear performance of both titanium and Nitinol. Ion implantation or deposition of TiN or DLC coatings on both counterparts was found to be less effective.

The current study indicates the importance and potential of reducing the reliance on titanium alloy by using Nitinol for patients with scoliosis and especially in those cases where relative moment of the fixtures is required, such as in growing patients.

ACKNOWLEGMENTS

I would like to thank Professor Gordon Blunn for his supervision. This Thesis would not have been possible without the opportunity Professor Blunn gave me to be part of John Scales Center for Biomedical Engineering, University College London. I am grateful to Professor Blunn for his support, his patience and his enthusiastic attitude to the research which was very inspiring.

I would also like to thank him for sharing his vast knowledge comparable with an iceberg which reveals just its minor part at the certain moment while leaving the feeling that another huge part is underneath.

I would like to thank my big supervision team from Kingston University, London and personally Edith Sim, Peter Mason and Paul Wagstaff for their supervision, support and valuable advice and comments which allowed the constant improvement of my Thesis.

I am grateful to the Russian collaborator of this project Professor Mikhail Kollerov from Moscow State Technological University for his valuable advices and discussions especially on the fatigue performance of Nitinol.

I would like to thank Professor Aleksandr Laka from (Center of Scoliosis correction, Medical Faculty of the Peoples' Friendship University of Russia) for his extensive support of my work and providing the retrieved components and tissues for investigation. I would also like to thank clinicians from Royal National Orthopedic Hospital in Stanmore, UK and personally Mr. Hilali Nordeen and Wai Yoon for their support, advice and inspiration.

I would like to thank everyone in at the Institute of Orthopedics for their help and support and personally Dr. Jay Meswania for valuable advice, Mark Harrison for his technical support and inspiring optimism and Josie Marshall for never-ending smiles. I would like to thank David Wertheim for his great help with the application of the MATLAB software in my work.

I am also grateful to Jackie Deacon and Annette Geraghty for their patience and help.

I would like to thank my new friends in the UK, Othman, Andrea, Arash, Alex and Kana for the great time spent together.

Eventually, I would like to thank this country, Great Britain for the true hospitality and enjoyable life experience. I am happy that I have had an opportunity in my life to come to know this country having a huge historical and scientific history and its in many ways traditional, but so open-minded people.

NOMENCLATURE

EOS	early onset scoliosis
TiN	titanium nitride
DLC	diamond like carbon
TGR	traditional growing rods
MCGR	magnetically controlled growing rods
Ti	Titanium alloy
CoCr	cobalt chromium alloy
SS	stainless steel
SME	shape memory effect
SE	superelasticity
UTS	ultimate tensile strength, MPa
YS	yield strength, MPa
σ_{-1}	fatigue limit, MPa
SMA	shape memory alloy
A	austenite
M	multivariant martensite
S	single variant martensite
M_s	martensite start temperature at cooling, °C
M_f	martensite finish temperature at cooling, °C
A_s	martensite start temperature at heating, °C
A_f	martensite finish temperature at heating, °C
THP	total hip implant
TKP	total knee implant
TDP	total disk implant

SEM	scanning electron microscopy
EDAX	energy dispersive X-ray analysis
SPB	sodium phosphate buffer
ICP-MS	Inductive Coupled Plasma Mass Spectrometry
σ	stress, MPa
ε_{cr}	strain, %
σ_M	stress of the martensite re-orientation, or its stress-induced formation in Nitinol, MPa
σ_{slip}	stress at which deformation caused by the dislocation slip mechanism starts, MPa
ε_{cr}	critical strain, which is maximal strain which Nitinol sample can completely recover after unloading and heating to the temperature higher than A_f, %
TEM	transmission electron microscopy
E	elastic modulus, GPa
ε_a	strain amplitude, %
ΔV	volume wear loss, mm^3
m	weight, g
ρ	density of the material, g/mm^3
HV	nano-hardness, GPa
h	indentation depth, nm
Lc_1	first critical load, N
Lc_2	second critical load, N

TABLE OF CONTENTS:

LIST OF FIGURES:

LIST OF TABLES:

CHAPTER 1

INTRODUCTION

1.1. SCOLIOSIS AND METHODS OF TREATMENT

1.1.1. Scoliosis

Scoliosis is a complex three-dimensional deformity of the spinal column that causes structural changes in the three planes of the spine (frontal, sagittal and transverse plane) and may occur in all vertebral segments. Scoliosis is typically classified as either congenital (caused by vertebral anomalies present at birth), idiopathic (scoliosis with unknown cause, the most common) or neuromuscular (developed as a secondary symptom of another condition). In most cases scoliosis presents itself, or worsens, during adolescent growth and is more frequently diagnosed (3-6 times) in females than males (Movshovich, 1964).

Full-length standing spine X-ray is the standard method for the evaluating the severity and progression of scoliosis by measuring the Cobb angle (Figure 1.1), which is the angle between two lines, drawn perpendicular to the upper endplate of the uppermost vertebrae involved and the lower endplate of the lowest vertebrae involved. For patients with two curves, Cobb angles are followed for both curves (Benzel, 2001, p.85).

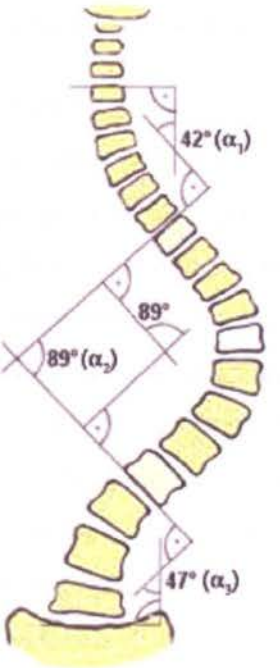

Figure 1.1. Method of assessing scoliosis curvature by the measurement of the Cobb angle α (by Benzel, 2001)

Chaklin classification (Movshovich, 1964) of scoliosis degrees is given in Table 1.1.

Table 1.1. Scoliosis degrees (Chaklin classification)

Scoliosis degree	Cobb angle α
I	$1\text{-}10^0$
II	$11\text{-}25^0$
III	$26\text{-}60^0$
IVA	$60\text{-}80^0$
IVB	$80\text{-}100^0$
IVC	$100\text{-}120^0$

1.1.2. Methods of scoliosis treatment

In all cases of scoliosis there are four treatment options which are physiotherapy, bracing, and surgery. Physiotherapy may be effective in stopping progression of the scoliotic curve when the Cobb angle is less than 15^0. For Cobb angles between 20 and 35 degrees a brace is often indicated, however in such cases children are considered to be at high risk of progression. Surgery is usually recommended when the Cobb angle is more than 45 degrees (Rohmiller & Akbarnia, 2006, p.116).

Instrumentation for surgery on skeletally mature patients

During the surgery of the skeletally mature patients the scoliotically deformed spine is straightened to reduce the curve, usually with the help of metal rods. Surgical procedures include traditional fusion as well as more novel fusionless techniques. Spinal fusion, also called arthrodesis, has become the "gold standard" and most widely performed surgery for scoliosis. In performing fusion, the goal is to permanently hold a joint in a fixed position, and allow bone to grow across that joint, which means the joint will never bend again. In this procedure the growth plates between the vertebrae affected are removed; bone (either harvested from elsewhere in the body (autograft) or from a donor (allograft) is then grafted to the vertebrae. After a period of time, one solid bone mass forms and the fused part of the spine column becomes rigid with no further growth or bending in the operated spine levels (Cluett, 2012).

Until 1962 spinal fusions were performed without metal implants. In 1962, Paul Harrington introduced a metal rod spinal system of instrumentation (fig. 2A) that assisted with straightening the spine by implanting parallel compression and distraction rods, which were hooked on the posterior elements of the spine (Radin et al., 1992).

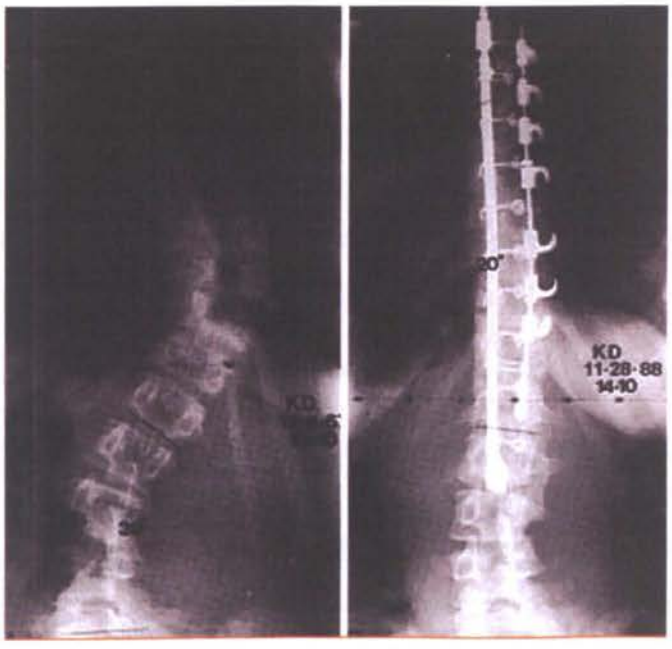

(A)

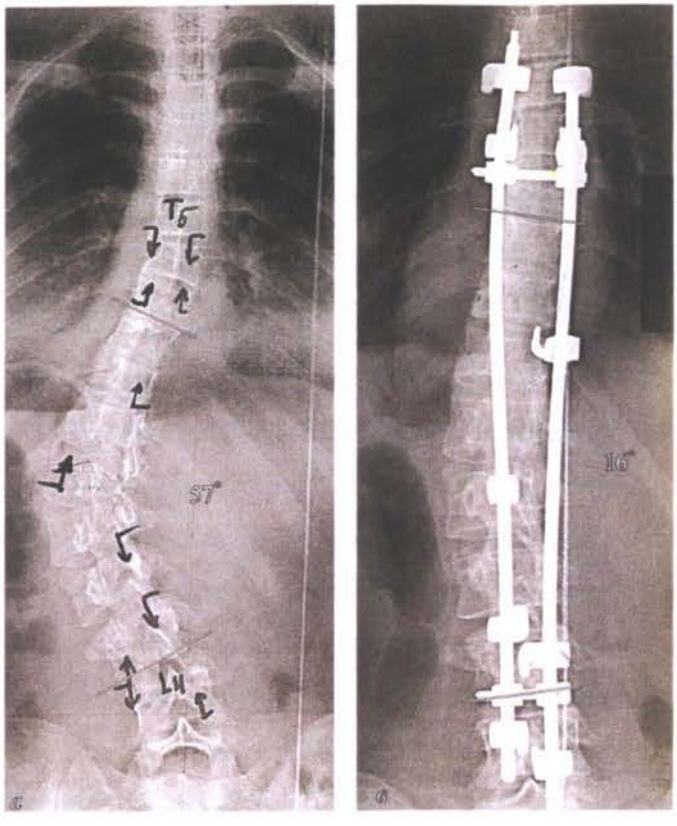

(B)

Figure 1.2. (A) Harrington and (B) Cotrel-Dubousset spine instrumentation for fusion surgery on skeletally mature patients

This method did not address the rotational component of scoliotic deformation. However, subsequent improvements to the instrumentation systems have been made. Currently, the most widely used systems are based on the Cotrel-Dubousset

instrumentation (fig. 2B). Following the placement of screws or hooks into or onto the appropriate vertebrae, two rods pre-bent to the shape of the deformed spine, are first rotated and then attached. This corrects the spine to a more "normal" physiological shape and position. The two rods are linked by the cross-sections then to stabilise the system. In general, modern spinal fusions have good outcomes with high degrees of correction and low rates of failure (Lenke, 2005, p. 582).

Instrumentation for surgery on skeletally immature patients

A very important area for development is how to deal with juvenile and adolescent scoliosis, where the spine is immature and still growing. Surgery is indicated at Cobb angles starting from 45^0 (early onset scoliosis), however, spinal fusion at this stage in a child's development is very inappropriate. Postponing the surgery until the child is fully grow can cause further progression of the curve which can cause problems with lung and heart function as well as hindering good correction results as an adult. The main goal of instrumentation for children is to enable the patient's inherent spinal growth to continue and redirect it to achieve correction, rather than progression of the curve.

According to the literature, instrumentation for surgery on skeletally immature patients includes: (1) anterior vertebral body stapling; 2) growing rods and 3) growth guidance sliding devices like Shilla or LSZ. Each will be considered in turn.

1) Anterior vertebral body stapling (fig. 1.3) presents installation of staples on the scoliotically deformed part of the spine and offers a single intervention that may provide a permanent solution to the spinal deformity (Betz et al., 2003). Furthermore, correction of a spinal deformity in the absence of a rigid fusion mass allows mobility of the operated segments and hence long-term problems related to spinal fusion such as adjacent level degeneration are avoided. The disadvantage of this method is that the forces developed by the staples are limited and as a result only moderate curves less that 35° can be successfully treated. It is now acknowledged that more severe cases of scoliosis require implantation of spinal rods (Betz et.al., 2010 & O'Leary et.al., 2011). For that reason vertebral body stapling is now considered to be a more effective alternative to bracing for the treatment of moderate scoliosis (Theologis et al., 2013).

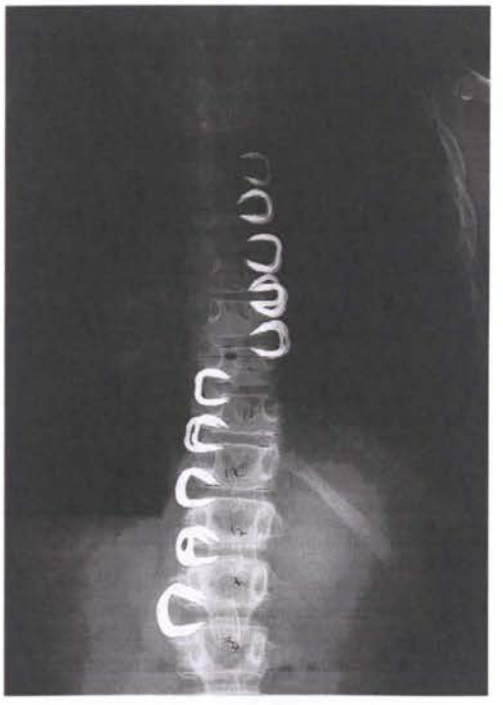

Figure 1.3. Anterior vertebral body stapling for EOS correction

2) Growing rods (Ellipse. USA) (fig. 1.4) allow the control of the progression of spinal deformity by using extendable rods to cater for the child's growth. Modifications of this device include traditional growing rods (TGR) and magnetically controlled growing rods (MCGR). The drawback of growing rods is the forperiodic extension as the child grows (at least twice a year) requiring a multi-year commitment of semi-annual intervention from the family and patient for successful results (Noordeen, 2011 & Akbarnia et al., 2013). Another disadvantage of growing rods is the high rate of post-surgery complications. Watanabe et al (2013) reported proximal junctional kyphosis complication, defined as kyphosis measured from one segment head-ward to the upper end instrumented vertebra to the proximal instrumented vertebra, with an abnormal value defined as 10 degrees or greater (Herkowitz et.al., 2011). This is observed in 24% of patients implanted with growing rods. Rod breakage occurs in approximately 20% of cases while other complications include distal screws loosening and proximal hook migration (Sedra et al., 2013).

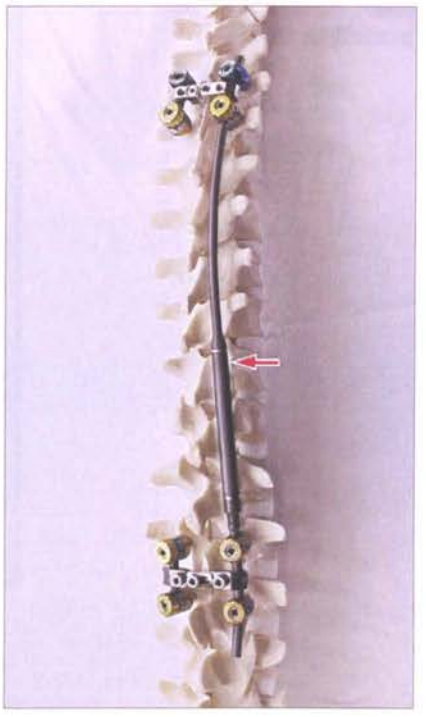

Figure 1.4. Magnetically controlled growing rods for EOS correction, (Ellipse, USA)

3) Growth-guidance sliding devices such as the Shilla (Medtronic, USA) or LSZ (Conmet, Russia) are relatively new products on the market. These devices do not require periodical extension as only a few of the fixtures are locked stiffly (marked red) while the remaining fixtures allow the rods to slide (fig. 1.5 and 1.6). Thus, these devices do not impede the child's growth and following insertion just one further operation may be necessary to fix the sliding elements when the child becomes mature to prevent instrumentation fracture. These systems have correction results comparable with traditional fusion instrumentation while providing unrestricted growth of the spine up to 10-13 cm (McCarthy et al., 2014, Laka, 2008 & Sampiev et al., 2013).

Shilla devices are made of stainless steel and have round section rods (fig. 1.5B), while the benefit of LSZ-4D device is the application of more corrosion-resistant and biologically compatible titanium alloy (Ti6Al4V) and the use of rectangular cross-section rods (fig.1.6B) which provide improved rotational correction compared with round cross-section rods (Laka, 2008 & Sampiev et al., 2013).

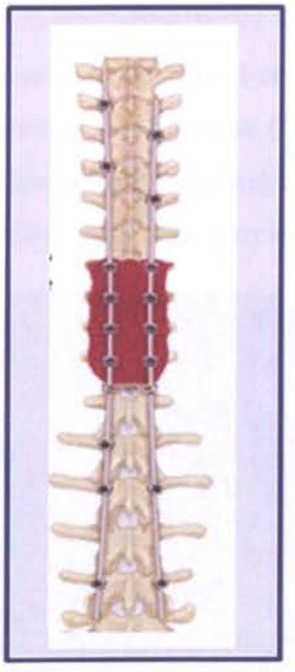

(A)

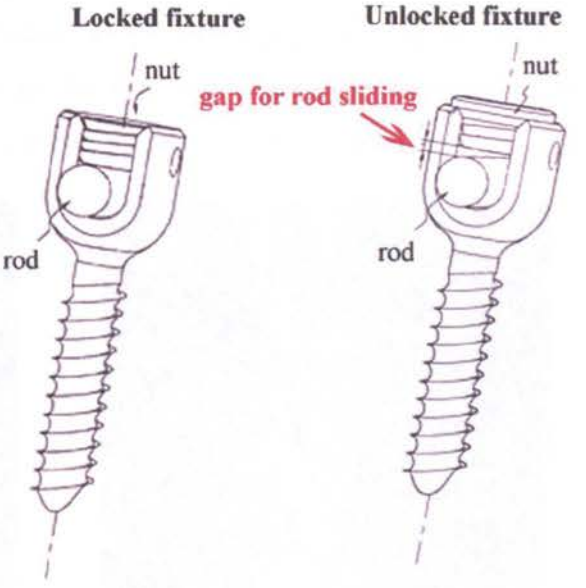

(B)

Figure 1.5. Growing guidance Shilla (Medtronic, USA) device for EOS correction: (A) overall view of device; (B) locked and unlocked fixtures (by McCarthy et.al., 2010)

(A)

(B)

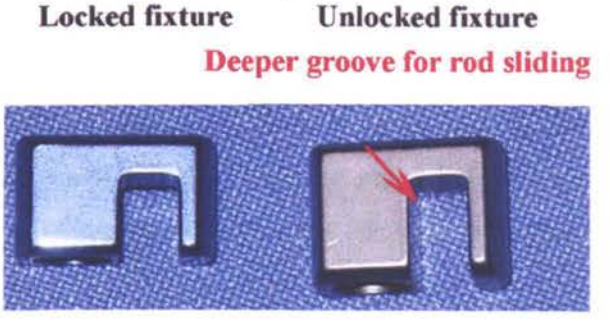

(C)

Figure 1.6. Growing guidance LSZ-4D device (Conmet, Russia) for EOS correction: (A) overall view of device; (B) locked fixture unit; (C) locked and unlocked clips (by Sampiev et al., 2013)

The LSZ-4D sliding device consists of two 6x4 mm rods with fixture units consisting of hooks, screws and clips. For the first stage of implantation all the hooks are attached to the vertebrae using screws (fig. 1.7A). Following this the rods are introduced and fixed to the hooks with attaching clips, which are fitted to the screws using nuts (fig. 1.7B). Tightening of the nuts provides the correction of the scoliotic deformation.

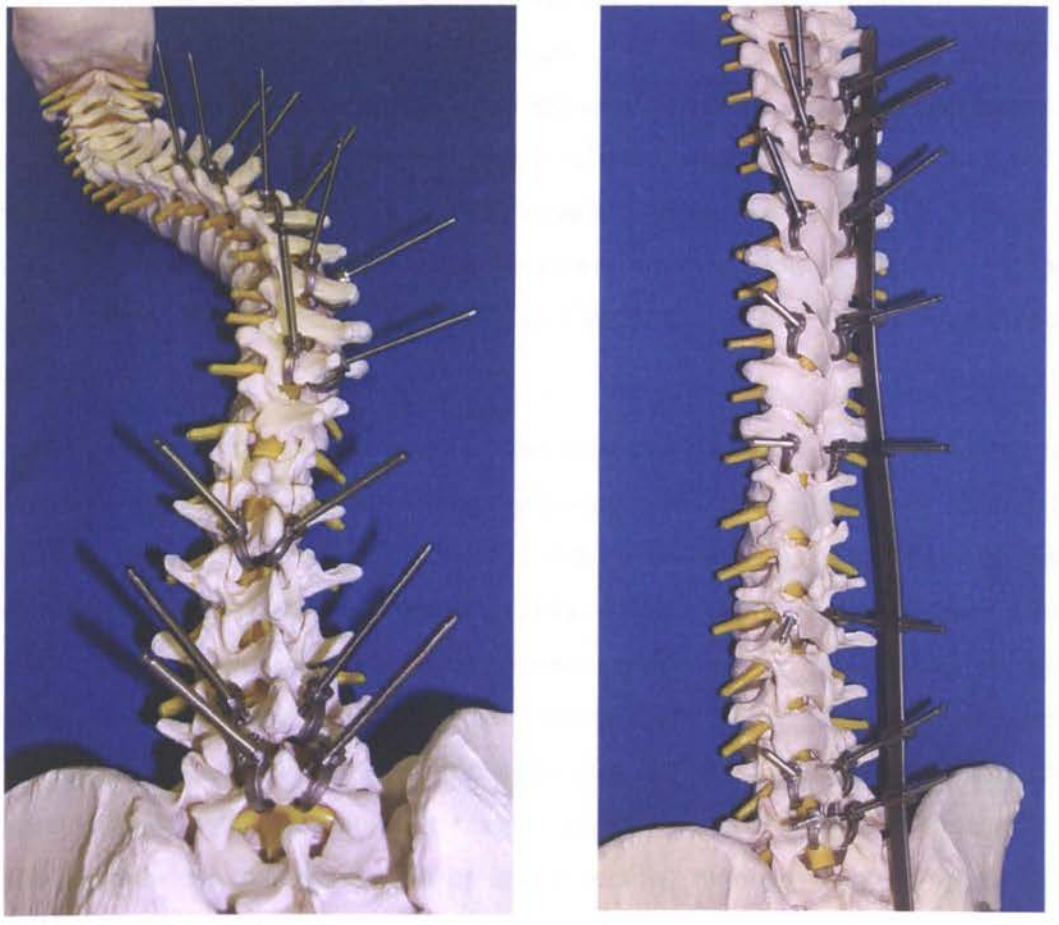

(A) (B)

Figure 1.7. Stages of LSZ-4D sliding device implantation: (A) on the first stage all the hooks are attached to the vertebrae using screws; (B) on the next stage the rods are introduced and fixed to the hooks with attaching clips, which are fitted to the screws using nuts (by Sampiev et al., 2013)

Locked clips which stiffly attach the rods to the hooks and thus to the spine are used on one thoracic spine level, while other clips are unlocked (sliding). Unlocked clips have deeper grooves (fig. 1.6B) which allow the rods to slide in the longitudinal direction and permits growth of the patient's spine without extension of the implanted device.

However, complications for fusion-less devices for EOS have not yet been thoroughly investigated. Due to the absence of fusion, there is relative movement between the rods and the fixtures. This may result in the generation of wear debris in such devices. However, this is likely to be more pronounced in growth-guidance devices which have unlocked sliding fixtures. Excessive amounts of even biologically compatible titanium wear debris produced by spinal implants have been reported to cause inflammation and osteolysis (Hallab et al., 2003; Cunningham et al., 2003 & Mochida et al., 2000). Additionally, wear debris produced by hip and knee prosthesis is normally accompanied by increasing metal ion levels in the patients' whole blood and serum (Hart et al., 2011). Increases in the titanium, aluminium and vanadium concentration of up to 300% in the serum of patients with implanted titanium spinal instrumentation was reported by Kasai et al. (2003), Richardson et al. (2008) & Cundy et al. (2013) even in arthrodesis procedures.

Traditional fusion procedure leads to the solid bone block formation without any mobility of the joint between the fused spine segments. This significantly reduces the loads on the implanted rods (ASTM F1717, rationale). On the other hand, in fusion-less sliding devices rod fracture is possible since the absence of arthrodesis results in greater cyclic loading of the rods. The main activities which impose cyclic loads on spinal implant rods are walking and physical exercise like flexion, extension and lateral bending (Rohlmann et.al., 1997 & Rohlmann et.al., 2002). Walking imposes frequently repeated loads with low amplitude bending moments of 0.5-1 Nm (Rohlmann et.al., 1997), while less frequent flexion or lateral bending moments may be up to 4 Nm (Rohlmann et.al., 2002).

For this reason the fatigue resistance of spinal implant constructs is required to be tested according to the standards ASTM F1717 or ISO 12189. For fusion spinal devices, this test imitates cyclic loading of the rods in spinal constructs during the first two years after surgery, which is the normal time required for the arthrodesis to take place. Since the sliding LSZ-4D device for early onset scoliosis is fusion-less and arthrodesis may not take place for 5-8 years, while the patient's spine is growing, an increase in the probability of fatigue fracture is likely and these spinal devices require higher fatigue resistance of the rod material.

Formation of seromas in the lumbar part of the spine after sliding LSZ-4D device implantation and fatigue fractures of the rods were acknowledged by one of the

developers of LSZ instrumentation Laka (personal communication, 2011) who has been implanting the devices for the several years. Nevertheless, quantitative analysis of the percentage of such complications has not been undertaken to date.

1.2. MATERIALS USED FOR SCOLIOSIS CORRECTION DEVICES

One of the main factors affecting the performance of spinal instrumentation is the materials they are made of. It is well known that materials for medical application must have excellent mechanical properties, high corrosion resistance, must not cause toxic reactions, and should have good biological and biomechanical compatibility. That is why only a limited number of materials are allowed to be used for implantation (Davis, 2003, p.13). Metallic materials traditionally used for spinal instrumentation include titanium (Ti), cobalt chromium (CoCr) alloys and stainless steels (SS). Nitinol, a metallic material having shape memory effect (SME) and superelasticity (SE) is also one of the prospective materials for the rods in spinal instrumentation for treating scoliosis (Yoshihara, 2013).

1.2.1. Stainless steels

Stainless steels have been employed as surgical implant materials since the time of their development between 1900 and 1915. The main alloying element introduced in these steels for improving corrosion resistance is chromium (not less than 12 wt.%). Corrosion resistance is improved because of the formation of a protective film based on chromium oxide Cr_2O_3. Addition of nickel (minimum 10 wt.%) and small amounts of molybdenum further improve the corrosion resistance of SS in chloride solutions. Content of Ni and Mo in the oxide layer is reported to be 5-10 wt.% and 4-5 wt.% respectively (Lowery & Roll, 1998 & Fredriksson et al., 2011). Type 316L stainless steel (Fe – balance, Cr – 17.0-19.0 wt.%, Ni – 13.0-15.0 wt.% , Mo – 2.25-3.0 wt.% , Mn $\leq$ 2.0 wt.% , C $\leq$ 0.03 wt.%, S $\leq$ 0.01 wt.% and P $\leq$0.025 wt.%.) was developed in 1950 and has become the most frequently selected choice for implantation due to its superior corrosion resistance in comparison with other stainless steels. For medical application this steel is used in the annealed condition and has a satisfactory combination of mechanical properties (UTS 490-690 MPa, YS $\geq$ 190 MPa, elongation $\geq$ 40%, elastic modulus is 190-200 GPa, $\sigma_{-1} \geq$ 440 MPa). The first spinal device (Harrington instrumentation) was made of this steel (Davis, 2003, p.26).

However, the relatively low resistance of stainless steels to localized corrosion, especially in stressed and oxygen depleted regions (such as the contacts under hooks or screws of the rod attachments) is the main disadvantage of this material. Thus, stainless steels are more suitable for temporary use and the reason why long-term applications were later substituted by cobalt-based alloys (Park, 2003, p.3).

1.2.2. Cobalt-chromium alloys

Within the overall range of cobalt-chromium, there are three alloys which are currently used for surgical applications: F-75, F-90 and F-562. Of these, F-75 is the most common (Co- balance, Cr - 26-30 wt.%, Mo- 5-7wt.%, Ni $\leq$ 1 wt.%, C$\leq$ 0.35 wt.%, N$\leq$ 0.25 wt.%, Fe$\leq$ 0.75 wt.%, Mn $\leq$ 1,0 wt.%, Si $\leq$ 1,0 wt.%). In the forged, hot isostatically pressed and annealed condition this alloy has good mechanical properties: UTS $\geq$ 895 MPa, YS $\geq$ 515 MPa, $\sigma_{-1} \geq$ 750-800 MPa. These alloys have high corrosion resistance in biological environments (Davis, 2003, p.31) due to formation of passive layer Cr_2O_3 on its surface (Lin & Bumgardner, 2004). CoCr alloys have the best wear resistance among metal materials used for implantation and thus are materials of choice for articulating components in total hip and knee prosthesis. However, biocompatibility of CoCr alloys is a concern, particularly for long-term use due to the release of chromium and cobalt ions. Chromium is reported to have some cancer causing action, and particles of cobalt in in-vitro studies were shown to be toxic to human osteoblast-like cells and to inhibit synthesis of collagen in the culture medium (Granchi et al., 1996, p.186).

Another disadvantage of CoCr alloys is their relatively high elastic modulus (220-230 GPa) which is about ten times the value for the bone-ligament structures (35 GPa, 20 GPa and 10 GPa for cortical, spongy bone and cartilage-ligament structures respectively (Long & Rack, 1998, p. 1630)). Thus, if used for the spinal rods, these alloys add more rigidity to the instrumentation and as a result may cause overstressing of the adjacent segments (Kim et al., 2007).

1.2.3. Titanium alloys

Titanium alloys were introduced about 20 years ago for medical applications and have had clinical success due to their superior biocompatibility and good combination of mechanical properties and corrosion resistance. The alloy, Ti6Al4V (Ti balance, Al 5.5-6.75 wt.%, V 3.5-4.5 wt.%, Fe $\leq$ 0.3 wt.%, O $\leq$ 0.2 wt.% C $\leq$ 0.08 wt.% N $\leq$ 0.05 wt.% H $\leq$ 0.015 wt.%), is predominantly used for surgical implants because of the combination of its biocompatibility, corrosion resistance and mechanical strength, however, other alloys are also approved to be used for internal implantation (grades of commercially pure titanium, and alloys based on a Ti-Nb-Zr-Ta system).

Corrosion resistance of the Ti6Al4V alloy is higher than that of 316L stainless steel and medical cobalt-based alloys in the biological environment (Karimi et al., 2012) due to the formation of a passive TiO_2 layer on its surface. Titanium alloys have an extremely low toxicity and are well tolerated by both bone and soft tissue. Animal experiments have revealed that the material may be implanted for an extensive length of time and fibrous encapsulation of the implants in the bone environment is minimal to non-existent (Brunette et. al., 2001).

Typical Ti6Al4V alloy properties in the annealed condition are as follows: UTS $\geq$ 860MPa, YS $\geq$ 780 MPa, elongation is 10%, σ_{-1}=550 MPa. A very important advantage of titanium alloys is that the elastic modulus (110 GPa for Ti6Al4V) is approximately half that of the stainless steels and cobalt-based alloys which results in less rigidity of the spinal instrumentation.

The main drawback of titanium alloys which limits its applications in friction conditions is its low wear resistance due to high chemical activity of titanium, micro-welding to the counter-body and intensive damage once the oxide layer is removed from its surface as a result of friction (Gorinin & Chechulin, 1990). This leads to the adhesion of titanium to the counter-body Nevertheless, application of surface treatments such as nitriding, ion implantation as well as deposition of wear resistant coatings such as titanium nitride and diamond like carbon are reported to significantly improve wear resistance of titanium alloys (Shenhar et al., 2000, Wang et al., 2013, Wiklund & Hutchings, 2001& Costa et al., 2010, Alves-Claro et. al., 2008).

Nitinol is new compared to Ti, CoCr and SS metal material. It has attracted attention lately for use as a rod material in scoliosis instrumentation due to having such unique

properties as shape memory effect (SME) and super-elasticity (SE) (Otsuka & Wayman, 1998). More gradual and sustained correction associated with its SME is reported by Cheung et al., 2011, while its super-elastic properties (with an "effective" elastic modulus of 40-80 GPa) may potentially reduce adjacent segment degeneration.

1.3. NITINOL AS A MATERIAL FOR SCOLIOSIS CORRECTION DEVICES

1.3.1. Shape Memory Effect and Superelasticity

Nitinol is a shape memory alloy (SMA). SMAs are special metallic materials which spontaneously recover their shape after being subjected to macroscopic deformation higher than their elastic limit. Recovery of shape may occur after the release of load (superelasticity or pseudoelasticity) or after additional heating (shape memory effect). Nitinol is a stoichiometric compound of titanium and nickel. Composition limits of Nitinol range from 54.5 to 57 wt.% of Ni; O ≤ 0.004 wt.%, N ≤ 0.004 wt.%, C ≤ 0.002 wt.%, H ≤ 0.0005 wt.%, (titanium balance) (Otsuka & Wayman, 1998).

At high temperatures, Nitinol has cubic B2 (CsCl, space group Pm3m) crystal structure referred to as austenite (also known as the parent phase). At low temperatures, Nitinol transforms to B19' crystal structure which has a rhombic crystal structure with monoclinic distortion known as martensite (space group $P2_1/m$). In particular, the martensite can exist in two configurations: (i) the stress-free martensite, characterised by a twinned multivariant (*M*) crystallographic structure, which minimises the misfit with the surroundings (austenitic phase), hence not associated with any macroscopic deformation which forms if the transformation takes place without any external load; (ii) the stress-induced martensite, characterized by a configuration with a single twin variant (*S*) crystallographic structure, which aligns variants along a predominant direction, hence associated with macroscopic deformation which forms if the transformation takes place with the external load applied (fig. 1.8).

The temperature at which austenite transforms to martensite is generally referred to as the transformation temperature. More specifically, there are four transition temperatures. When the alloy is fully austenite, martensite begins to form as the alloy cools at the so-called martensite start, or M_s temperature, and the temperature at which the transformation is complete is called the martensite finish, or M_f temperature. When

the alloy is fully martensite and is subjected to heating, austenite starts to form at the A_s temperature, and finishes at the A_f temperature (Kumar & Lagoudas, 2008, p. 6).

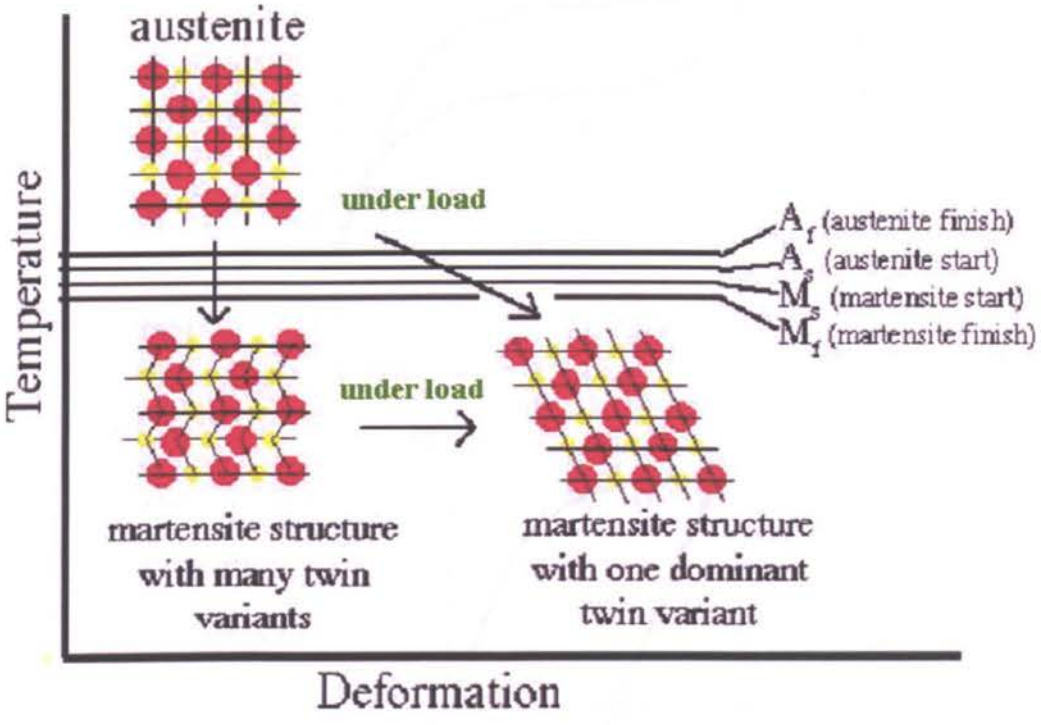

Figure 1.8. Transformations in Nitinol: multivariant twin martensite not associated with any macroscopic deformation forms if austenite - martensite transformation takes place without any external load; single twin variant martensite associated with macroscopic deformation forms if austenite - martensite transformation takes place with an external load applied; single twin variant martensite can also develop from multivariant martensite under an external load (by Kumar & Lagoudas, 2008).

In particular, when the material is mechanically deformed at a temperature greater than A_f (ABC), the stress induces the transformation from austenite to single variant martensite ($A \rightarrow S$). Because the martensite is not stable for $T > A_f$, when the load is removed (CDA) the reverse transformation ($S \rightarrow A$) occurs and the material recovers its original shape. This peculiar behaviour above A_f (fig. 1.9A) is the so-called superelasticity or pseudoelasticity. The ability of the complete restoration of high deformations indicates that the "effective" elastic modulus of Nitinol is in the range of 40-80 GPa, which is similar to bone and cartilage-ligament structures.

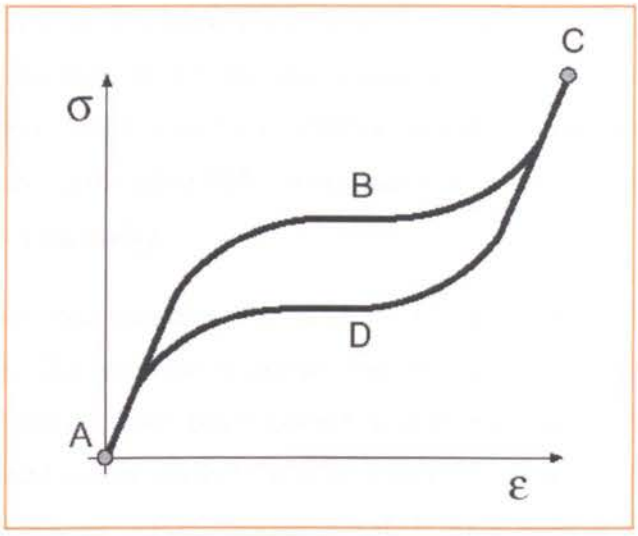

(A)

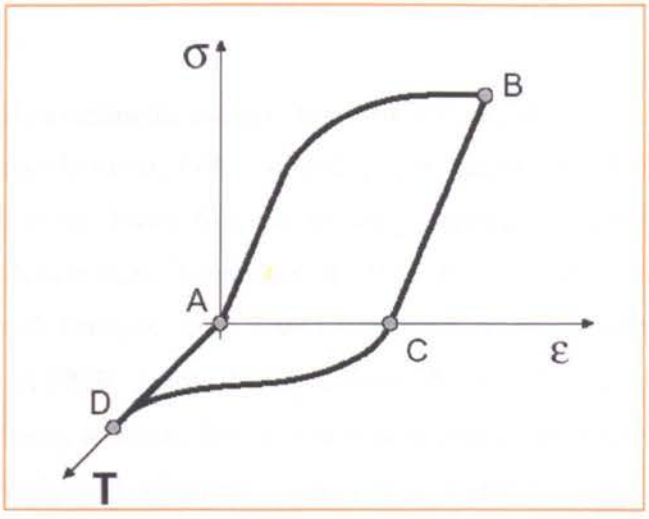

(B)

Figure 1.9. Stress (σ) – strain (ε) – temperature (T) dependence of Nitinol demonstrating: (A) superelastic (pseudoelastic) effect ($T > A_f$) and (B) shape memory effect ($T < A_s$) (by Kumar & Lagoudas, 2008)

On the contrary, as the material is mechanically deformed at a temperature lower than A_s (ABC) a transformation from austenite to stress-induced single variant martensite (A→ *S)* or from multivariant to single variant martensite ($M \rightarrow S$) at the deformation temperature lower than M_f occurs (fig. 1.9B). When the stress is removed (BC), a residual deformation remains (AC). Hence, heating the material above A_f (CDA) at zero stress allows the material to recover the residual strain: indeed, the single-variant martensite is no more stable at this temperature and the reverse transformation ($S \rightarrow A$) takes place. This behaviour is the so-called shape memory effect.

If boundary conditions do not allow the original shape recovery, the material is able to produce a high reaction based on the constraints: this phenomenon is called "constrained recovery" and is used for generating compressive forces in medical Nitinol devices. Temperature A_f for using SME in medical devices must be 35 ± 1^0C (correspond to the temperature of the body).

Realisation of SME can significantly facilitate rod installation during surgery for scoliosis correction. The rods can be pre-strained to any shape (including lordosis and kyphosis of spinal curve); after being cooled in cold water prior to surgery, the rods become malleable and can be easily bent according to the shape of the deformed spine. After heating to body temperature they recover their prestrained shape (the recoverable deformation can be up to 6%) and thus correct scoliotic deformation (Otsuka et al. 1998 & Yoshihara, 2013)

The first successful experiments using Nitinol for scoliotic deformation correction were performed on animals between 1993 and 2002; subsequently they have been performed on humans. It has been shown that the forces generated in Nitinol are sufficient to improve scoliotic deformation (Sanders et al., 1993 & Wever et al., 2002). However in the experiments with humans Nitinol was used only to assist with the initial spinal correction, using its SME, before being replaced by a rod made from conventional material (Wang, Zheng & Zhan, 2011). The first results using a permanent Nitinol rod were reported recently and described successful short-term results indicating that the use of Nitinol rods provides gradual and better correction of the scoliotic curve (Cheung, 2011).

Another long-term complication after the surgery with spinal fusion can be overstressing of the adjacent spinal segments due to the rigidity of the fused segments, which can cause the need for additional surgery later on. There is little in the literature concerning this particular issue regarding scoliosis instrumentation. However, it has been extensively recognized for transpedicular devices when they are used to treat degenerative spinal disease. Consequently, alternative approaches have and are being developed to enable fusion-less and less rigid spinal instrumentation (Burton, 2010 & Guille et al., 2007).

In this respect the low modulus of elasticity of Nitinol, comparable with that of human structures, could provide flexibility of the operated segments of the spine. Based on 20 years' experience of using Nitinol in spinal instrumentation (predominantly staples) for

disc degeneration or spine traumas it has revealed that the problems associated with overstressing of adjacent segments, referred to earlier, has been dramatically reduced (Kollerov et.al., 2002 & Kim et.al., 2007). However, implementation of this unique material for long-term implantation is slow because its fatigue and wear properties have not been extensively investigated.

1.3.2. Structure and mechanical properties of Nitinol

Irrespective of the preparation method, besides austenite (B2) and/or martensite (B19') phases, Nitinol always contains a small quantity of $Ti_4Ni_2(O)_x$ particles. Nickel-enriched alloys with nickel content higher than 55.1 wt.% of Ni are characterised by the additional formation of nickel rich precipitates $Ti_{11}Ni_{14}$, Ti_3Ni_4, Ti_2Ni_3, $TiNi_3$. So, transformation temperatures of Nitinol are strongly dependent on Ti/Ni content in the B2 phase. Increases of 0.1 wt.% Ni in the B2 phase results in an A_f decrease of 10^0C. Chemical composition of the B2 phase depends not only on the chemical composition of the alloy, but also on the volume fraction of all these precipitates.

Nitinol also has high mechanical properties: UTS 800-1400 MPa, YS 600-700 MPa. In spite of the fact that stress-controlled fatigue strength σ_{-1} is 350 MPa. This parameter is not good for describing the material for spinal rod application as due to the high elasticity of Nitinol such stress levels correspond to extremely high strains (more than 5-8%) which are unlikely to be encountered in spinal rods due to the limited mobility of the spinal column. Consequently, in this situation, strain-controlled fatigue will better describe its behaviour.

1.3.3. Fatigue behaviour of Nitinol

Over the past 10 years the number of publications in the literature addressing fatigue properties of Nitinol, and devices made from this material, have increased dramatically due to growing importance of the material in medical device applications.

Most of the testing involves strain-controlled testing as this is thought to best represent the in-vivo condition of the predominant part of the device. It is acknowledged that strain-controlled fatigue of Nitinol is much better than that of traditional titanium, cobalt-based alloys and steels (Adler, 2007, Kollerov et al., 2008 & Robertson et al, 2012). Nevertheless, it should be taken into consideration that since the modulus of elasticity of Nitinol is lower compared with that of CoCr, SS and Ti alloy, the same load (stress) will result is higher strain amplitude in Nitinol. Bending moments encountered

by spinal rods in the lumbar part of the spine can achieve 4 Nm (Rohlmann et al., 2002) resulting in stresses of approximately 300 – 330 MPa in ∅ 5.5-6mm rods. Corresponding strains would be 1.5% for Nitinol and 0.65% for Ti alloy (elastic modulus values for Ti and Nitinol, of 110 and 70 GPa respectively, were deduced from stress-strain curves presented by Kollerov et al. (2008).

Comparing the number of cycles to failure for Nitinol tested at strain amplitude ε_a=1.5% with that observed for Ti alloy tested with ε_a=0.65% (fig. 1.10) reveals that Nitinol has similar fatigue resistance to Ti alloy thus further improvement in the fatigue resistance of Nitinol would help to avoid fatigue failures if it is used as a rod material in fusion-less instrumentation for scoliosis correction.

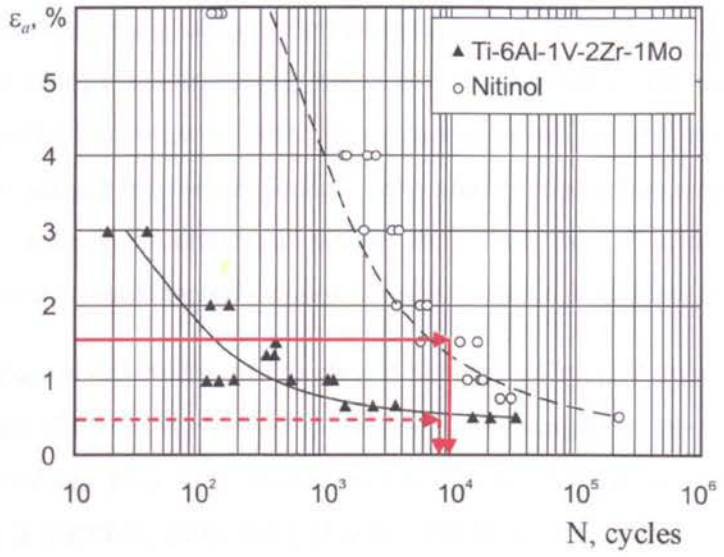

Figure 1.10. Number of cycles to fatigue failure (N) plotted against applied strain amplitude (ε_a) for Nitinol and Ti alloy (by Kollerov et al., 2008)

A significant effort has been made lately by scientists to establish the various factors that influence fatigue in Nitinol. Research concentrated on the influence of strain level, and temperature of the tests. Investigation of martensite transformation temperatures influence on the fatigue behaviour of Nitinol have revealed that its fatigue resistance is higher in the range where stress-induced martensite transformation occurs. It was concluded that it is the martensite mechanism of deformation that provides Nitinol's higher strain-controlled fatigue in comparison with traditional materials having a

slipping mechanism of plastic deformation (Tolomeo, Davidson & Santinoranout, 2000). On the other hand it was established that when the mechanism of deformation is predominantly slipping (for instance at temperatures much higher than A_f) the fatigue behaviour of Nitinol becomes similar to that of traditional metallic materials (Tabanli, Simha & Berg, 2001 and Morgan, Painter & Moffat, 2003). Efforts have been made to establish the strain levels at which Nitinol provides the best fatigue resistance. However, generalisations are often made without taking into consideration that the strain level at which the onset of slipping starts greatly depend on the Nitinol structure, chemical composition of the main phases and the difference between the testing and martensite temperatures (A_f, As) in the material.

Furthermore, many fatigue investigations suffer from two other issues: first the structure of Nitinol (including homogeneity, secondary phase size and volume fraction, thermo-mechanical processing) is not properly taken into consideration. Therefore, the results from these investigations must be critically evaluated before using them for predictions about the alloys' fatigue behaviour. Second, early studies focused on materials that were tested in the annealed condition, which may not be relevant to heat and thermomechanically treated materials used in today's medical devices (Pelton, 2011).

There are few papers devoted to the treatment and microstructure influence on Nitinol fatigue resistance. The results reported in the literature showed that the processing route and thermal treatment play very important roles in the fatigue resistance of Nitinol (Patel, Plumley & Bouthot, 2006 and Gal et al., 2008). Specifically it was revealed that aging or thermomechanical treatment improve Nitinol fatigue resistance significantly, however the influence of the precipitate particles and their volume fraction has not been addressed (Wurzel & Hornbogen, 2000). That is why it may be concluded that more systematic investigations are needed, to address the influence of microstructural parameters on the strain-controlled fatigue of Nitinol in order to safely utilise this unique material in fusion-less scoliosis instrumentation.

1.3.4. Corrosion resistance and biocompatibility of Nitinol

The two main factors that determine biocompatibility of a material are: degradation of the material in the body environment and the host's reaction induced by the material. Therefore, biocompatibility is directly related to the corrosion behaviour of the material in a specified solution and the tendency for the alloy to release potentially toxic ions (Davis, 2003, p.14).

Generally it is indicated (Shabalovskaya, 2002) that Nitinol has good biocompatibility, due to the formation of a passive titanium-oxide layer (TiO_2) similar to that found on Ti and its alloys. This oxide layer on Nitinol serves two purposes:

- It increases the stability of the surface layers by protecting the bulk material from corrosion.

- It creates a physical and chemical barrier against Ni release.

Studies have shown that in simulated physiological solutions Nitinol is less resistant to chemical breakdown than Ti-6AI-4V, but more resistant than 316L stainless steel (Es-Souni et al., 2005). Moreover, it has been established that Nitinol stents which are electropolished, or electropolished and chemically etched, have very high corrosion resistance (Shabalovskaya, Anderegg & Humbeeck, 2008).

Additionally, it was revealed that Nitinol has a high corrosion resistance to galvanic corrosion when coupled with titanium alloys (Venugolapan & Trepanier C, 2000).

Another important aspect of the behaviour of implant alloys is their corrosion performance under static stress and under dynamic loading–unloading conditions in the body. Studies of the effect of applied stress on the corrosion parameters of SS, CoCr, and Ti alloys show that loading, even within the elastic limits, results in enhanced metal ion release (Bondy et al., 1991). Applied stresses higher than the yield strength, resulting in plastic deformation, lower the breakdown potentials and increase the corrosion current. On the other hand, no changes in localised corrosion resistance has been observed in Nitinol when samples were strained in the recoverable regime and martensite was induced, which demonstrates the resistance of the passive Nitinol surface layer to the damaging tensile stress that triggers stress corrosion cracking (Rondelli & Vicentini, 2000).

However there is still a concern about possible release of Ni ions from Nitinol since Ni ions are known to be toxic and can cause an allergic reaction (Goyer, 1986 & Lacy et al., 1996). Trepllnier (1999) revealed that Nitinol released a very small quantity of ions (an average of 13.05 μg per day of Ni, which is significantly below the estimated average dietary intake of 200-300 μg per day. Ryhänen et al. (1997) and Wever et al. (1998) revealed that the Ni ions release rate from Nitinol is slightly higher compared with that from SS but only during the first 8-10 days of immersion in biological solution. After this period the level of Ni ions starts to reduce in spite of the fact that

Nitinol contains more than 50 wt.% of Ni, while SS only 10 wt.%, which may be explained by the formation of a TiO_2 based passive surface layer on Nitinol. After special surface preparation, including electro-polishing and/or etching, the nickel content in this layer was reported to be less than 2-7 wt. % (Shabalovskaya, 2008 & Pohl, 2004), which is comparable to the Ni content in a Cr_2O_3 based passive layer on SS (Lowery & Roll, 1998 & Fredriksson et al., 2011).

However, the chemical composition of Nitinol wear particles generated in-vivo is not well understood which is why such particles could be the source of Ni ion release. Thus, better understanding of the wear resistance of Nitinol is required for its safe application in fusion-less EOS correction, especially so for sliding spinal instrumentation. (Lowery & Roll, 1998 & Fredriksson et al., 2011).

1.3.5. Wear resistance of Nitinol

The wear resistance of Nitinol is not completely understood and is reported to be ten to twenty times better in dry sliding or fretting conditions compared to Ti, 304 (18 wt.% Cr, 10 wt.% Ni, $\leq$ 2 wt.% Mn, Fe – balance) or CCr15 steels (1 wt.% C, 1.5 wt.% Cr) (Zhang et al., 2009, Li et al., 2000 & Linmao et. al., 2005). On the other hand, Lui & Lee (2009) who studied wear resistance of Nitinol in oil lubrication revealed it to be two orders of magnitude higher compared to 304 stainless steel.

Many authors explain the high wear resistance of Nitinol by superelastic deformation of its surface layers in friction. Superelastic behaviour results in reversible deformation of asperities during articulation thus reducing contact stresses and asperity wear (Quain et a.l, 2005 & Yan et al., 2006).

However in most experiments Nitinol was mainly tested against dissimilar materials like tungsten carbide and little is known about its wear behaviour in body-simulated fluid when sliding against Ti which is the most likely fixture material for Nitinol rods.

Surface modification techniques have demonstrated significant improvements in the friction and wear behaviour of titanium alloys and it may be possible to use these to improve the wear properties of Nitinol. Diamond-like carbon deposition, ion implantation and titanium nitride TiN deposition seem to be the most promising since they provide high surface hardness, corrosion and wear resistance (Geetha, 2009, Dearnaley & Arps, 2005, Laskovski, 2011), and some are being used now to prevent Ni ion release from Nitinol. However, further research is necessary to evaluate the wear

resistance of Nitinol – titanium alloy friction pairs in a biological environment in addition to the capacity of surface treatments to further improve their wear performance.

1.4. LITERATURE REVIEW CONCLUSIONS AND AIMS

This Literature Review has revealed that a very important area for further development is healing early on-set scoliosis in young children where the spine is immature and still growing. Surgery for early onset scoliosis (EOS) often requires instrumentation which enables the pediatric patient's spine to grow. The drawback of growing rods (Ellipse Technologies, USA) is the requirement of periodical extension (at least twice a year). In contrast, in growth-guidance sliding devices such as the Shilla (Medtronic, USA) or LSZ-4D (Conmet, Russia) the extension procedure is not necessary since only one or few fixtures are locked whilst other fixtures make it possible for rods to slide allowing growth of the spine. However, due to the absence of fusion in sliding devices increased rates of rod fracture are possible. Additionally, movement of rods against fixtures may result in the generation of wear debris. However, complications for these devices are not yet thoroughly investigated. Susceptibility of stainless steels to localized corrosion and possible release of toxic cobalt and chromium ions from CoCr alloys are the drawbacks of these traditional metal materials used for scoliosis instrumentation. Additionally, both SS and CoCr have a high modulus of elasticity which might result in the problem of adjacent segment degeneration in the long term. On the other hand, titanium alloys are the most corrosion resistant, biocompatible, have doubly lower modulus of elasticity and are now widely used both for rod and fixture manufacture. A disadvantage of Ti alloys is their poor wear resistance which might result in wear debris formation and metallosis in the case of using sliding devices where rods articulate within fixtures. Nevertheless, TiN, DLC and ion implantation are surface treatments reported to improve wear performance of Ti components. Nitinol, an alloy with shape memory effect, is a promising material for rods in devices for scoliosis correction due to its potential for more gradual and sustained correction associated with its shape memory effect and potentially reducing adjacent segment degeneration due to its super-elastic properties. However, further improvement of Nitinol fatigue performance by optimization of its bulk structure would be beneficial. In addition, investigation of Nitinol wear resistance in a biological environment, and tested against Ti alloy, the most

likely material for fixtures, is necessary for the safe application of Nitinol rods in growth-guidance sliding devices.

The **aim** of this thesis was to investigate the complications associated with implantation of current growth-guidance sliding LSZ-4D systems in pediatric patients and to investigate Nitinol and titanium alloy (Ti6Al4V) as alternative materials for this application.

The **objectives** were:

1. To analyse retrieved components of LSZ growth-guidance sliding devices (LSZ-4D) made from titanium alloy Ti6Al4V, together with associated surrounding tissues, implanted in paediatric patients for EOS correction and to evaluate the complications associated with this implantation device;

2. Establish the effect of various structural parameters including increased dislocation density, size of Ni-rich (Ni_4Ti_3 and Ni_3Ti_2) particles and volume fraction of Ti-rich ($Ti_4Ni_2O_x$) particles on the fatigue behaviour of Nitinol.

3. Investigate the wear resistance of Nitinol – Ti6Al4V friction combination in a biological environment and compare this with Ti6Al4V - Ti6Al4V and CoCr – Ti6Al4V combinations which are commonly used for scoliosis instrumentation.

4. Investigate the influence of TiN, DLC coatings and ion implantation on the wear resistance of Nitinol – Ti6Al4V friction combination.

CHAPTER 2

ANALYSIS OF RETRIEVED LSZ-4D SLIDING DEVICES FOR THE CORRECTION OF EARLY ONSET SCOLIOSIS

2.1. INTRODUCTION

Surgery for the correction of early onset scoliosis often requires fusionless instrumentation as early fusion may result in complications such as trunk shortening, pulmonary dysfunction and overloading of the spine (Karol et al., 2008). That is why instrumentation which does not impede the spine growth of pediatric patients is required. Suitable devices currently available include extended growing rods (Akbarnia et al., 2013) and guided-growth systems, such as the Shilla or LSZ devices (McCarthy et al., 2014 & Sampiev et al., 2013). Periodic extension of the growing rods device is required as the child grows (at least twice a year) This procedure is not required in guided-growth devices where only a few of the fixtures are locked stiffly while the remaining fixtures allow the rods to slide and will not impede growth of the spine.

However, due to the absence of fusion in devices for EOS, relative movement between the rods and the fixtures may result in the generation of wear debris. This is likely to be more pronounced in growth-guidance devices with unlocked sliding fixtures.

While absolute amounts of wear debris produced by joint prostheses such as total hip, knee and spinal disk replacements (THP, TKP, TDP) which have a high range of motion, are extensively covered in literature (Lord et al., 2011 & Lee et. al., 2008), there is limited information on the quantitative measurement of volume wear loss of spinal implants used for the correction of EOS.

One of the main factors affecting the amount of debris is the wear resistance of the materials used for spinal instrumentation. Metallic materials traditionally used for such instrumentation include titanium, cobalt chromium alloys and stainless steels (Yoshihara, 2013). Titanium alloys are the most biocompatible, however, without special protection they have lower wear resistance compared to CoCr and SS and can produce wear debris where movement occurs (McKellop et al., 2001).

Villarraga et al., (2006) reported prominent wear scars both on Ti and SS scoliosis instrumentation. Wang et al., (1999) also reported high concentrations of Ti in tissues collected from areas near pedicle screw-rod junctions.

Excessive amounts of even biologically compatible Ti wear debris produced by spinal implants have been reported to cause inflammation and osteolysis (Hallab et al., 2003; Cunningham et al., 2003 & Mochida et al., 2000). Additionally, wear debris produced by THP and TKP is normally accompanied by increasing metal ion levels in the patients' whole blood and serum (Hart et al., 2011). Increases in the titanium, aluminium and vanadium concentration of up to 300% in the serum of patients with implanted titanium spinal instrumentation was reported by Kasai et al. (2003), Richardson et al. (2008) & Cundy et al. (2013) even in arthrodesis procedures. However tissue reactions to wear debris generated by fusion-less implants for EOS correction and metal ion concentration in pediatric patients with implanted fusionless devices have not been thoroughly investigated. This information would be useful in making decisions on the necessity of replacing fusion-less devices with traditional instrumentation once the pediatric patient is fully grown thus avoiding any further wear debris production from sliding devices.

The purpose of the work described in this chapter was to analyse retrieved components of LSZ growth-guidance sliding devices (LSZ-4D) made from titanium alloy Ti6Al4V implanted in paediatric patients for EOS correction. The aims were:

1. **To evaluate complications associated with LSZ-4D devices;**
2. **To measure specific amounts of volumetric wear loss in LSZ-4D devices;**
3. **To establish the mechanisms of wear damage in LSZ-4D device components;**
4. **To evaluate tissue reactions to titanium wear debris produced by LSZ-4D devices;**
5. **To establish the content of titanium, aluminium and vanadium in whole blood samples of patients with implanted LSZ-4D devices.**

2.2 MATERIALS AND METHODS

2.2.1. Description of LSZ-4D sliding device

The LSZ-4D guided-growth sliding device produced by Conmet, Russia for early onset scoliosis correction is shown in figure 2.1. This device consists of two 6x4 mm rods of rectangular cross-section and their fixture units. Locked fixtures are normally located on one spinal level while unlocked fixtures are used at the distal and proximal ends of the device, thus enabling sliding during the spine growth (fig. 2.1A). Each fixture consists of a clip and a hook (fig. 2.1B). All components of the LSZ-4D device are manufactured from titanium alloy (Ti6Al4V). Devices were retrieved from 25 patients undergoing routine surgery to exchange sliding LSZ-4D devices with traditional fusion instrumentation when the child became skeletally mature. Devices were retrieved at the Medical Faculty of the Peoples' Friendship University of Russia (PFUR), and brought to the John Scales Center for Biomedical Engineering (University College London UCL), for investigation under a Material Transfer Agreement between PFUR and UCL.

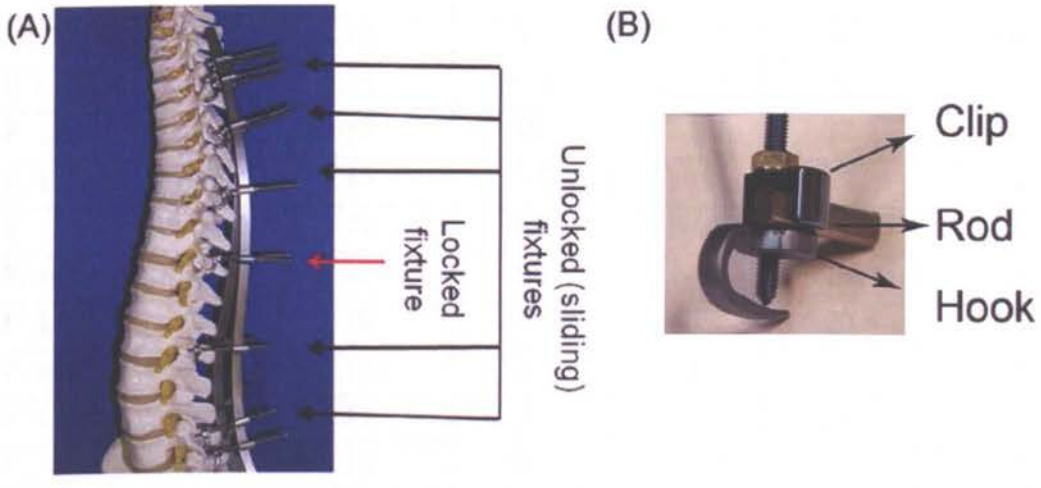

Figure 2.1. Illustration of the LSZ-4D sliding growth guidance device (A) and fixture unit (B). Locked fixtures are used at one spinal level. Unlocked fixtures are used at the distal and proximal end of the device enabling sliding and continued spinal growth.

2.2.2. Patient samples

Clinical information (age of patients at the time of primary surgery, degree of scoliosis, number of fixture units, levels and implantation time) is presented in Table 2.1. for the study group of 25 patients

Table 2.1. Patients clinical information

	Gender	Age at implantation	Scoliosis degree	Levels	Fixture units number	Implantation time, years
P. 1R	Female	13	IVC	T2-L4	24	5.8
P. 2R	Female	12	IVB	T4-L2	20	3.5
P. 3R	Male	10	IVA	T2-T12	16	3.5
P. 4R	Female	11	IVA	T2-L3	20	5
P. 5R	Female	12	III	T2-L4	20	10.1
P. 6R	Female	11	IVA	T2-L4	20	5
P. 7R	Female	13	III	T3-L5	16	5.4
P. 8R	Female	12	IVB	T2-L4	20	6
P. 9R	Female	12	IVC	T2-L5	24	10
P. 10R	Female	13	IVA	T2-L4	20	6
P. 11R	Female	10	III	T2-L4	22	3.5
P. 12R	Male	13	IVC	T2-L5	22	8.2
P. 13R	Female	11	III	T1-L5	22	6.2
P. 14R	Male	13	III	T2-L5	18	5.3
P. 15R	Female	10	IVA	T2-L4	20	7.3
P. 16R	Female	13	IVA	T3-L5	16	8.2
P. 17R	Female	10	III	T2-L4	20	4.2
P. 18R	Female	12	IVA	T2-L4	24	1.5
P. 19R	Female	11	IVA	T4-L2	20	4.2
P. 20R	Female	10	IVA	T2-L4	20	5.5
P. 21R	Female	11	III	T3-L5	16	5.5
P. 22R	Female	10	IVB	T2-L4	20	4.5
P. 23R	Female	12	IVC	T2-L4	22	5.1
P. 24R	Female	11	III	T2-L5	22	4.1
P. 25R	Female	10	IVA	T2-T12	16	5.2

Sliding LSZ-4D devices for EOS correction had been implanted in these patients for several years before they were retrieved during routine surgery as described above. Patients in this group were denoted as P.1R – P.25R. Complications in these patients, analysis, general inspection and metal ion contents were recorded for all 25 patients. Volume wear loss was measured for three patients; histological analysis of the tissues surrounding the implants was carried out on tissue obtained from 5 patients. Analysis of wear scars and wear particles was carried out for 3 patients.

Metal ion levels were measured in a control group consisting of patients with no implanted devices. There were 10 patients in this group. Nine of them female and 1 male. The average age of the patients was 11±1.2 years. These patients were denoted P.1I-P.10I.

2.2.3. Volume wear loss measurements

Visual inspection of retrieved LSZ-4D devices was carried out for all 25 patients and photography was carried out on devices with typical and characteristic wear patterns. Volume wear loss was measured on instrumentation retrieved from P.1R, P.2R and P.3R (1 male, 2 females). In total six rods and sixty fixture units (30 hooks and 30 clips) were analyzed from 3 patients. The components were implanted for periods of time between 3.5 and 5.8 years (average: 4.3 years). None of these patients had any clinical complications (Table 2.1.).

MATLAB software (The MathWorks Inc., Natick, MA, USA) was used to calculate the volume of grooves. Images of wear scars observed on LSZ-4D components were recorded using a Bruker interferometer microscope. The interferometry data was then incorporated into MATLAB including pre-processing involving mean filtering and saving the data as depth image files. The system then calculates the displaced volume in parallel planes with 1 pixel spacing lines along the length of the groove. The median height over 20 pixels is calculated at the end of each line. Using linear interpolation, the volumes under the lines are calculated and summed over the length of the groove. In case one edge of the groove was worn out, the system also allowed the volume to be calculated with respect to the mean of a region; in this mode the user could select the top surface and the displaced volume beneath is computed taking into account the tilting of the image. The depth image files were used in Amira (Visualization Sciences Group, USA) to form 3D visualisations of the data allowing translation, zooming and rotation.

Photos of the most severely damaged components of retrieved LSZ-4D devices and their restored images are presented in figure 2.2.

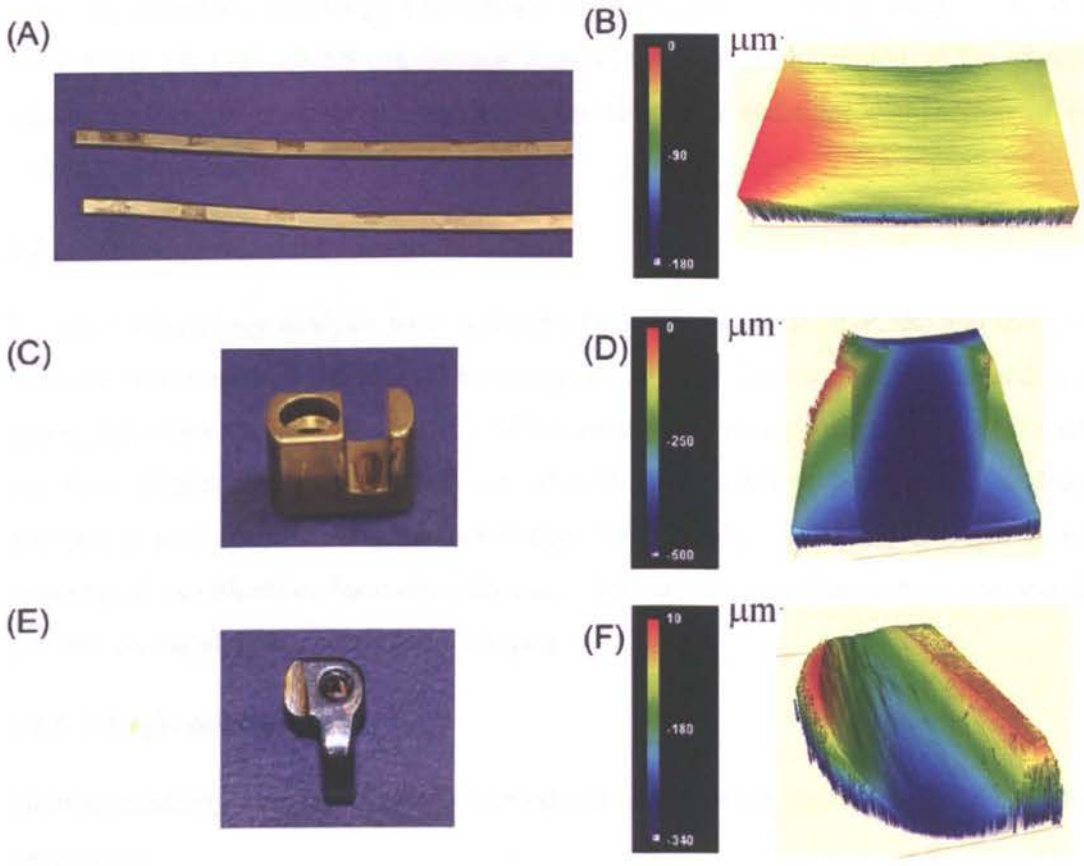

Figure 2.2. Photos of the worn surface of rods (A), clip (C) and hook (E) and the images of the wear scars on them (B, D and F respectively). Images of wear scars were taken using a Bruker interferometer microscope followed by incorporation into MATLAB software for volume loss calculations and afterwards into Amira software for visualization.

Validation of the volume calculations was made by measuring the volume wear loss of the grooves on disks used in our pin-on-disk wear test gravimetrically and by the method described above. The difference in measurements was less than 5%.

2.2.4. Analysis of wear scars

Measurement of roughness (Ra parameter) of wear scars on retrieved LSZ-4D instrumentation was carried out using a TESA Rugosurf 90g surface roughness gage. The direction of roughness measurements on wear scars was across the sliding direction

in order to evaluate the maximum values (ISO 4288). Three measurements for each sample were made.

Scanning electron microscopy (SEM) and energy dispersive X-ray analysis (EDAX) using EVO 50, Carl ZEISS microscope were carried out in the region of the of wear scars. The EDAX analysis on the wear scar formed a basis for comparison of the isolated wear particles.

2.2.5. Histology analysis

Tissues for histology analysis were collected from 5 patients (P.1R-P.5R) and stored in formalin before being processed for histological analysis. Tissues were dehydrated in an ascending series of alcohols (50, 70, 95%), processed through chloroform, infiltrated and then embedded into wax. Sections of 6-10 μm thickness were cut on a sledge microtome and attached to glass cover-slips followed by de-waxing in Xylene. For histological examination, haematoxylin and eosin staining was then carried out and the sections on the glass slide was cover slipped.

2.2.5.1. Light microscopy

Light microscopy investigation was carried out using a Carl Zeiss AXIOSCOP 2 plus microscope.

2.2.5.1. SEM and EDAX

Analysis of wear debris within tissues was carried using SEM and EDAX analysis. For this examination tissues were processed as described above without final stage of staining and cover slipping. Since the tissues are non-conductive, a 5 nm layer of gold palladium was deposited on the tissues for SEM and EDAX examination by sputter coating.

2.2.6. Analysis of wear particles

Wear particles were extracted from tissues surrounding LSZ-4D device. Digestion and examination of particles was implemented according procedures recommended by ISO 17853:11.

2.2.6.1. Digestion procedure

The main stages of digestion included washing in sodium phosphate buffer (SPB), incubation in papain solution (4.8 units in 1.5 ml of SPB) at 65^0C for 24 hours, washing, centrifuging, incubation in proteinase K (0.2mg in 1 ml of 50mM TRIS-HCl) at 65^0C for 24 hours, washing, centrifuging and stored in distilled water at $+1^0$C. After digestion particles were put on plastic coverslips using drop-evaporation method. Coverslips were attached to aluminum stubs by double-side carbon taper.

2.2.6.2. Shape, size and elemental analysis of particles: SEM and EDAX

Before examination, particles were coated with 5 nm layer of Au/Pd. The shape and size of particles were analysed using SEM at magnifications 10,000 – 60,000. Distribution of particle size was made by analysing several micrographs at 30,000 magnification. Fifty particles per samples were measured as required by ISO17853. Image analyser ImagePro3 (Nexis, Russia) software was used for particle size and shape measurements and developing of their size distribution.

2.2.7. Metal ion content in the blood

2 ml of the whole blood have been collected intravenously using cannulas to avoid contamination of the blood from needles. Blood was stored at $+1\pm1^0$C before analysis. Titanium, aluminium and vanadium contents were measured using Inductive Coupled Plasma Mass Spectrometry (ICP-MS) on quadrupolar Nexion 300D (Perkin Elmer, USA). The blood sample of each patient was measured three times and an average value was recorded.

2.2.8. Analysis of fractured spinal rods

Light and SEM microscopy was used for the analysis of the fracture surfaces of the rods rods.

2.2.9. Statistics

Statistical analysis was performed with SPSS 14.0 software.

Comparisons of metal ions level in the whole blood of patients between study and control groups were made using the Mann Whitney U test. A p-value$\leq$0.05 was considered a significant result.

2.3. RESULTS

2.3.1. Analysis of complications in patients with implanted LSZ-4D sliding device

Complications observed in the study patients group (N=25, 3 males and 22 females, age 1,4±1,2, implantation time 5,6±2) revealed breakage of rods in 16% of cases (4 patients) and formation of seromas and fistulas in 20% (5 patients) as indicated in Table 2.2.

Table 2.2. Complications observed in the study group of patients with implanted LSZ-4D sliding devices for EOS healing

	Implantation time, years	Complications	
		Rod breakage	Other
P. 1R	5.8	-	-
P. 2R	3.5	-	-
P. 3R	3.5	-	-
P. 4R	5	+ 1.5 years after surgery	Fistula with inflammation
P. 5R	10.1	-	Seroma, paleness, elevated body temperature, weight loss
P. 6R	5	-	Seroma
P. 7R	5.4	-	Seroma, fistula without inflammation
P. 8R	6	-	Seroma
P. 9R	10	+ 2 years after surgery	-
P. 10R	6	-	-
P. 11R	3.5	-	-
P. 12R	8.2	-	-
P. 13R	6.2	-	-
P. 14R	5.3	-	-
P. 15R	7.3	-	
P. 16R	8.2	+ 1 year after surgery	-
P. 17R	4.2	-	-
P. 18R	1.5	-	-
P. 19R	4.2	-	-
P. 20R	5.5	+ 2.1 years after surgery	-
P. 21R	5.5	-	-
P. 22R	4.5	-	-
P. 23R	5.1	-	-
P. 24R	4.1	-	-
P. 25R	5.2	-	-

In 5 cases seromas and fistulas were observed locally in the lumbar part of the spine over the implanted device. Seromas were seen in 4 patients, fistulas in 2 cases (one with inflammation). All seromas and fistulas were localized in the lumbar part of the spine. Excretion of serous liquid was observed in the 2 cases in patients with fistula formation. Tissues surrounding the implanted device were blackened by the metal debris (fig. 2.3). After removal of LSZ-4D sliding devices during routine exchange due to cessation of growth, the seromas and fistulas disappeared.

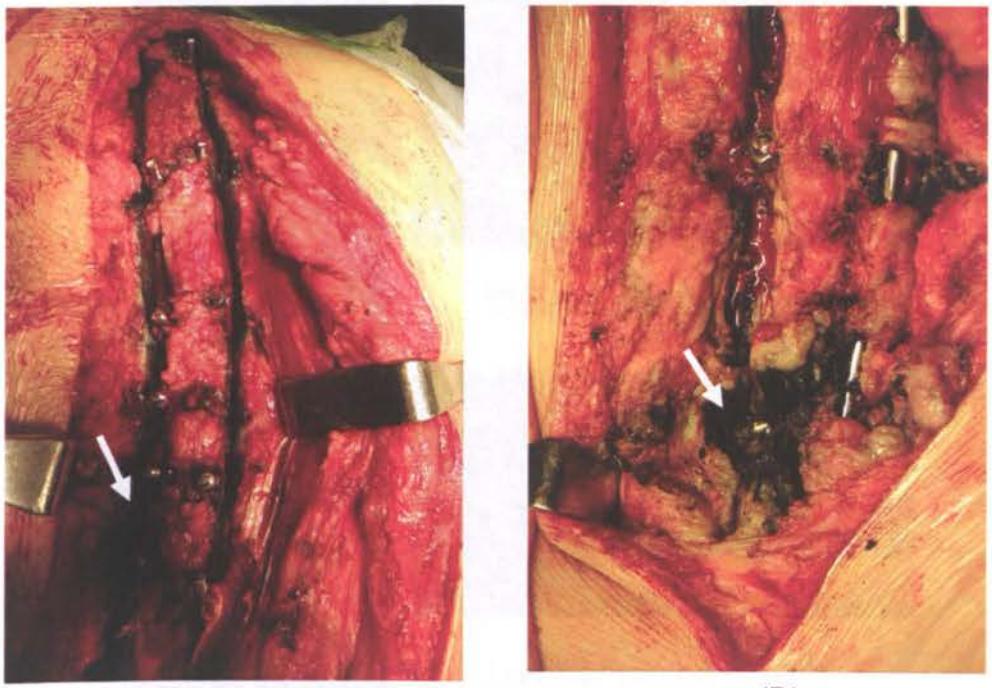

Figure 2.3. Photo of the tissues surrounding LSZ-4D sliding device for EOS made during routine surgery of its interchanging for fusion instrumentation, revealing metal debris in the lumbar part of the spine: (A) patient P.1R, 5.8 years of implantation; (B) patient P.5R, 10.1 years of implantation.

Localization of seromas and fistulas, the presence of black metal wear debris in adjacent tissues and the discoloured serous liquid suggests that these complications are associated with metallosis.

2.3.2. General inspection of retrieved LSZ-4D sliding device components

Examination of wear scars on rods revealed larger scars on the distal and proximal parts of rods (normally located in the cervical and lumbar part of the spine) and minor wear of the rods in the central region near the level with the locked screws (normally in thoracic spine level). Typical photographs of two retrieved rods are shown in figure 2.4. The average width of scars was 10±2 mm.

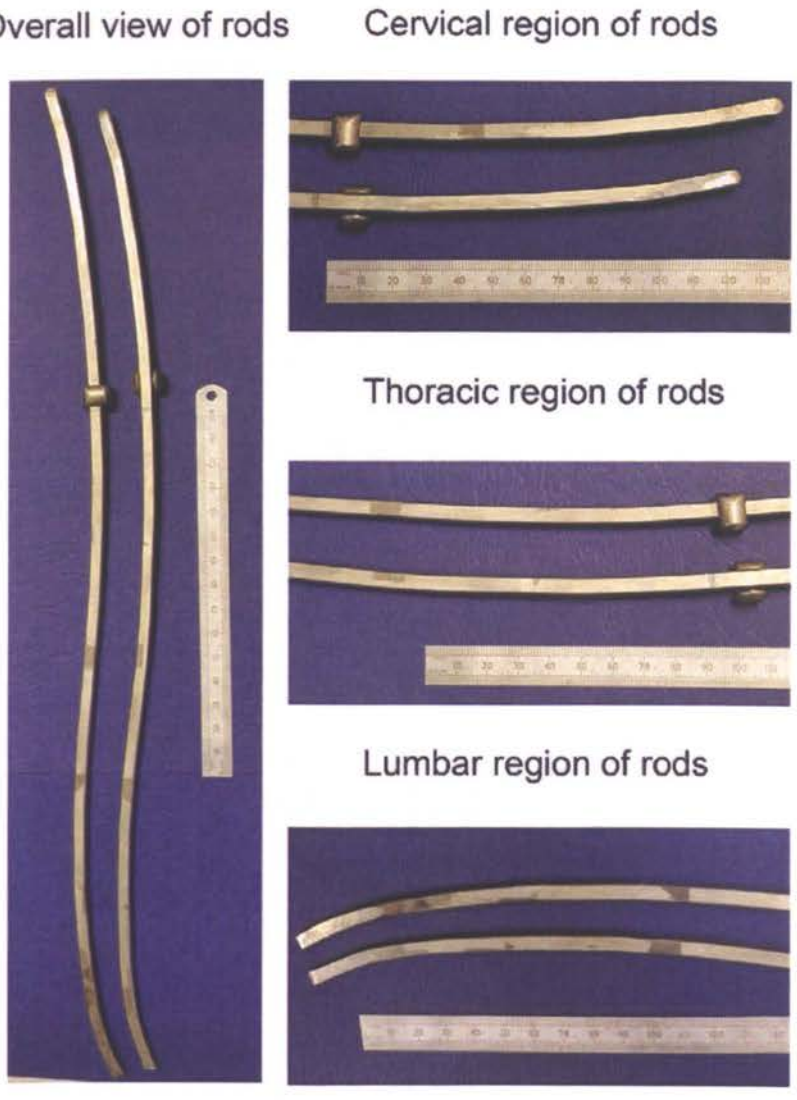

Figure 2.4. Photos of retrieved rods of LSZ-4D sliding device for EOS: (A) overall view of rods; (B) cervical region of rods; (C) thoracic region of rods; (D) lumbar region of rods. Implant retrieved from patient P.1R (5.8 years of implantation).

The wear of hooks and clips was uneven (fig. 2.5). Approximately 30% were severely damaged (red arrows on fig. 2.5) while another 20% revealed minor damage (green arrows) and the rest (50%) had minor scratches with no measurable damage. Larger numbers of more severely damaged fixtures were retrieved from the distal part of LSZ-4D instrumentation located in the lumbar region (fig. 2.5).

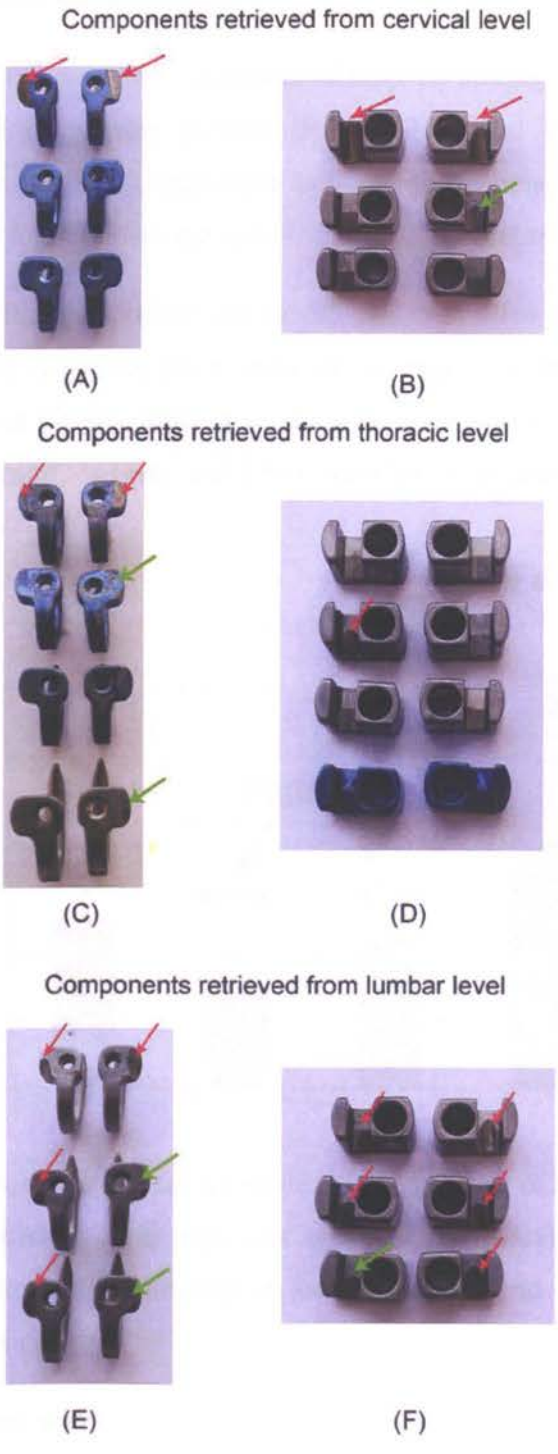

Figure 2.5. Photos of retrieved fixtures (clips and hooks) of LSZ-4D sliding device for EOS. Implant retrieved from patient P.1R (5.8 years of implantation): (A and B) components retrieved from cervical level; (C and D) components retrieved from thoracic level; (E and F) components retrieved from lumbar level

2.3.3. Volume wear loss measurements

Volume wear loss of the complete assembles of LSZ-4D sliding devices were analysed for devices retrieved from three patients (P. 1R, P.2R and P.3R, Table 2.1). The duration of installation of these implanted devices ranged between 3.5 and 5.8 years (average: 4.3 years). None of these patients had any clinical complications (Table 2.2).

The whole assembly for each patient included 2 rods with 40±8 fixture elements (20±4 hooks and 20±4 clips). Assuming linear wear, the average wear rate for the whole LSZ-4D sliding device, was 12.5±1.5mm^3 per year with contribution from two rods, hooks and clips being 5±1.2mm^3, 3±1mm^3 and 4.5±1.5mm^3 per year respectively (figure 2.6).

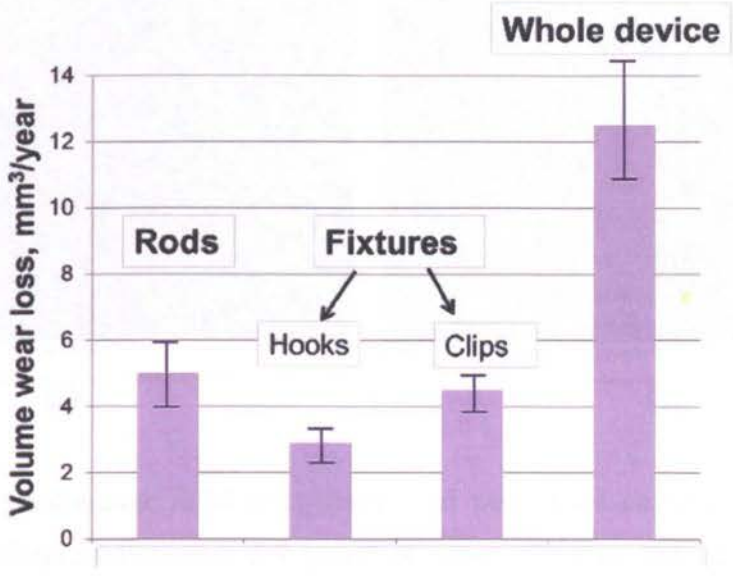

Figure 2.6. Average volumetric wear for retrieved components of LSZ-4D devices made of titanium alloy Ti6Al4V. The data was obtained from devices retrieved from 3 patients. Instrumentation from each patient included 2 rods and 40±8 fixture elements (20±4 hooks and 20±4 clips).

2.3.4. Analysis of wear scars

SEM analysis of wear scars on retrieved rods, hooks and clips of LSZ-4D devices revealed that approximately 20% could be classified as being severely damaged, while the remaining 80% could be classified as being mildly damaged (fig. 2.7A) and had only mild scratches (fig.2.7B). Severely damaged areas had Ra roughness parameter 0.7±0.1 μm, while mildly damaged only 0.1±0.05 μm.

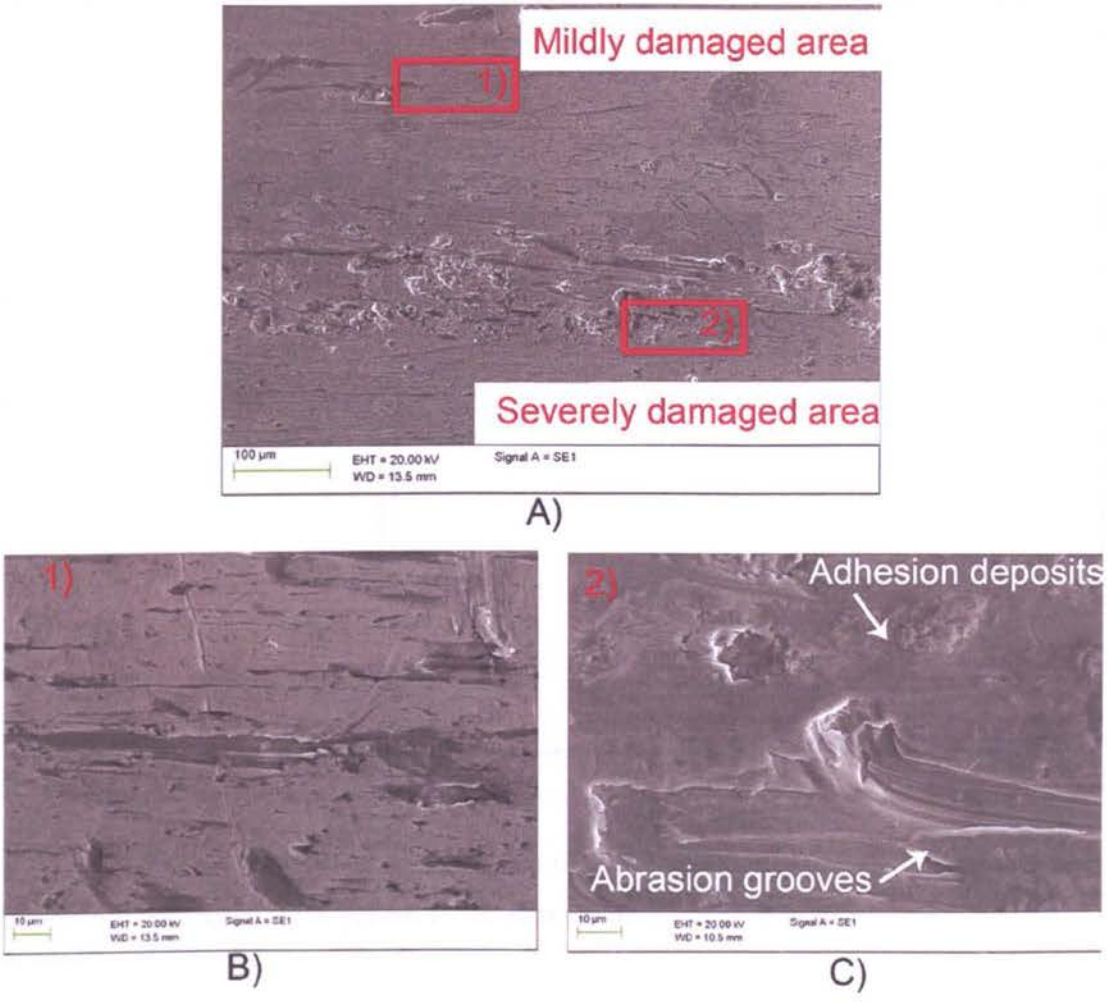

Figure 2.7. Representative SEM micrographs of wear scars on retrieved rods from patient P.1R, (implantation time 5.8 years) revealing abrasive and adhesion damage mechanisms: (A) general view; (B and C) areas 1) and 2) respectively at higher magnification.

Deep abrasive grooves and adhesion deposits of titanium (fig. 2.7C) indicating abrasive and adhesion mechanisms of Ti6Al4V alloy wear damage was observed on severely damaged areas.

EDAX analysis of adhesion deposits revealed typical titanium, aluminum and vanadium peaks characteristic of Ti6Al4V alloy (fig. 2.8).

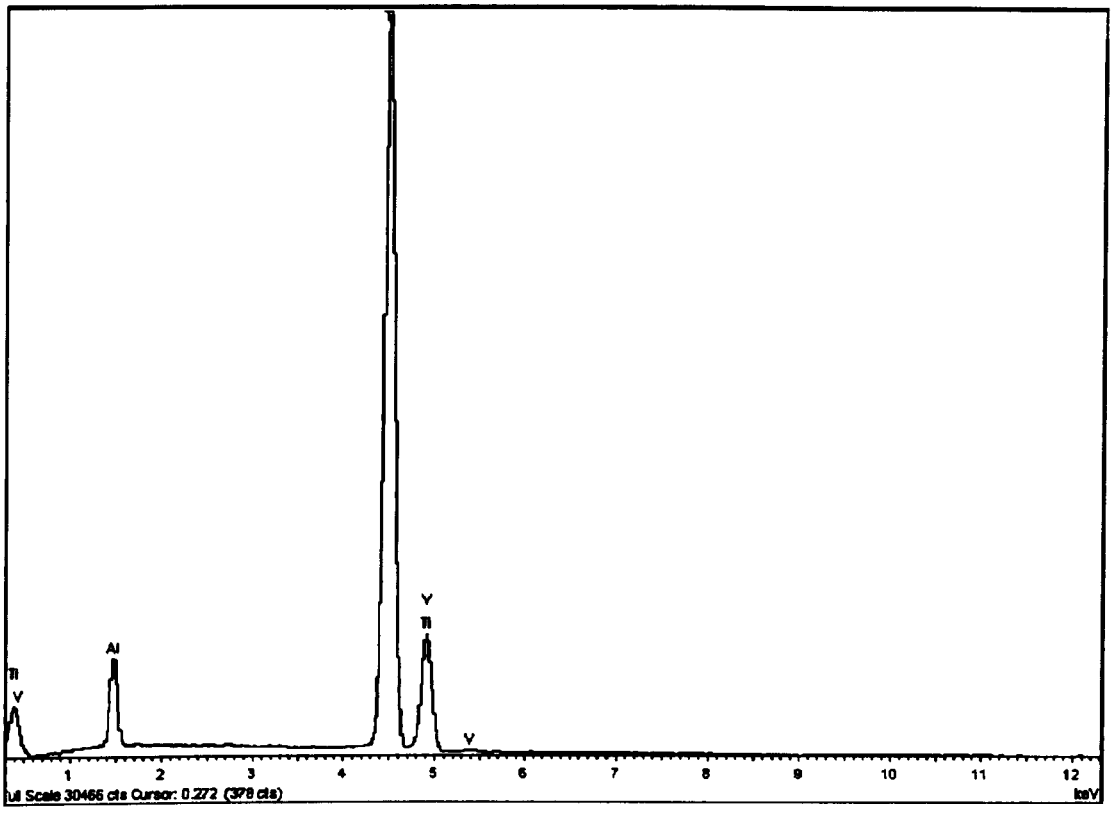

Figure 2.8. EDAX analysis of adhesion deposits on the severely damaged areas of wear scars (rods retrieved from patient P.1R, implantation time 5.8 years)

2.3.5. Analysis of wear particles

2.3.5.1. Shape and size: SEM

The average particles size determined by analyzing SEM images taken at 30,000 magnification (fig. 2.9A) using ImagePro3 (Moscow, Russia) software was 0.46μm (range from 0.09 to 1.59μm). Average aspect ratio was 1.2-1.5 and they were classified as round to oval according to ISO 17853:2011. The size distribution of the particles is shown in figure 2.9B. It can be seen that approximately 50% of particles have a size less than 0.4 μm.

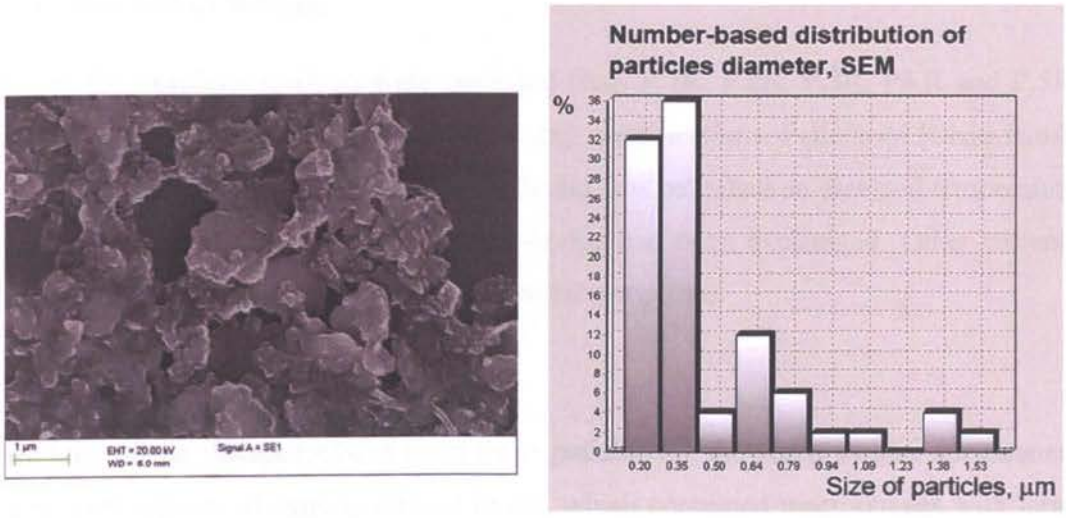

Figure 2.9. Scanning electron micrograph of wear particles enzymatically digested from retrieved tissues (A) and number-based distribution of particle diameters (B).

2.3.5.1. Elemental analysis: EDAX

EDAX analysis of the chemical composition of wear particle agglomerates demonstrated typical profiles of Ti6Al4V alloy with titanium and aluminum peaks (fig. 2.10). Oxygen peaks indicate that these particles were oxidized in biological environment. Gold and palladium peaks appear from the nanosize coating deposited on particles for EDAX analysis.

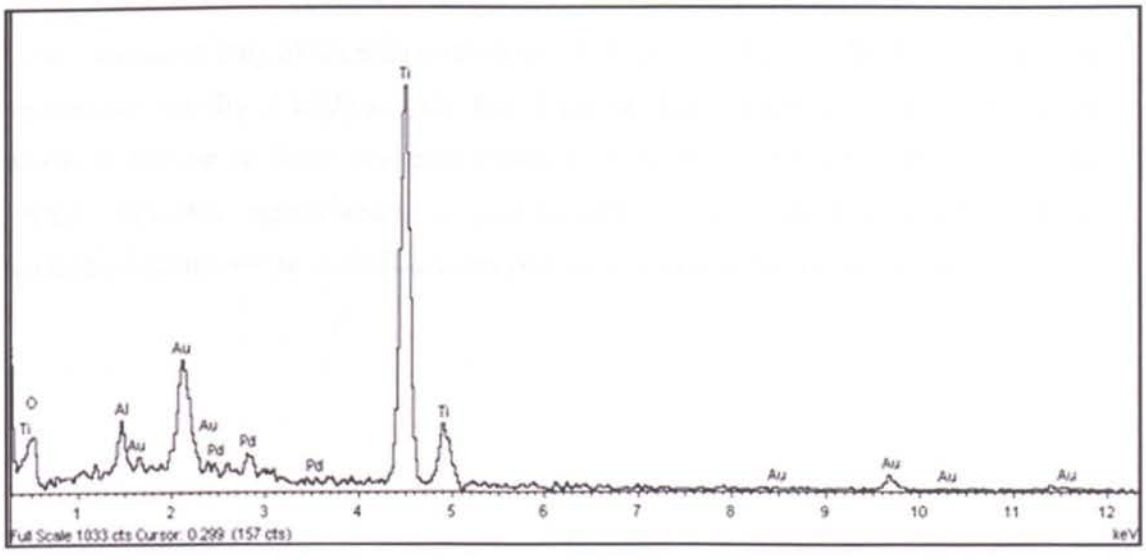

Figure 2.10. The chemical composition of particle agglomerates reveals presence of Ti and Al (EDAX analysis).

2.3.6. Histological analysis

Tissues for histology analysis were collected from P.1R, P.2R, P.3R, P4.R and P.5R. Patients P.1R, P.2R and P.3R did not have any complications. Patient P4.R had fistula with inflammation. Patient P.5R had seroma and was pale, had an elevated temperature and weight loss which resolved once the device had been exchanged. Other patients although not as severe also demonstrated similar symptoms.

2.3.6.1. Light microscopy

Histology of the tissues isolated from these patients all showed a similar appearance. There were regions of densely stained tissue, which contained macrophages with large numbers of titanium particles. Individual particles could not be seen as there were of a small size. These macrophages often occurred in well vascularised tissue and there was an infiltration of plasma cells within the tissue. In other regions particularly in patient P. 5R there were regions of necrosis where the cell number was reduced and a-cellular regions of collagenous tissue were observed.

2.3.6.2. SEM and EDAX

Analysis of tissues surrounding LSZ-4D devices using scanning electron microscopy in backscattered and secondary electron modes revealed the presence of particles in the tissues (fig. 2.12 A-C). EDAX analysis revealed agglomeration of smaller particles consisted of Ti and Al (EDAX 1, fig. 2.13A) whereas bigger, separate particles 2-5 μm in size consisted only of Ca with no traces of Ti (EDAX 2, fig. 2.13B). Most particles in agglomerations (fig. 2.12D) are less than 1 μm in size and have a round to oval shape which is similar to those particles digested from tissues discussed in the previous section. However, quantification of particle size was difficult since distinct particle boundaries could not be identified when particles were incorporated in tissues.

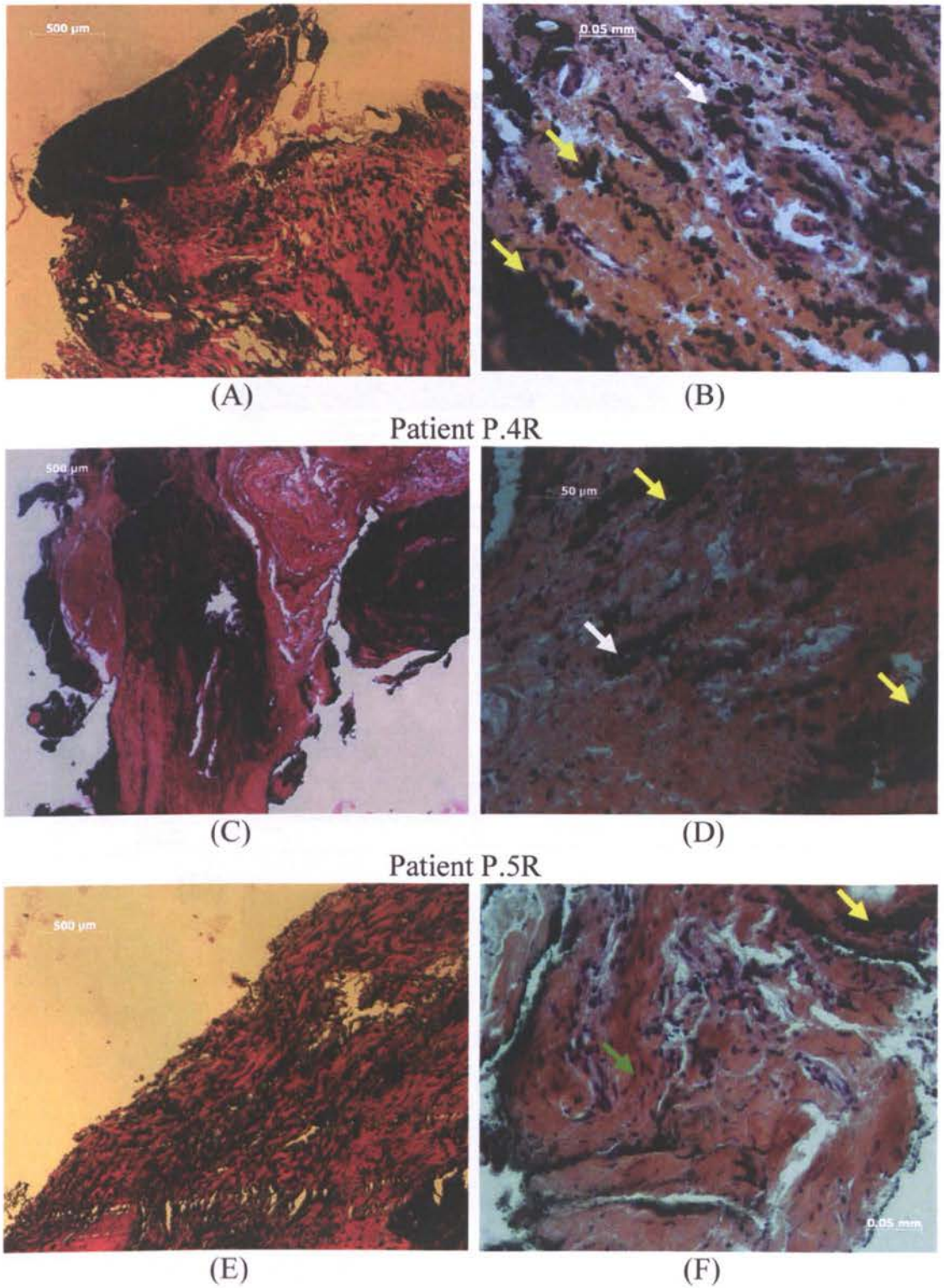

Figure 2.11. Histology analysis of tissues from patient P.1R (A and B), P.4R (C and D) and P.5R (E and F) surrounding LSZ-4D sliding device, showing densely stained tissue (yellow arrows), macrophages (white arrows) and necrosis (green arrows)

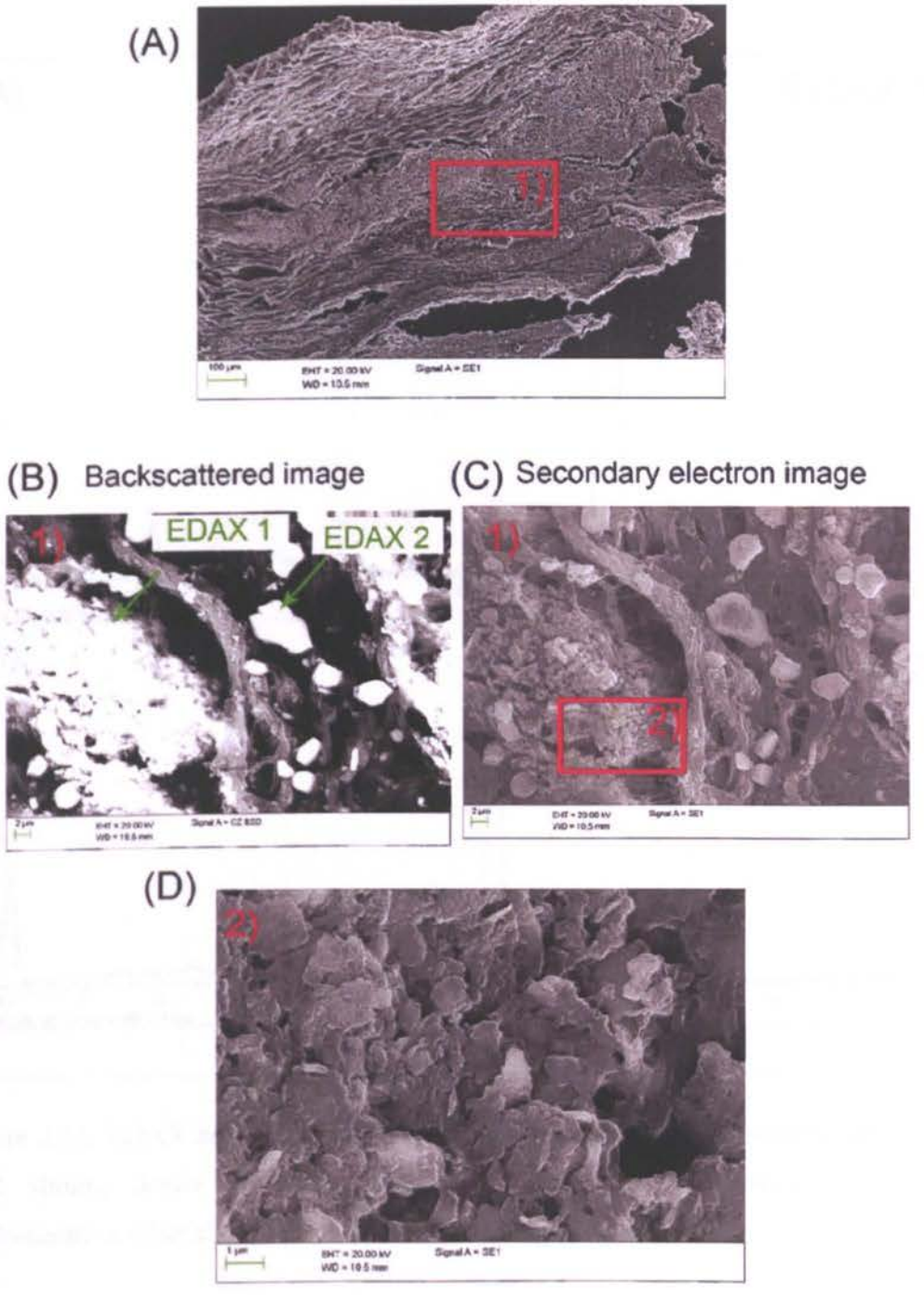

Figure 2.12. Scanning electron micrograph of tissues surrounding LSZ-4D sliding device revealing incorporated particles: A) general view; (B and C) area 1); D) area 2) at higher magnification. (A, C and D) are secondary electron SEM image; B) backscattered SEM image

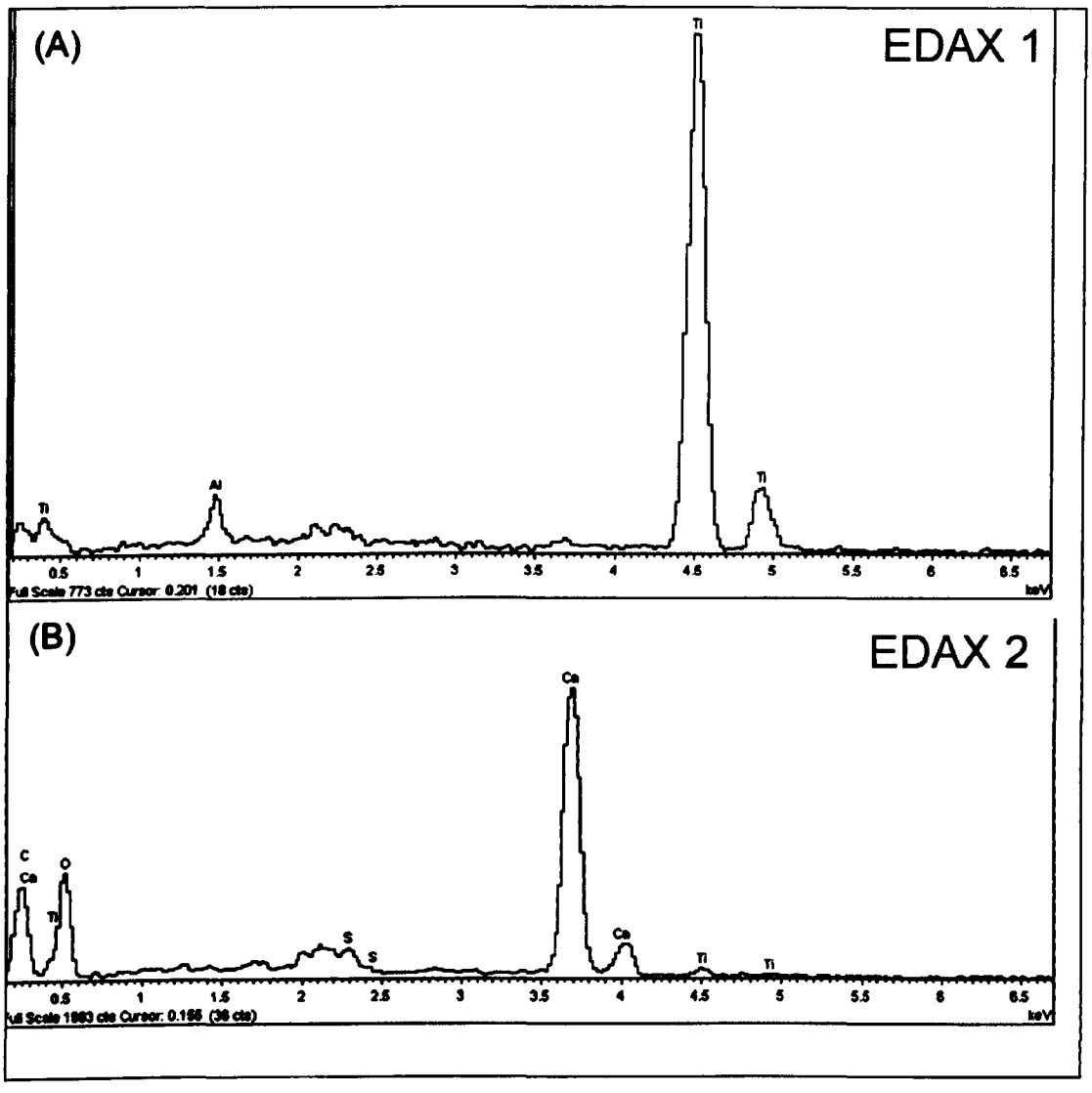

Figure 2.13. EDAX analysis of small (A) and big (B) particles in tissues surrounding LSZ sliding device revealing large (2-5μm) particles consisting of Ca and agglomeration of smaller particles below consisting of Ti and Al

2.3.6. Metal ion content in the blood

The titanium, aluminium and vanadium content in the whole blood of patients from control group without implants (P.I1-P.I10) was 32±3.5 ppb for titanium, 28±6 ppb for aluminium and 0.08±0.02 ppb for vanadium. Patients with implanted LSZ-4D sliding devices had much higher ion levels with 89±46 ppb of titanium, 44±32.5 ppb of aluminium and 0.33±0.11 ppb of vanadium (fig. 2.14-2.16). Statistical analysis of these results using Mann-Whitney non-parametric test revealed statistically significant raised levels of titanium and vanadium (2.8 and 4 times respectively) in the whole blood of patients with implanted LSZ-4D devices. Statistically significant difference in aluminum content was not observed for the compared control patients due to the high degree of scattering of ion content in the blood of patients with implanted devices ($p=0.16$).

The content of titanium, aluminium and vanadium for patients with implanted LSZ-4D devices who had seromas and fistulas (N=5: P. 4R, P. 5R, P. 6R, P. 7R, P. 8R) was also compared with that observed in patients who did not have these complications (N=20, all the rest from P.R group, Table 2.2). In the group of patients with complications of titanium, aluminium and vanadium content was found to be 59±16; 68±50 and 0.26±0.08 ppb respectively. In the group without complications it was 102±48; 33±12 and 0.36±0.10 ppb for titanium, aluminium and vanadium respectively. Statistical analysis revealed that the patients who developed seromas or fistulas did not have higher content of titanium, aluminium or vanadium.

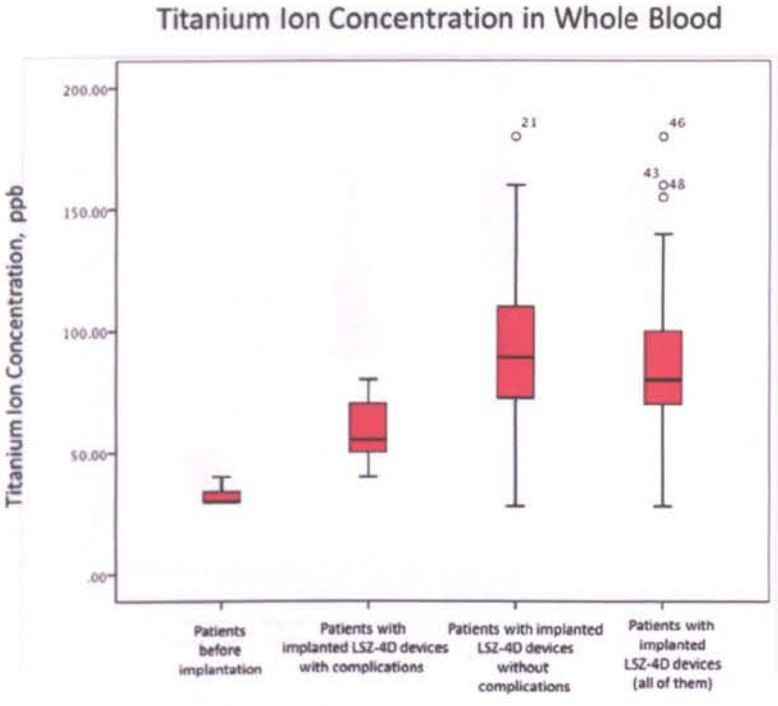

Figure 2.14 Content of titanium measured using ICP-MS method, in the whole blood of patients before and after implantation of LSZ-4D devices

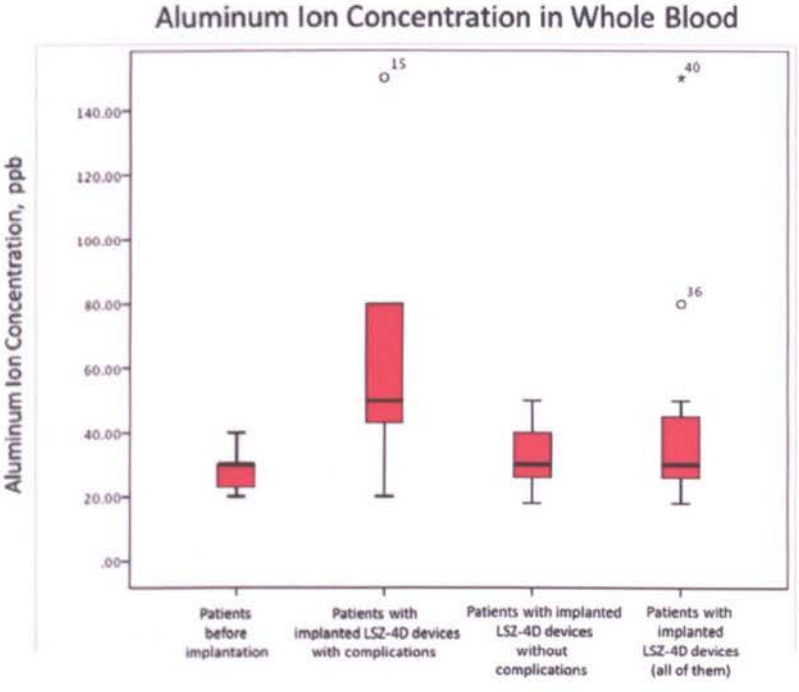

Figure 2.15 Content of aluminium measured using ICP-MS method, in the whole blood of patients before and after implantation of LSZ-4D devices

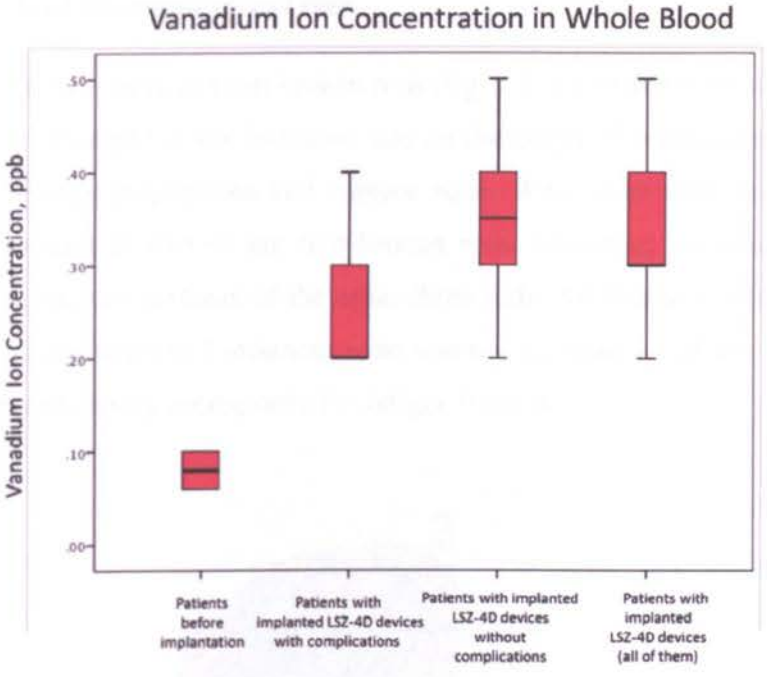

Figure 2.16 Content of vanadium measured using ICP-MS method, in the whole blood of patients before and after implantation of LSZ-4D devices

2.3.7. Analysis of fractured spinal rods

Analysis of fracture surfaces from broken rods (fig. 2.17) revealed typical fatigue failure with evidence of fatigue crack initiation site on the edges of rectangular cross-section rods, zone of crack propagation and rupture zone. Wear scars near fractured surface have been revealed in two of the five broken rods. However, no wear damage was observed near fracture surfaces of the other three rods. All fractures initiated from the edge of the rod and since in 3 instances wear was not associated with the initiation point it may not be a necessary prerequisite for fatigue fracture.

Figure 2.17 Fracture surface of the rod in patient P. 4R after 1.5 years of implantation reveals features of fatigue failure: crack initiation site (1), propagation zone (2) and rupture zone (3).

2.4. DISCUSSION

The frequency of rod breakage for LSZ-4D sliding devices was 16% which is similar to that recently reported by McCarthy et al. (2013) for Shilla rods made of SS (Medtronik, USA) and by Sedra et al. (2013) for Ti growing rods (Ellipse Tech, USA). Obviously the absence of fusion in these devices results in a higher range of spine mobility and thus to higher stresses and strains encountered by these rods due to the functional activities of the patients. This makes the testing of fusion-less devices for EOS correction using ISO12189 very important, since it evaluates fatigue resistance of spinal implants. Another complication for LSZ-4D devices was found to be metallosis associated with the formation of seromas, and fistulas (20%). Complications associated with metallosis have not been reported for growing rods or for Shilla devices. It can be assumed that growing rods encounter less movement in fixed devices, but no long-term results for Shilla devices are available.

The volume wear rate measured for the retrieved components of LSZ-4D devices made of Ti alloy Ti6Al4V was found to be 12.5 mm^3 per year with $5mm^3$ and 7.5 mm^3 per year contributed from rods and fixtures respectively. Due to the large number of fixtures in LSZ-4D devices, the wear rate was measured on three devices which had typical wear scars on visual observation of instrumentation retrieved from 25 patients. Wear loss values observed in LSZ-4D devices are greater when compared to Shilla growth-guidance devices (made of SS which were reported to be 0.78 per year (Singh et al., 2013). One of the reasons for this could be the higher wear resistance of SS compared to Ti. However, absolute values of the wear rate will also depend on the design of device, number of fixtures and, patient activity etc. Nevertheless, the wear rate measured for LSZ-4D devices, is similar to values reported for metal-on-metal THR made of CoCr alloys (15-26 mm^3 per year) which are known for their superior wear resistance (Lord et al., 2011, Morlock et al., 2008 & Witzleb et al., 2009) (McKellop et al., 2008). Such amounts of CoCr wear debris often result in bone resorption, inflammation and implant failure. Taking into consideration the poor wear resistance of titanium alloys, it may imply that the contact area and possibly the loads in sliding growth-guidance devices are lower compared to THR. Analysis of complications in patients with implanted LSZ-4D devices revealed no cases of loosening of the device. However, there were cases of seroma and fistulas near the devices.

Abrasive and adhesion mechanism of wear damage have been identified on retrieved components of LSZ-4D device wear scars. Abrasive mechanism of wear damage is typical for many metal materials, while adhesion mechanisms are considered to be specific for titanium alloys due to removal of the protective TiO_2 oxide film during friction. The high chemical activity of titanium results in micro-welding of titanium to the counter-bodies and is considered to be one of the main reasons for its poor tribological properties (McKellop et al., 2001).

Examination of wear particles retrieved from tissues which surrounded LSZ-4D devices using image analysing of SEM micrographs at 30,000 magnification, revealed the size of particles to be 0.09 to 1.59μm with 50% of wear particles being less than 0.400 μm in size and round to oval in shape. The smallest particles observed in this work were 0.09 μm. It should be noted that there could be particles less than 0.09 μm in size; however high-resolution field emission gun SEM or transmission microscopy is necessary for imaging them. The values found here are similar to those described for cobalt chromium particles retrieved from THR which are reported to be 0.02-0.8 μm for CoCr and 0.04-0.9 μm for Ti analysed using transmission electron microscopy by Doorn et al. (1998). Larger wear particles observed for Shilla devices (Sign et al., 2013) might possibly be explained by their use of laser scattering methods for measuring particle size where the effect of particle agglomeration or particles settling down to the bottom during measurement is unclear.

Statistically significant increased levels of titanium and vanadium (2.8 and 4 fold respectively) in whole blood of patients with implanted LSZ-4D sliding devices was revealed. In total hip replacement abnormal wear resulting in osteolysis and loosening for metal-on-metal THR was associated with an increase in Co ion concentrations in whole blood of 7-10 fold (Hart et al., 2013). Although implantation of sliding LSZ-4D devices resulted in increasing levels of titanium and vanadium this increase was less than that found in THRs. There was no statistically significant difference in metals ions in the blood of patients who developed seromas and fistulas compared with patients who did not develop these complications.

However the incidence of seroma and fistula formation was observed to be 25% and this level indicates that is necessary to is exchange the growing device for instrumentation with locked fixtures once the patient has matured. However metallosis

was a common problem even in growing patients and this may be reduced using wear-resistant coatings on titanium spinal instrumentation, which is the subject of the next experimental chapters

2.5. CONCLUSIONS

1. Analysis of complications for 25 patients with implanted growth-guidance LSZ-4D devices revealed metallosis associated complications in 20% of patients (seromas, fistulas and inflammation). A further 16% encountered fatigue breakage of rods.

2. The volume wear rate measured for the retrieved components of LSZ-4D device made of titanium alloy Ti6Al4V was found to be 12.5 mm^3 per year from which 5mm^3 per year is derived from the rod wear debris and 7.5 mm^3 per year is contributed by fixtures.

3. Abrasive and adhesion wear damage mechanisms were observed on retrieved LSZ-4D device components.

4. Histological analysis revealed regions of densely stained tissue, which contained macrophages with large numbers of titanium particles.

5. Statistically significant increases of titanium and vanadium concentration (2.8 and 4 times respectively) in the whole blood of patients with implanted LSZ-4D devices have been revealed.

CHAPTER 3

THE INFLUENCE OF THE STRUCTURE ON THE FATIGUE BEHAVIOUR OF NITINOL

3.1. INTRODUCTION

The rods in the devices designed for the correction of spinal scoliosis encounter repeated cyclic loading. Analysis of complications after implantation of LSZ-4D sliding devices carried out in Chapter 2 revealed significant percentage of the fatigue breakage of the rods (16%).

Analysis of literature reveals that Nitinol has good fatigue performance in strain-controlled conditions and is now being used for the manufacturing of endovascular stents (Duering et al., 1999) and orthopaedic devices such as spinal fixings (Kim et al., 2007). When loaded up to strains equivalent to 300-330 MPa stress reported by Rohlmann et al. (1997) for spinal rods implanted into lumbar part of the spine, Nitinol demonstrates fatigue performance comparable to titanium. Nevertheless, since rods in spinal sliding instrumentation operate in a corrosive environment and may also have wear damage, further improvements in the fatigue resistance of Nitinol by optimization of its microstructure would be beneficial.

Research into the factors which influence the fatigue performance of Nitinol indicates that the microstructure which develops as a result of thermo-mechanical processing and thermal treatments significantly affects its fatigue behaviour (Melton & Mercier, 1979; Heckmann & Hornbogen, 2002; Pelton, 2011; Wagner at al., 2010; Wessels et al., 2012). Nevertheless, due to the complex structure of the Nitinol (the phase composition of which may include austenite, martensite, Ti-rich and Ni-rich particles), predicting its fatigue behaviour is difficult. As a result, adjusting of thermo-mechanical treatment is recommended even for each batch of ingots (Pelton et al., 2011).

An attempt to explain the complex influence of various structural parameters was made by Melton and Mercier (1979) who assumed that the larger the strain Nitinol can accommodate by the development of stress-induced martensitic transformation the better the fatigue performance.

Subsequently, this idea was developed further by Heckmann and Hornbogen (2002) who suggested that the improvement of Nitinol fatigue-resistance in strain-controlled conditions can be achieved by the creation of the microstructure which provides $\sigma_M/\sigma_{slip} \Rightarrow$minimum, where σ_M is the stress of the martensite re-orientation, or its stress-induced formation, and σ_{slip} is the stress at which deformation caused by the dislocation

slip mechanism starts. It should be noted that changes in microstructure may result in corresponding changes in both σ_M and σ_{slip}. However due to the difficulty of measuring σ_{slip} these considerations have thus far been qualitative. In the current work it has been assumed that the critical strain (ε_{cr}), is defined as the maximal strain which the sample can completely recover after unloading and heating to the temperature higher than A_f (Kollerov et al., 2008), and is a measure of the differences in σ_M and σ_{slip}.

Significant change of the fatigue slope of Nitinol is observed when testing at lower strain amplitudes starting from 1.5-1% as reported by Pelton et al. (2008) and Tolomeo et al. (2000) and may indicate a change in the fatigue fracture mechanism. That is why, the influence of the structure parameters should be established separately for high- and low-strain cyclic loading.

Since recent research (Moumni et al., 2005; Runciman et al., 2011; Maletta et. al. 2012) revealed that the strain-controlled fatigue curve of Nitinol can be described by a modified Coffin-Manson relationship, it will be useful to establish if this relationship can be used with structure-influenced coefficients.

Consequently, the <u>purpose</u> of the study detailed in this Chapter was to establish the effects of various structural parameters on the fatigue behaviour of Nitinol including increased dislocation density, the size of Ni-rich (Ni_4Ti_3 and Ni_3Ti_2) particles and the volume fraction of Ti-rich ($Ti_4Ni_2O_x$) particles.

The <u>aims</u> were:

1. **Establish the effect of structural parameters (increased dislocation density, size of Ni-rich (Ni_4Ti_3 and Ni_3Ti_2) particles and volume fraction of Ti-rich ($Ti_4Ni_2O_x$) particles on high-strain fatigue performance of Nitinol.**
2. **Establish the effect of structural parameters (increased dislocation density, size of Ni-rich (Ni_4Ti_3 and Ni_3Ti_2) particles and volume fraction of Ti-rich ($Ti_4Ni_2O_x$) particles on low-strain fatigue performance of Nitinol.**
3. **Establish the possibility of using a modified Coffin-Manson relationship with structure-controlled parameters for describing and prediction of the strain-controlled fatigue behaviour of Nitinol.**

3.2 MATERIALS AND METHODS

3.2.1. Materials

The test samples were prepared from three ingots. Ingot 1 was produced by scull melting combined with subsequent vacuum arc re-melting. Ingots 2 and 3 were produced by vacuum induction melting. The chemical composition of all three ingots provided by the supplier is presented in Table 3.1 below. Wire semi-products were supplied in the warm rolled condition without additional annealing.

Table 3.1. Chemical composition of Nitinol alloys

Alloy	Elements content, [wt.%]								
	Ti	Ni	Fe	Co	O	C	H	N	Si
Ingot 1	balance	55.7	0.1	0.01	0.17	0.015	0.0015	0.009	0.15
Ingot 2	balance	55.8	0.05	0.016	0.013	0.012	0.0011	0.006	0.01
Ingot 3	balance	54.7	0.08	0.012	0.017	0.013	0.0016	0.006	0.015

Ingot 1 was used to investigate the influence of increased dislocation density, as and the presence and size of Ni-rich (Ni_4Ti_3 and Ni_3Ti_2) particles, on the fatigue behaviour of Nitinol. A portion of the samples were investigated in the initial warm rolled state (group 1, Table 3.2). Vacuum annealing (V.A.) and aging of Nitinol samples in order to modify their structure was carried out in vacuum furnace SVN-1.31/16-I4 (Russia) and air furnace SNOL-1.6 (Russia) respectively (groups 2-4, Table 3.2).

In order to investigate the influence of the volume fraction of $Ti_4Ni_2O_x$ on the fatigue behaviour of Nitinol, ingots 1 and 2 were compared. These ingots had approximately the same Ni content which was in the range of 55.7-55.8 wt.%, however they differed in the oxygen content which is known to affect the formation of $Ti_4Ni_2O_x$ phase (Chuprina et al., 2002).

Ingot 3 had decreased Ni content (54.7 wt.%) for comparison reasons as low Ni content was expected to provide a high ε_{cr} parameter as described below.

Table 3.2. Heat treatment of Nitinol wire samples for fatigue testing

	Group of samples	Ingot number	Heat treatment
1.	Group 1	Ingot 1	Initial state, warm rolling
2.	Group 2		Vacuum annealing at 700^0C for 1 h
3.	Group 3		Vacuum annealing at 700^0C for 1 h and aging at 500^0C
4.	Group 4		Vacuum annealing at 700^0C for 1 h and aging at 450^0C
5.	Group 5	Ingot 2	Vacuum annealing at 700^0C for 1 h and aging at 500^0C
6.	Group6	Ingot 3	Vacuum annealing at 700^0C for 1 h and aging at 500^0C

The diameter of wire samples was 1.5 mm. Oxide surface layers were removed by the wire supplier by chemical and mechanical polishing.

After heat treatment all samples were then ground and electro-polished in a mixture of 20% of $HClO_4$ and 80% of CH_3COOH acids.

3.2.2. Methods

3.2.2.1. Analysis of microstructure: optical microscopy, SEM, transmission electron microscopy (TEM), X-ray analysis

The microstructure of the materials was analysed (using a Carl Zeiss) Neophote 30 optical microscope. Before investigation all samples were ground, electro-polished and etched in 5% HF + 35% HNO_3 + 60% distilled water solution.

Chemical composition of Ti_2Ni_4Ox particles was identified using SEM and EDAX analysis. The volume fraction of Ti_2Ni_4Ox particles was evaluated on electro-polished samples without subsequent etching by taking 10 micrographs per sample which were then processed using ImagePro3 (Nexis, Russia) software.

Bright field transmission electron microscopy was carried out using JEOL 2800 with acceleration voltage 125 kV.

X-ray analysis was carried out using DRON 4 (BUREVESTNIK, Russia) in filtered Cu Kα radiation at 40 kV. Samples were etched in a mixture of 25% HF + 75% HNO_3 acid.

3.2.2.2 Mechanical behaviour characterization

Stress-strain curves which characterize mechanical behaviour of Nitinol were measured using three point bending tests at 21 ± 1°C using TIRAtest 2300 machine (HECKERT, Germany). Curves were plotted on 3 samples per each structural state.

Elastic modulus E was measured as $E=\sigma/\varepsilon$ on the rectilinear part of the stress-strain curve.

σ_M was identified as a stress at which rectilinear stress – strain dependence terminates.

3.2.2.3 Measurement of A_f temperature

The A_f temperatures for the wires were determined using a bend and free recovery method according to ASTM standard F2082 at the temperature 21 ± 1°C.

3.2.2.4 Measurement of ε_{cr}

The critical strain ε_{cr} of Nitinol alloy samples for all structural states was measured at the temperature of the fatigue tests (21 ± 1°C) by subsequent loading of the samples up to various strains by bending over holders having various diameters (D). Strain amplitude was calculated according to the following relationship:

$$\varepsilon_a = (d/(D+d))x100, \qquad (3.1)$$

where d – wire sample diameter, mm; D – diameter of the holder, mm

After loading samples were unloaded then heated to a temperature above A_f. If no unrecoverable strain was detected afterwards, another sample was loaded up to the higher strain. The process was repeated until unrecoverable strain of 0.2% was reached, which is minimal strain which can be measured by this method. This value was named as $\varepsilon_c^{0.2}{}_r$. Three samples were tested for each structural state.

3.2.2.5 Fatigue tests

The fatigue tests were performed on Nitinol wire samples according a total life strain-controlled approach by combined bending and rotation as shown in Figure 3.1 below. The tests were carried out in a circulating, temperature-controlled water bath at a temperature of 21 ± 1°C. The rotation frequency was 1.5 Hz and the mean strain was zero.

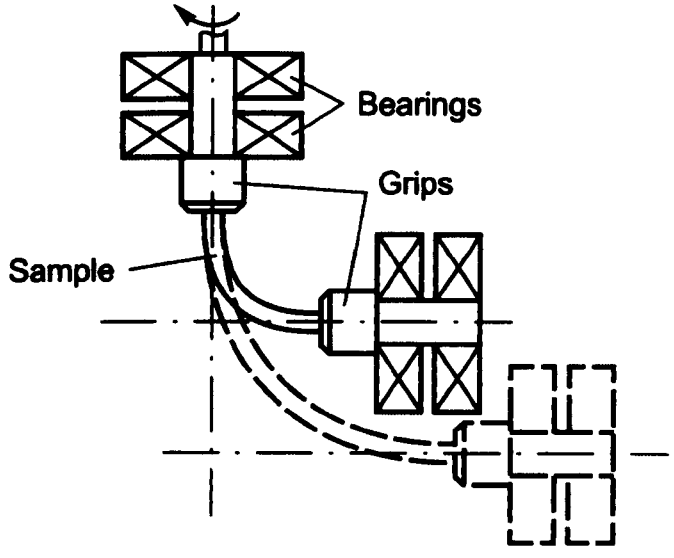

Figure 3.1. Loading unit of the machine for the fatigue test by bending and rotation of wire samples.

Cyclic changes of the bending moment in spinal rods during walking were reported to be 0.5 Nm (Rohlmann et al., 1997). This would result in low strain amplitude loading (corresponding to a strain amplitude of up to 0.07% for the modulus of elasticity of Nitinol of 70 GPa) while the maximal bending moment was measured to be 8Nm (corresponding to high strain amplitudes of 1.5-2%). Therefore fatigue tests were carried out at both low and high strain amplitudes. Since it is difficult to perform tests at

amplitudes lower than 0.5-0.75%, the strain amplitudes (ε_a) used in these tests was in the range of 0.75-4.8%. For imposing these strains the wire samples were bent over holders having various diameters (D). Strain amplitude was calculated according to the relationship 3.1.

SEM microscopy of the wire surface adjacent to the fatigue fracture was carried out using EVO 50 microscope.

3.2.2.6 Statistics

Statistical analysis was performed with SPSS 14.0 software.

3.3. RESULTS

3.3.1. Analysis of microstructure

Ingot 1

Analysis of microstructure revealed that Nitinol samples in initial warm rolled state (Group 1, Table 3.2) had a typical deformed structure with elongated grains (fig. 3.2A) of austenite B2 phase (fig. 3.2C). TEM revealed increased dislocation density in these samples (fig. 3.4B).

Samples in Group 2 (Table 3.2) were subjected to vacuum annealing which led to the development of fully re-crystallized B2 phase structure (fig.3.3A and C). No dislocations or Ni-rich particles known to dissolve at temperatures higher than 600^0C (Otsuka et al., 1998) were identified in these samples (fig. 3.3B).

Samples of group 3 and 4 (Table 3.2) were aged after vacuum annealing at 500^0C and 450^0C which resulted in the formation of Ni_4Ti_3 and Ni_3Ti_2 particle sizes of 100-200 nm (fig. 3.4 A and B) and 25-30 nm (fig. 3.4 C and D) respectively.

Since the difference between A_f and the test temperature is known to affect the fatigue performance of Nitinol (Eggeler et al., 2004), in order to make the correct decision about the influence of the particle size, the time of aging at 500 and 450^0C differed slightly in order to provide the same A_f temperatures, which were measured to be 18-19^0C.

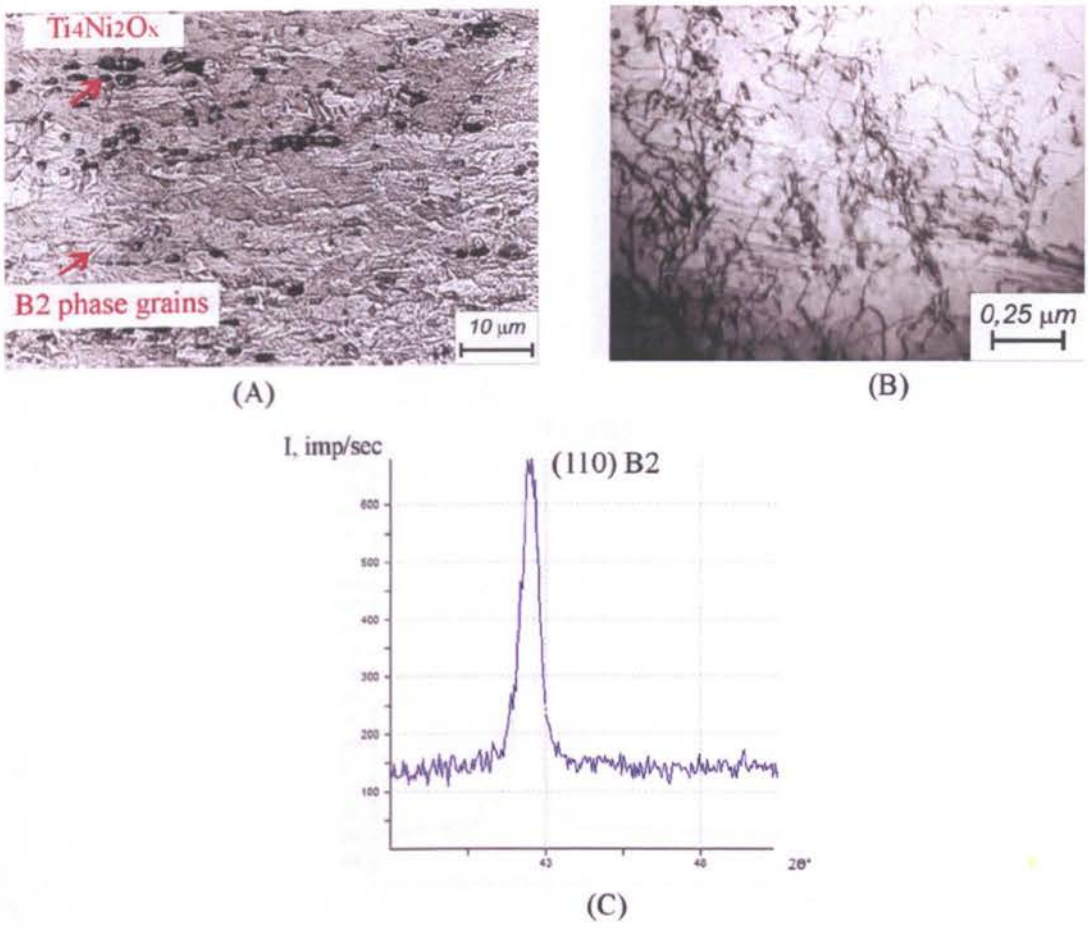

Figure 3.2. Microstructure of the Nitinol samples, Group 1 (ingot 1, warm rolling): (A) optical microscopy, (B) TEM, (C) X-ray analysis

Particles of $Ti_4Ni_2O_x$ phase were present in all samples of ingot 1. EDAX analysis revealed its chemical composition to consist of 60±2 wt.% of Ti and 40±2 wt.% of Ni. Despite the fact that no oxygen was revealed in their chemical composition, these particles still were named $Ti_4Ni_2O_x$ as oxygen has been reported to stimulate their formation (Chuprina et al., 2002) and the lower limit of oxygen detection by EDAX analysis is less than 5 wt.%.

No difference was found in the volume fraction and size of $Ti_4Ni_2O_x$ particles after various treatments of ingot 1 samples. The volume fraction and size of $Ti_4Ni_2O_x$ particles averaged for all four groups of Nitinol samples in ingot 1 was measured to be 15±1 % and size to be 1.5±0.5 μm.

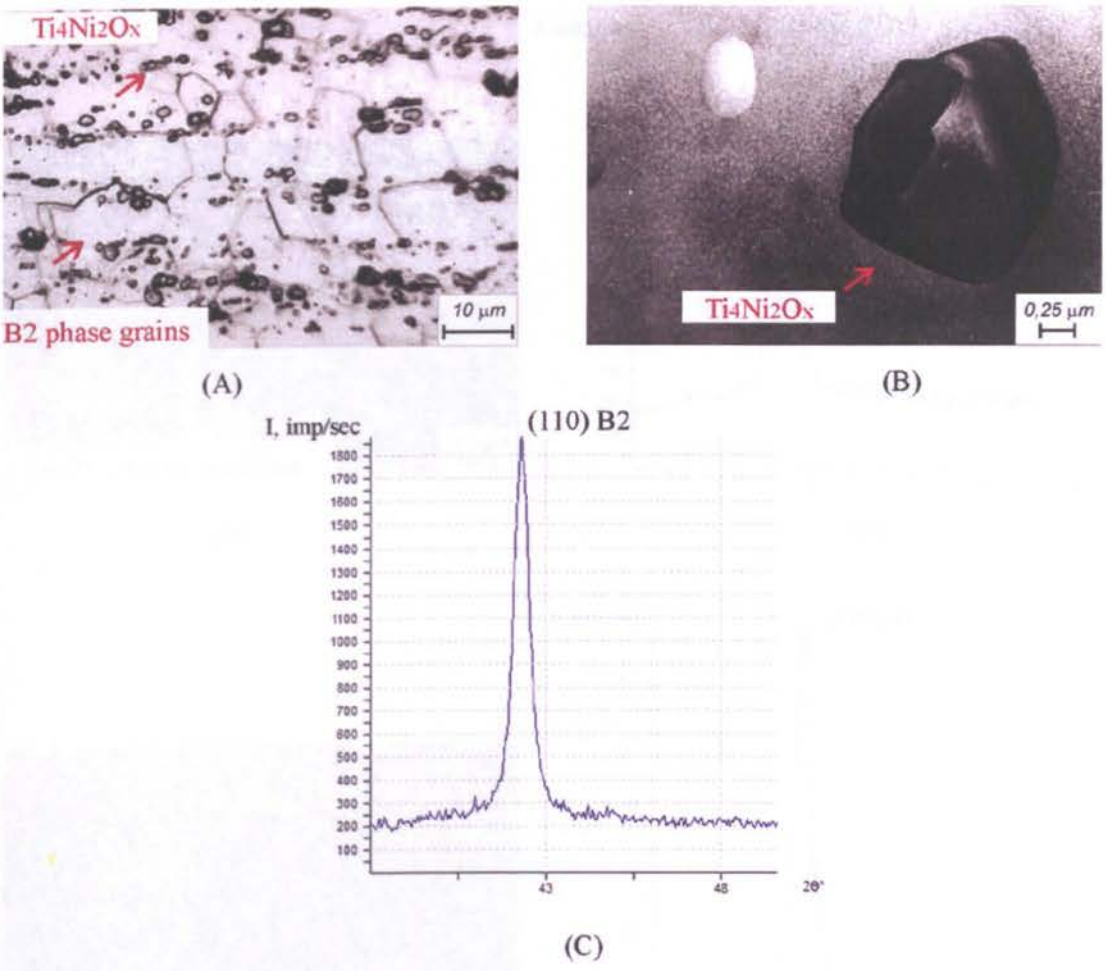

Figure 3.3. Microstructure of the Nitinol samples, Group 2 (ingot 1, vacuum annealing at 700^{0}C for 1 h: (A) optical microscopy, (B) TEM, (C) X-ray analysis

Ingot 2

The influence of the volume fraction of $Ti_4Ni_2O_x$ particles was also investigated. The samples from ingots 1 and 2 which differed in oxygen content in the alloy (ingot 1 had 0.17 wt.% and ingot 2 only 0.013wt.%) were compared. Before testing the samples were subjected to vacuum annealing at 700^{0}C for 1 h and subsequent aging at 500^{0}C (Group 3 and 5 respectively, Table 3.2). The microstructure and X-ray analysis of samples made from ingot 2 is given in Figure 3.5. The average size of $Ti_4Ni_2O_x$ particles in ingot 2 was 1.5±0.5 microns. The volume fraction was 6±1.5%.

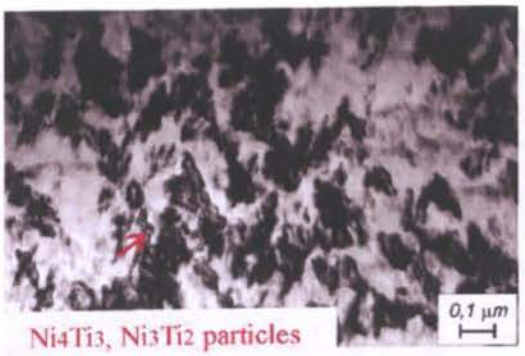

(A)

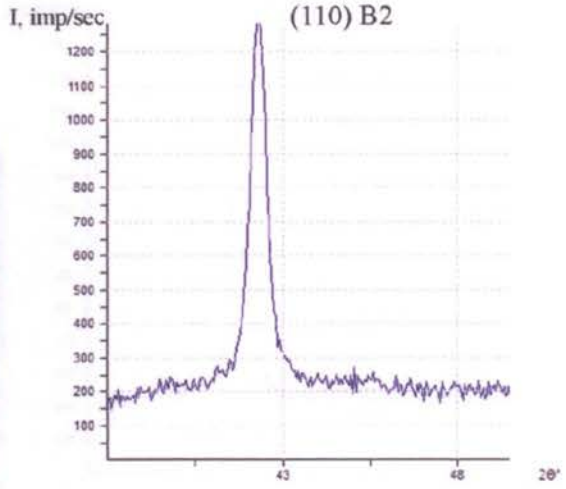

(B)

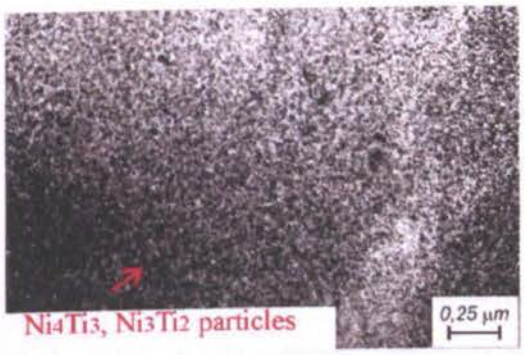

(C)

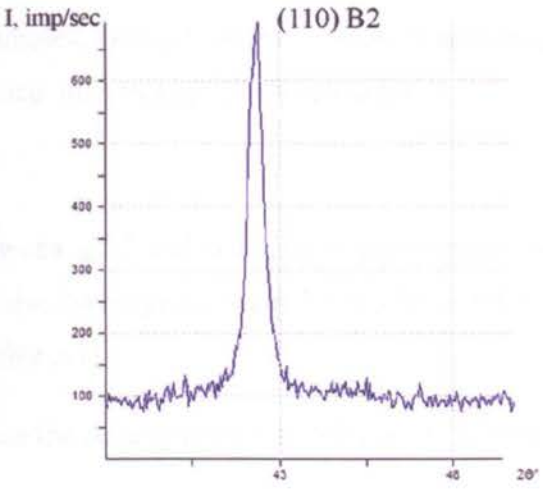

(D)

Figure 3.4. Microstructure of the Nitinol samples: (A) TEM, (B) X-ray analysis for Group 3 (ingot 1, vacuum annealing at 700^0C for 1 h and aging at 500^0C; (C) TEM, (D) X-ray analysis for Group 4 (ingot 1, vacuum annealing at 700^0C for 1 h and aging at 450^0C)

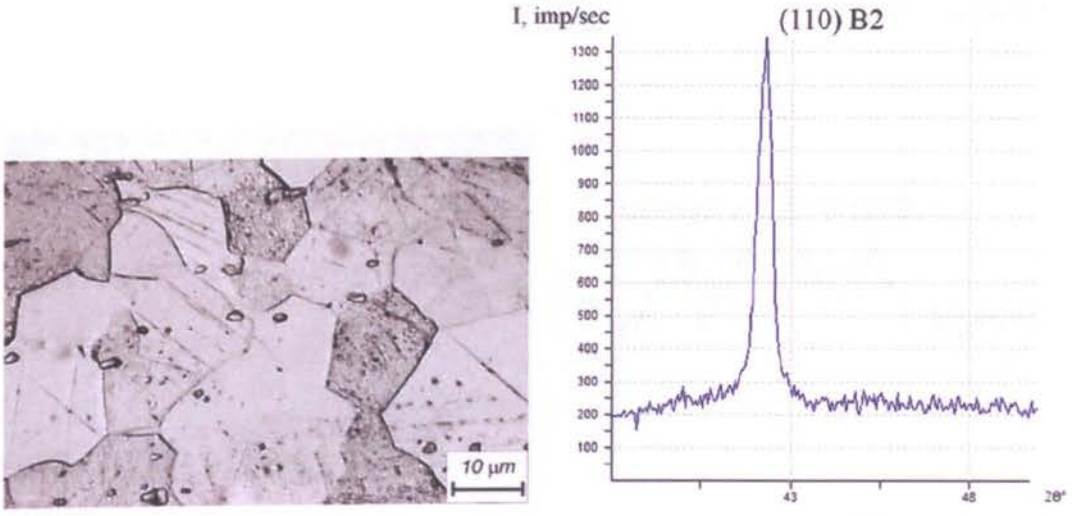

Figure 3.5. Microstructure of the Nitinol samples, Group 5 (ingot 2, vacuum annealing at 700^0C for 1 h and aging at 500^0C: (A) optical microscopy, (B) X-ray analysis

Ingot 3

In an attempt to establish correlation between $\varepsilon_c^{0.2}{}_r$ and the fatigue performance of Nitinol the wire samples from ingot 3 were also investigated. Ingot 3 had a lower Nickel content in comparison to ingots 1 and 2. (Table 3.1)

A reduction in Ni content is known to reduce the A_f temperature of NiTi alloys (Otsuka et.al., 1998) and thus decrease its σ_M stress.

These samples were annealed at 700^0C for 1 hour and aged at 500^0C; their microstructure and X-ray analysis are given in Figure 3.6. The phase composition consisted of re-crystallised B2 grains, B19' martensite, Ni-rich precipitates of 100-200 nm size and Ti-rich particles of $Ti_4Ni_2O_x$. The volume fraction and size of the $Ti_4Ni_2O_x$ particles was 5.5±1.5% and size 1.4±0.5 microns respectively.

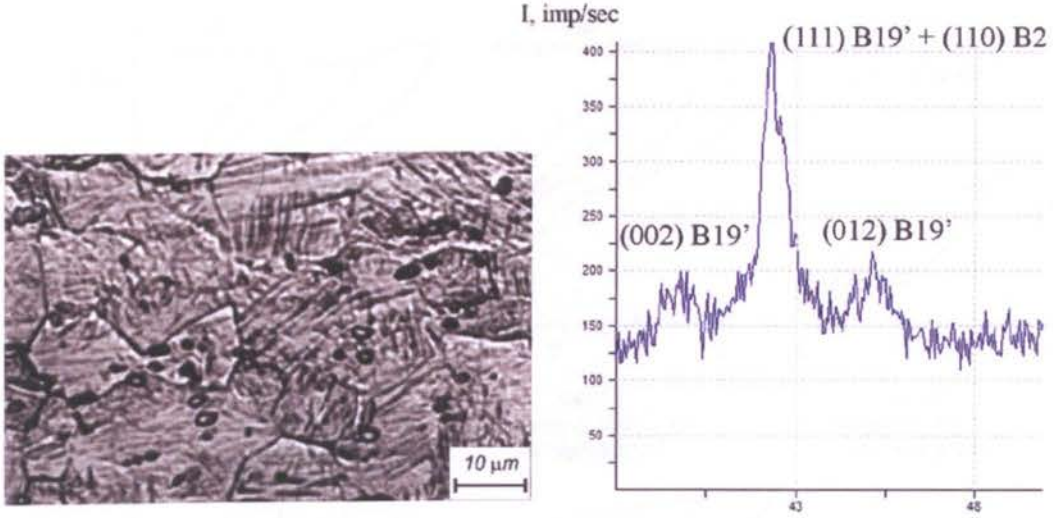

Figure 3.6. Microstructure of the Nitinol samples, Group 6 (ingot 3, vacuum annealing at 700^{0}C for 1 h and aging at 500^{0}C: (A) optical microscopy, (B) X-ray analysis

3.3.2. Characterization of mechanical behaviour and A_f temperature

Ingot 1

Stress-strain curves which characterize mechanical behaviour of Nitinol samples were obtained for three-point-bending at 21^{0}C on three samples for each structural state. Typical stress-strain curves are given in Figure 3.7.

All samples from ingot 1 demonstrated super-elastic behaviour. As can be seen, the upper plateau stress is relatively high for warm-rolled samples and for those after annealing at 700^{0}C; this is because of their low martensitic transformation temperatures. The martensite formation stress measured from these curves was 1000±40 and 850±30 MPa respectively. The values of parameter $\varepsilon_c^{0.2}$ were measured to be 2.8±0.5% and 3.0±0.5% for warm-rolled and vacuum annealed samples respectively (Table 3.3).

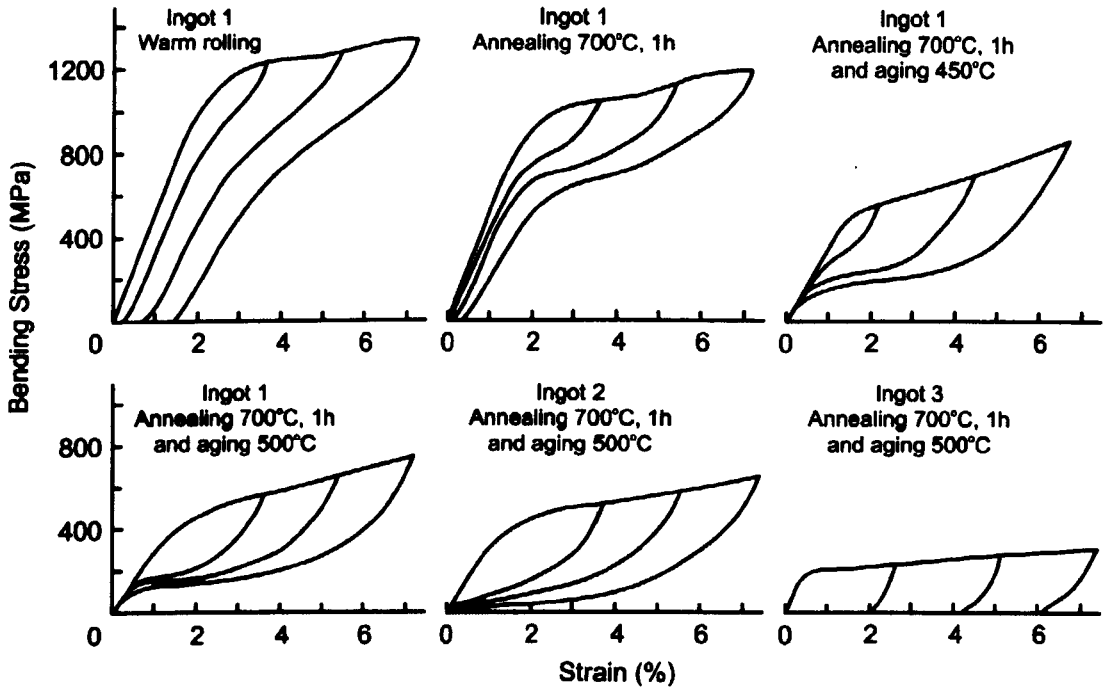

Figure 3.7. Stress-strain curves for Nitinol wire samples obtained by three point bending test at the temperature 21 ± 1°C.

Table 3.3. Elastic modulus, σ_M, shape recovery temperature and critical strain

Number	Shape recovery finish temperature, A_f, °C	E,GPa	σ_M, MPa	$\varepsilon_c^{0.2}$, %
Group 1.Ingot 1. Warm rolling	- 20±1	56±3	1000±40	2.8±0.5
Group 2. Ingot 1. V.A. 700°C,1h	- 30±1	54±2	850±30	3.0±0.5
Group 3. Ingot 1. V.A. 700°C,1h +aging 500°C	18±1	30±1.5	360±18	6.0±0.5
Group 4. Ingot 1. V.A. 700°C,1h +aging 450°C	19±1	36±1.5	420±20	5.5±0.5
Group 5. Ingot 2. V.A. 700°C,1h +aging 500°C	18±1	30±1	320±15	5.5±0.5
Group 6. Ingot 3. V.A. 700°C,1h +aging 500°C	46±1	42±1	150±10	8.5±0.5

It might be assumed that despite the lower σ_M values for the Nitinol samples after vacuum annealing, the solution of Ni-rich precipitates results in a decrease in the dislocation slip stresses as well, thus making the strain which these samples can accumulate by a martensitic mechanism equal to that for samples after warm rolling.

Much lower martensite formation stresses, equal to 360±18 MPa and 420±20 MPa, were observed for samples subjected to aging at 500 and 450^{0}C respectively. This reduction is caused by the decrease in Ni content in the B2 phase and the increase in the A_f temperatures (Otsuka et. al., 1998). The parameter $\varepsilon_c^{0.2}_r$ was measured to be 6.0±0.5% and 5.5±0.5% after aging at 500 and 450^{0}C respectively. Although the values of σ_M are lower, in the case of aging at 500^{0}C, the slip dislocation stress is also lower because of the larger size of Ni-rich precipitates. However, it should be noted that $\varepsilon_c^{0.2}_r$ after both aging schemes is twice that of samples in the warm-rolled or annealed condition.

Temperature A_f was measured to be -20±1^{0}C after warm rolling, -30±1^{0}C after vacuum annealing at 700^{0}C. Aging increased the A_f temperature to 18±1^{0}C and 19±1^{0}C after treatment at 500 and 450^{0}C respectively.

Ingot 2

Ingot 2 was subjected to vacuum annealing and aging at 500^{0}C. Time of aging for ingot 2 was adjusted in order to get equal A_f temperatures and $\varepsilon_c^{0.2}_r$ parameters with Ingot 1 subjected to the same heat treatment. The mechanical behaviour of these samples was very similar to that of ingot 1 which had been subjected to the same thermal treatment and $\varepsilon_c^{0.2}_r$ was measured to be 5.5±0.5%. The A_f temperature was 18±1^{0}C (Table 3.3).

Ingot 3

As expected, samples from ingot 3 had the lowest σ_M stress which was found to be 150±10 MPa and had the highest value of $\varepsilon_c^{0.2}_r$ equal to 8.5±0.5.

The A_f temperature of these samples was 46±1^{0}C (Table 3.3).

3.3.3. Fatigue test results

The results of the fatigue tests of the ingot 1 samples are presented in Figure 3.8. and partly summarized in Table 3.2 (for ε_a=4%; 2.5% and 1%). Comparison of the number of cycles to failure for the samples tested at strain amplitude was higher than 1.5% using parametric T-test revealed no statistically significant difference neither between warm rolled and vacuum annealed samples (for which $\varepsilon_c^{0.2}{}_r$ was 2.8-3.0%) nor between samples aged at 450^{0}C and 500^{0}C (for which $\varepsilon_c^{0.2}{}_r$ was 5.5-6%). However, the number of cycles to failure of the aged samples which had higher $\varepsilon_c^{0.2}{}_r$ values was also about 3 times higher (Table 3.4). This demonstrates the presence of a correlation between $\varepsilon_c^{0.2}{}_r$ and the low-cycle fatigue behaviour of Nitinol.

Comparison of the number of cycles to failure for the samples tested at 1.5 and 1% strain amplitudes demonstrated no correlation with $\varepsilon_c^{0.2}{}_r$ (Table 3.4). It was noted that for tests carried out at low amplitudes the samples which had nano-size precipitations of Ni-rich Ni_4Ti_3 and Ni_3Ti_2 particles (up to 30 nm), or which had increased dislocation density as a result of after warm rolling , demonstrated better fatigue resistance.

Ingot 2

The results of the fatigue tests (fig. 3.7C and E and in Table 3.4) demonstrate no statistically significant difference in the high-amplitude fatigue resistance, indicating that a change of oxygen content in the alloy from 0.17 wt.% to 0.013wt.% does not affect the high-amplitude fatigue resistance of Nitinol, provided their $\varepsilon_c^{0.2}{}_r$ parameters are kept the same.

It was also noted that a decrease in the $Ti_4Ni_2O_x$ particle volume fraction improved the low-amplitude fatigue resistance of Nitinol (Table 3.4).

Ingot 3

Comparison of the fatigue behaviour of samples made from ingot 3 (fig. 3.7F and Table 3.4) revealed that increasing $\varepsilon_c^{0.2}{}_r$ up to 8.5% further improves high-amplitude fatigue resistance of Nitinol (Table 3.4). However as before, no correlation was observed regarding low-amplitude fatigue. Specifically, at 1% strain amplitude the fatigue resistance was similar to that of samples from ingot 2, possibly due to the similarity in volume fraction and size of the $Ti_4Ni_2O_x$ particles which is probably due to the comparable oxygen content and equal size and volume fraction of Ni-rich precipitates in both of these alloys.

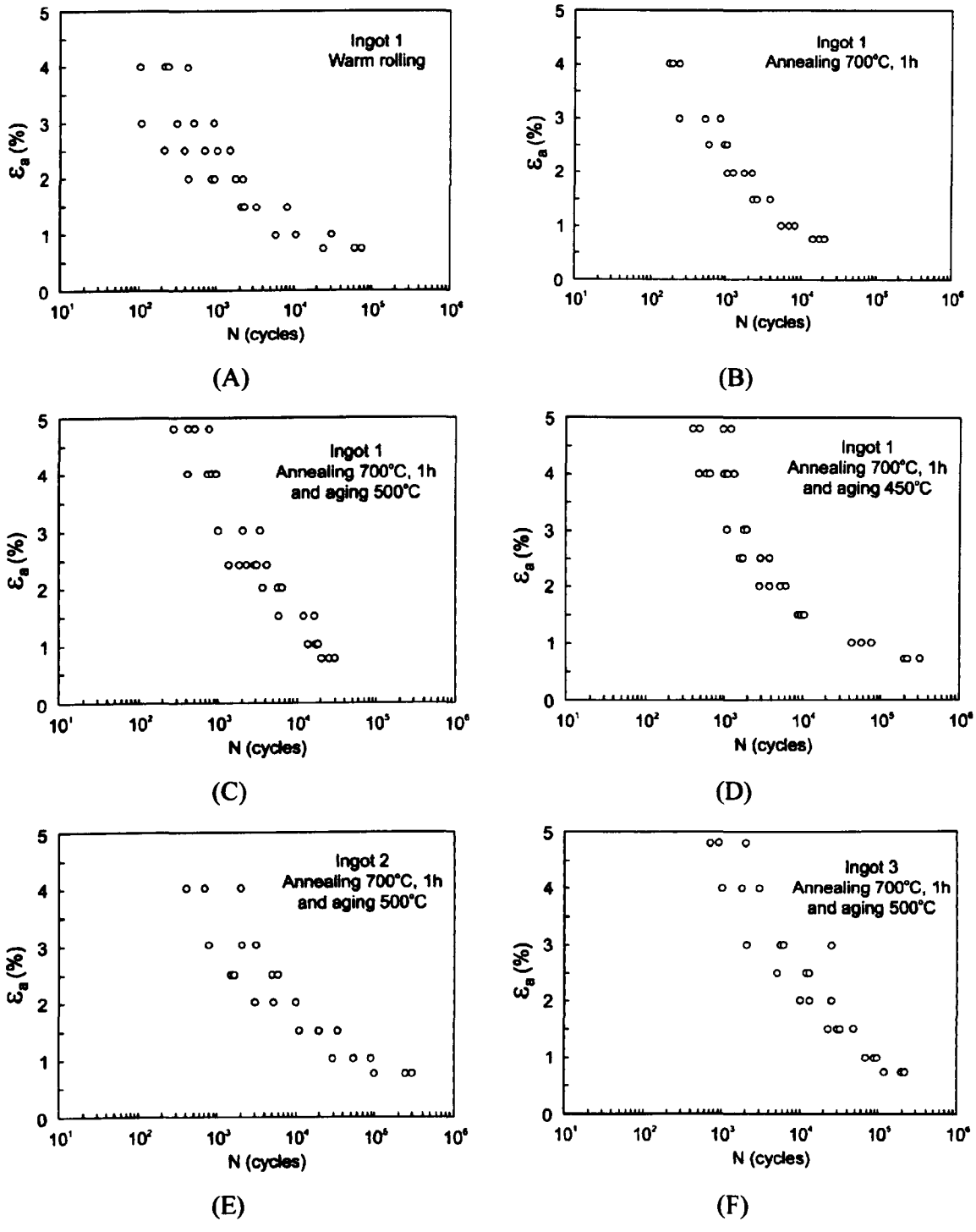

Figure 3.8. Number of cycles to fatigue failure plotted against applied strain amplitude (ε_a) for Nitinol in various structural states.

Table 3.4. Influence of Nitinol microstructure on the strain-controlled fatigue behaviour

Sample	$\varepsilon_c^{0.2}{}_r$,%	N, number of cycles to failure		
		ε_a=4%	ε_a=2.5%	ε_a=1%
Group 1.Ingot 1. Warm rolling	2.8±0.5	250±115	776±465	53,233±21,593
Group 2. Ingot 1. V.A. 700^{0}C,1h	3.0±0.5	204±25	842±183	17,833±2,690
Group 3. Ingot 1. V.A. 700^{0}C,1h +aging 500^{0}C	6.0±0.5	693±190	2,592±887	25,041±4,031
Group 4. Ingot 1. V.A. 700^{0}C,1h +aging 450^{0}C	5.5±0.5	836±334	2,544±934	179,256±49,641
Group 5. Ingot 2. V.A. 700^{0}C,1h +aging 500^{0}C	5.5±0.5	896±485	3,162±1,488	217,047±85,062
Group 6. Ingot 3. V.A. 700^{0}C,1h +aging 500^{0}C	8.5±0.5	1,939±822	9,356±3400	190,154±53,577

3.3.4. Scanning electron microscopy of samples after fatigue tests

Scanning electron microscopy images of the surface of Nitinol wire samples after fatigue tests at high amplitudes are given in Figure. 3.9. Development of multiple fatigue cracks across the longitudinal axis of wire before the fatigue failure was observed, which indicated that speed of fatigue cracks propagation will play important role in high amplitude zone. It can be seen that the number and width of the fatigue cracks on Nitinol after both schemes of aging ($\varepsilon_c^{0.2}{}_r$ is 5.5-6%), are lower in comparison with Nitinol samples after annealing or warm rolling ($\varepsilon_c^{0.2}{}_r$ is 2.8-3.0%).

On the other hand, almost no surface cracks were observed on Nitinol after testing at low amplitude (fig. 3.10) which indicates that the fatigue resistance of Nitinol in this case will depend on the fatigue crack initiation speed.

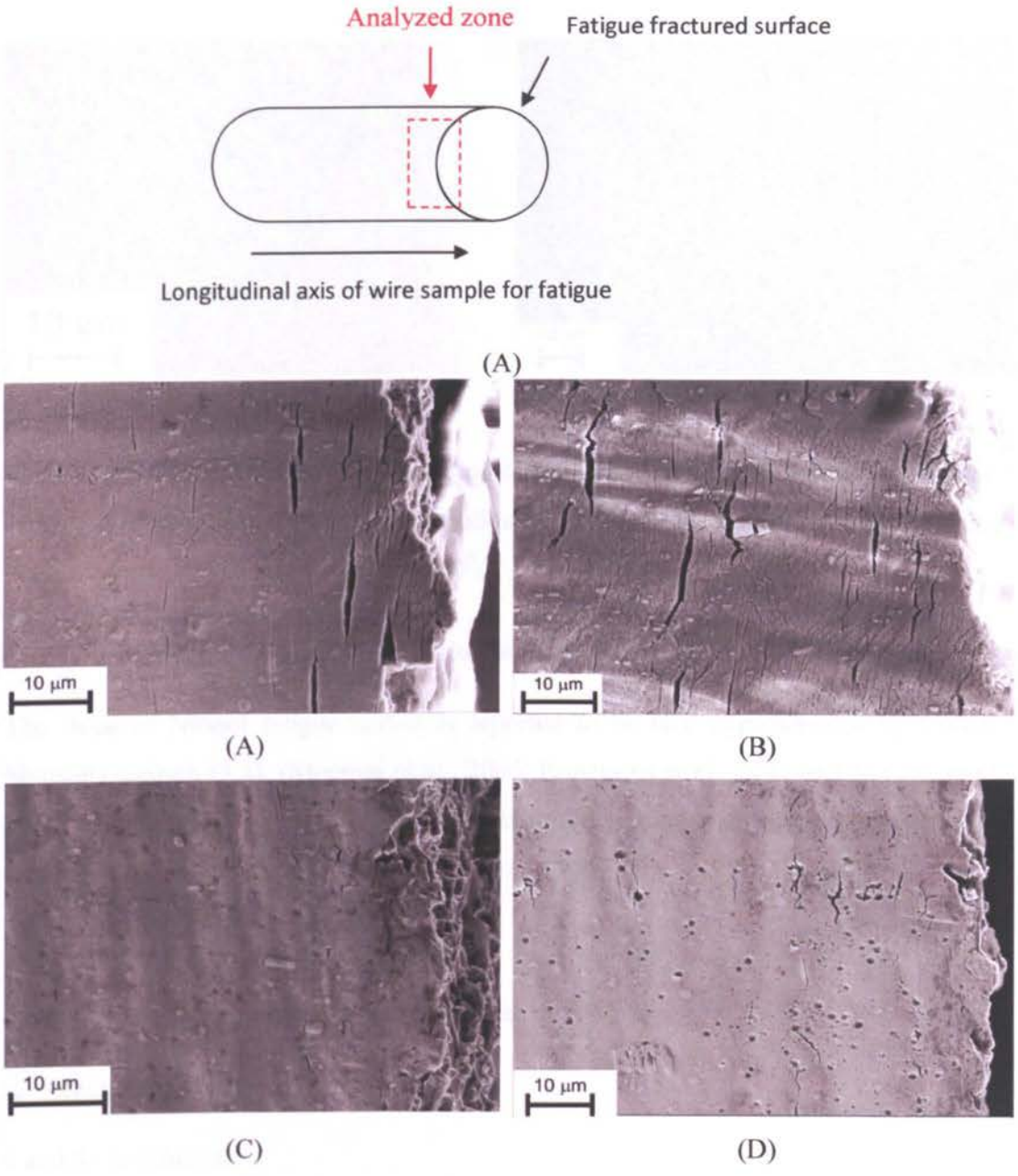

Figure 3.9. Scanning electron microscopy of the surface of Nitinol wire samples made from ingot 1 after fatigue tests at strain amplitude ε_a=4% : (A) Group 1:, warm rolling; (B) Group 2: vacuum annealing 700^{0}C, 1 hour; (C) Group 3: vacuum 700^{0}C, 1 hour and aging at 500^{0}C; (D) Group 4: vacuum 700^{0}C, 1 hour and aging at 450^{0}C

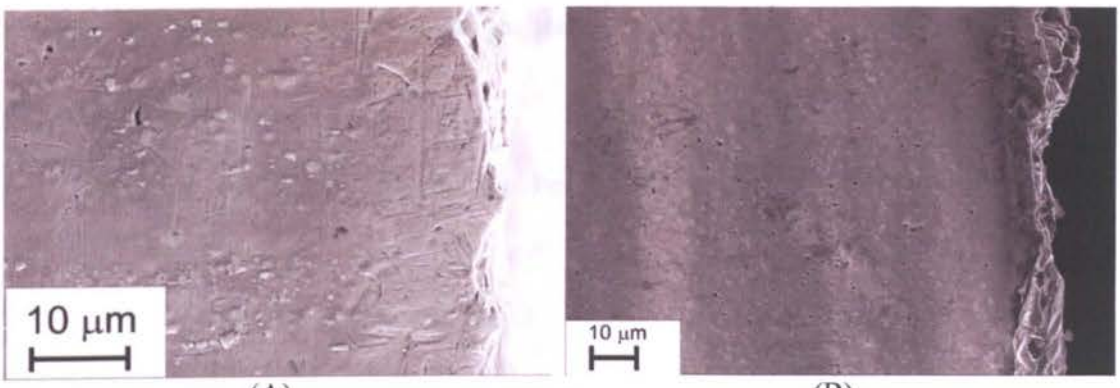

(A) (B)

Figure 3.10. Scanning electron microscopy of the surface of Nitinol wire samples made of ingot 1 after fatigue tests at strain amplitude ε_a=1% : (A) Group 2: vacuum annealing 700^{0}C, 1 hour; (B) Group 4: vacuum 700^{0}C, 1 hour and aging at 450^{0}C

3.3.5. Modified Coffin-Manson equation with structure dependent coefficients

The slope of Nitinol fatigue curves is reported to be well approximated by Coffin-Manson equation (3.2), (Moumni et al., 2005, Runciman et al., 2011 and Maletta et al. 2012) despite the fact that this equation was initially developed to relate plastic strain amplitude to lifetime (Coffin, 1959 & Manson, 1966).

$$N = \alpha\,(1/\varepsilon_a)^{\beta} \qquad (3.2),$$

where N – number of cycles to fatigue failure;

ε_a –strain amplitude;

α and β - coefficients

Since statistically significant differences in the number of cycles to fatigue failure was observed for Nitinol samples having various $\varepsilon_c^{0.2}_r$ values, a modified Coffin-Manson equation may be applied where both coefficients are structure dependent.

Critical strain $\varepsilon_c^{0.2}_r$ being the first coefficient:

$$N = \varepsilon_c^{0.2}_r\,(1/\varepsilon_a)^{\beta}, \qquad (3.3)$$

where N – number of cycles to failure;

$\varepsilon_c^{0.2}{}_r$ – critical deformation of the sample measured for a given microstructure of Nitinol measured at the temperature of the fatigue tests;

ε_a – strain amplitude;

β – empirical coefficient which can be calculated based on the bending test measurements, i.e.:

$$\beta = 3.3\,(1 - 11\,(\sigma_M / E)), \qquad (3.4)$$

where σ_M - stress of the martensitic re-orientation or its stress-induced formation;

E – elastic modulus (deduced from the slope of the rectilinear part of stress-strain curve).

σ_M and E were determined from stress-strain curves obtained during the bending test measurements (fig. 3.7) and are given in Table 3.3. The temperature of the tests was the same as that for the fatigue experiments.

Calculated values of β coefficients, together with $\varepsilon_c^{0.2}{}_r$ are given in Table 3.5.

Using the modified Coffin-Manson equation (3.3), curves were plotted as solid lines and compared with the experimental data (dots) as shown in Figure 3.11.

As seen in Figure 3.11, there is good agreement between the calculated curve (based on the newly proposed Coffin-Manson equation) and the experimental data (dots) for high amplitude fatigue testing (at strains $\varepsilon_a \geq 2\%$).

At the same time rather less correlation is observed in the region of low strain amplitudes ($\varepsilon_a \leq 1.0\text{-}1.5\%$).

Table 3.5 Coefficients for the suggested Coffin-Manson equation

Sample	$\varepsilon_c^{0.2}{}_r$,%	β
Group 1.Ingot 1. Warm rolling	2.8	2.65
Group 2. Ingot 1. V.A. 700^{0}C,1h	3.0	2.73
Group 3. Ingot 1. V.A. 700^{0}C,1h +aging 500^{0}C	6.0	2.86
Group 4. Ingot 1. V.A. 700^{0}C,1h +aging 450^{0}C	5.5	2.87
Group 5. Ingot 2. V.A. 700^{0}C,1h +aging 500^{0}C	5.5	2.91
Group 6. Ingot 3. V.A. 700^{0}C,1h +aging 500^{0}C	8.5	3.17

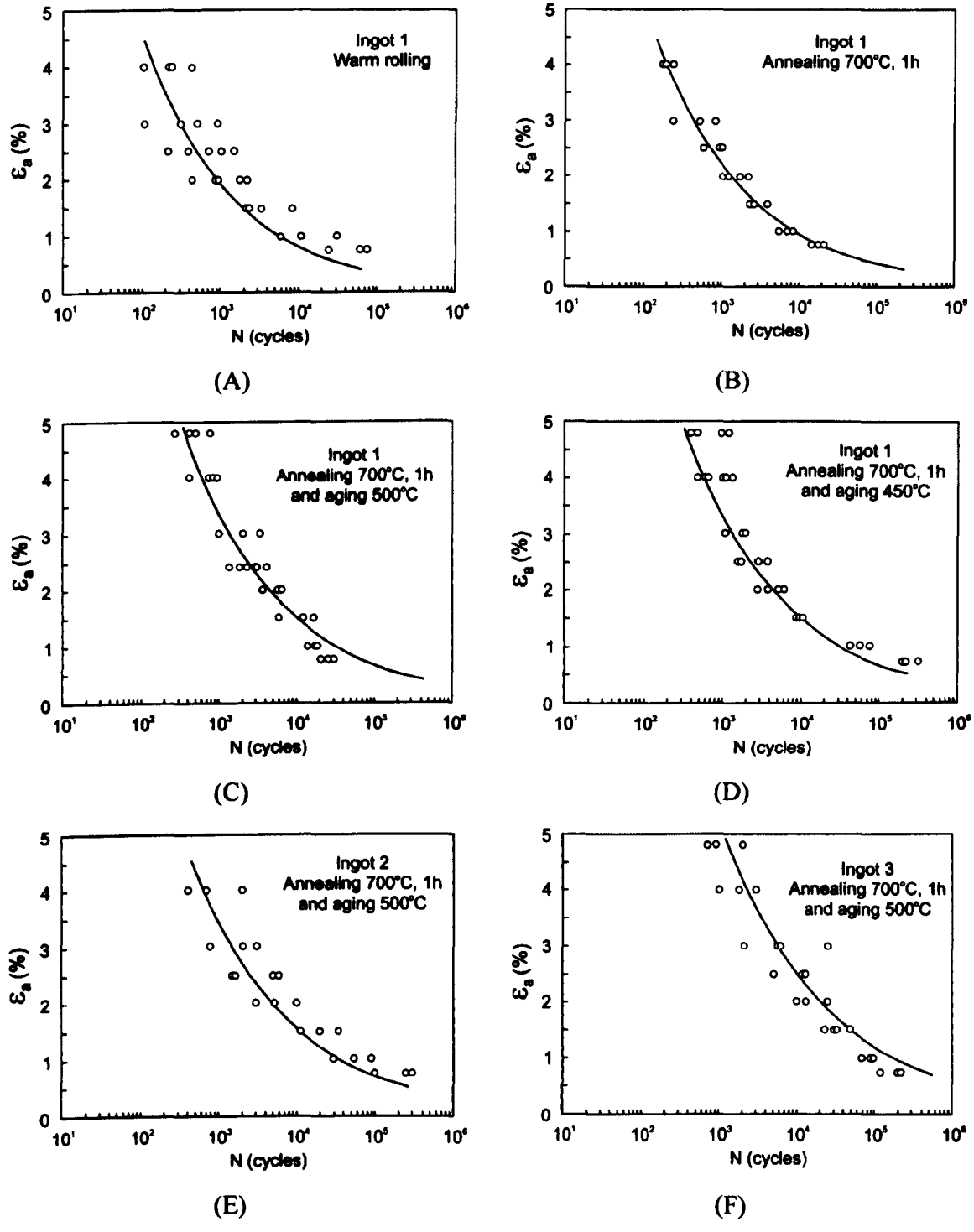

Figure 3.11. Number of cycles to failure (dots) plotted against applied strain amplitude (ε_a). Solid lines are calculated according to the newly proposed modified Coffin-Manson equation $N = \varepsilon_c^{0.2}{}_r (1/\varepsilon_a)^{\beta}$, where $\varepsilon_c^{0.2}{}_r$ – the critical degree of deformation, ε_a - the strain amplitude and β - empirical coefficient; $\beta = 3.3\ (1 - 11\ (\sigma_M / E))$.

3.4. DISCUSSION

Deformation accumulated by Nitinol at loading involves linear-elastic deformation, martensitic mechanism deformation (which is realized by stress-induced formation or re-orientation of martensitic crystals), and a dislocation slip deformation mechanism. As discussed above, in previous works (Melton et al., 1979, Heckmann et al., 2002) it was assumed that the improvement of Nitinol fatigue resistance after certain schemes of thermo-mechanical processing could be connected to the increase in the strain which Nitinol can accommodate by martensitic mechanism following these treatments. Accordingly, the higher the amount of deformation Nitinol can accommodate during fatigue cyclic loading by a martensitic mechanism, the better the fatigue performance should be. In other words the creation of the structure which provides the maximum difference between the stress of the martensite re-orientation, or its stress-induced formation (σ_M), and the stress at which the dislocation slip mechanism of deformation starts (σ_{slip}), will provide the best fatigue resistance of Nitinol. However, since the measurement of σ_{slip} is difficult such considerations were only qualitative.

In previous work it was assumed that for a given microstructural state, at a given temperature, the degree of deformation which Nitinol can accumulate by a martensitic mechanism can be estimated by measurement of the critical deformation strain (ε_{cr}). Critical strain (ε_{cr}) is defined as the maximal strain which a sample can completely recover after unloading and heating to a temperature higher than A_f. The tolerance for non-recovered strain in the sample upon unloading and heating was considered to be 0.2% ($\varepsilon_c^{0.2}_r$). Strains lower than critical are realized by the martensitic reorientation or its stress-induced formation mechanism. If the applied strain is higher than ($\varepsilon_c^{0.2}_r$), the sample will have non-recovered strain after unloading and heating. Since this non-recovered strain is caused by slip, critical strain characterises the transition from the martensitic to the slip deformation mechanism (Kollerov et al., 2008).

The results of these experiments have revealed that there is a statistically significant difference in the number of cycles to failure for Nitinol samples which have different $\varepsilon_c^{0.2}_r$ values in case of high amplitude fatigue testing. It was observed that higher $\varepsilon_c^{0.2}_r$ values improved the fatigue resistance of Nitinol. The presence of multiple fatigue cracks on Nitinol wire samples after testing at high strain amplitudes indicates that the fatigue resistance of Nitinol strongly depends on the fatigue crack propagation rate in

this case. The number and width of the fatigue cracks on Nitinol wire surfaces after both schemes of aging ($\varepsilon_c^{0.2}{}_r$ is 5.5-6%), are lower in comparison with Nitinol samples after annealing or warm rolling ($\varepsilon_c^{0.2}{}_r$ is 2.8-3.0%), indicating that Nitinol samples tested at high amplitudes have a lower rate of fatigue crack initiation and propagation for higher $\varepsilon_c^{0.2}{}_r$ values..

However no correlation between $\varepsilon_c^{0.2}{}_r$ parameter and fatigue performance of Nitinol was observed for low amplitude fatigue testing. In these testNitinol samples with nanosize Ni-rich particle precipitation or increased dislocation density, or a lower volume fraction of $Ti_4Ni_2O_x$ particles demonstrated better fatigue performance.

The absence of cracks on Nitinol surfaces for tests carried out at low amplitude indicates the importance of fatigue crack initiation speed. It could be assumed that when tests are carried out at low strain amplitudes the input of deformation occurred by the martensitic mechanism is comparable with that occurring by the elastic mechanism; in other words the Nitinol behaviour becomes more similar to structural metal materials which do not have a martensite mechanism of deformation.

The improved fatigue performance at low strain amplitudes for Nitinol samples containing nanosize Ni-rich particle precipitates or increased dislocation density can be explained by the development of dislocation activity during fatigue testing of specimens containing larger particles and the suppression of dislocation activity in specimens containing nano-size precipitates of Ni-rich Ni_4Ti_3 and Ni_3Ti_2. This was observed by Gall and Maier (2002), who found that the dislocation activity in Nitinol single-crystals was suppressed by nano-size (10 nm) Ni_4Ti_3 and Ni_3Ti_2 particles, whereas larger particles (500 nm) did not have any effect.

It might be assumed that the dislocation activity may result in the development of micro-plastic deformation and thus stimulation of fatigue crack initiation. Accordingly, it could be postulated that increased dislocation density may have the same effect as nano-size precipitates. Since the initiation of fatigue cracks is normally at the surface and as there are difficulties with TEM observations of surface regions, further work devoted to finite element analysis of the stress fields near different sizes of Ni-rich precipitates may produce further information on their effect on crack initiation which would be useful.

Analysis of literature on the role of the Ti-rich ($Ti_4Ni_2O_x$) particles on the Nitinol fatigue behaviour reveals contradictory opinions (Reinoehl et al., 2000, Patel et al. 2006 and Morgan et al., 2006). A possible explanation could be that the increased oxygen content might stimulate particle formation, thus resulting in a decrease in the titanium content of the B2 phase thus changing of the A_f temperatures (Chuprina et al., 2002 and Otsuka et al., 1998). It is known that differences in the temperature at which the fatigue tests are carried out (t_{test}) and the A_f temperature (t_{test} - A_f) of the Nitinol sample significantly affects the fatigue results (Eggeler et al., 2004). Accordingly when Nitinol samples have different A_f temperatures, it is difficult to separate the effect of the volume fraction of $Ti_4Ni_2O_x$ particles from the (t_{test} - A_f) temperature difference effects.

In this study the samples were heat treated in order to achieve equal A_f temperatures. The results of the fatigue tests demonstrate no significant differences for high amplitude fatigue resistance, indicating that a change of oxygen content in the alloy from 0.17 wt.% to 0.013wt.% does not affect high amplitude fatigue resistance of Nitinol. However, a decrease in the $Ti_4Ni_2O_x$ particles volume fraction improved the low amplitude fatigue resistance of Nitinol.

Recent investigations devoted to finite element analysis of local stress fields near $Ti_4Ni_2O_x$ particles (Cox et al., 2013) revealed increased local stresses near these particles. As a result, lower volume fractions of these particles decrease the driving force for fatigue crack initiation and thus improve the fatigue behavior of Nitinol in fatigue tests at low amplitudes.

The analysis of experimental fatigue curves by several researchers (Moumni et al., 2005, Runciman et al., 2011 and Maletta et al. 2012) revealed that the slope of the fatigue curves for Nitinol may be approximated by the Coffin-Manson equation (Coffin, 1959 & Manson, 1966), despite the fact that this equation was initially developed to relate plastic strain amplitude to lifetime. Runciman et al., (2011) have modified this equation in order to predict fatigue behaviour of Nitinol in multi-axial conditions. However, such equations are obtained for certain structural states of the material and the influence of structure modifications was not considered.

From the work carried out in this thesis a modified Coffin-Manson equation has been developed which has structure dependent coefficients. Critical strain was the first coefficient and an empirical equation was found for β coefficient in equation 3.3. Good

agreement between the calculated curve (based on the newly proposed Coffin-Manson equation) and the experimental data for high strain amplitude fatigue testing (at strains $\varepsilon_a \geq 2\%$) was observed. At the same time less correlation was observed in the region of low strain amplitudes ($\varepsilon_a \leq 1.0\text{-}1.5\%$).

Similar changes in the slope of experimental fatigue curve at strain amplitudes between 1-1.5% were also observed by Pelton et al., 2008 and Tolomeo et al., 2000 and could be explained by the relative increase in the elastic component of deformation compared with that due to martensitic mechanisms.

Thus, it has been established that the influence of the microstructure of Nitinol on its fatigue behaviour and the modified Coffin-Manson equation proposed provides a good prediction of the fatigue behaviour of Nitinol subjected to high amplitude ($\varepsilon_a \geq 2\%$) fatigue testing. It was revealed that the precipitation of nano-size Ni-rich particles, an increased dislocation density and decrease inthe $Ti_4Ni_2O_x$ volume fraction, may improve low amplitude fatigue performance.

3.5. CONCLUSIONS

1. It has been shown that under high amplitude conditions ($\varepsilon_a \geq 2\%$) the strain-controlled fatigue resistance of Nitinol may be improved by creating a microstructure which increases the deformation element resulting from martensitic mechanisms. It is proposed that this element can be estimated by measuring the parameter $\varepsilon_c^{0.2}{}_r$, as the maximal strain which sample can completely recover after unloading and heating to the temperature higher than A_f.

2. A modified Coffin-Manson equation is proposed for describing and predicting the strain-controlled fatigue behaviour in the range of high strain amplitudes ($\varepsilon_a \geq 2\%$), where $\varepsilon_c^{0.2}{}_r$ serves as one of the coefficients, while another coefficient may be deducted from the empirical relation based on bend test measurements. The correlation between experimental data and predictions based on this equation in this region is good.

3. No correlation between the strain-controlled fatigue resistance of Nitinol and $\varepsilon_c^{0.2}{}_r$ parameter was observed for the low amplitude conditions ($\varepsilon_a \leq 1.5\%$). In this case Nitinol fatigue performance may be improved by nanosize Ni-rich particle precipitation, the creation of increased dislocation density, or by decreasing the $Ti_4Ni_2O_x$ volume fraction.

CHAPTER 4

WEAR RESISTANCE OF NITINOL AND TITANIUM ALLOY (TI6AL4V) IN A SIMULATED BODY ENVIRONMENT

4.1. INTRODUCTION

Analysis of retrieved guided-growth sliding LSZ-4D devices made of titanium alloy (Chapter II) revealed prominent wear scars and increasing metal ion content in patients' blood with 25% of them having clinical complications such as seroma and fistula formation in the lumbar part of the spine, over the implants, as a result of metallosis. The specific amounts of wear debris generated by spinal implants depends on instrumentation design, number of fixtures, level of installation, patient activity and also on the wear resistance of the materials used.

Traditional metallic materials including Ti, CoCr alloys and SS steels are commonly used for spinal instrumentation. Ti alloys are considered to be the most biocompatible, however these have lower wear resistance compared to CoCr and SS and can produce wear debris when used as articulating surfaces (McKellop et al., 2001). However, the toxicity of cobalt and chromium ions (Campbell & Estey, 2013) and possible fretting-corrosion damage (Yoon et al., 2013) with titanium counterparts is a main disadvantage of CoCr rods. SS have lower corrosion resistance compared with Ti alloys (Park, 2003). Villarraga et al., 2006 reported both corrosion and wear marks on retrieved spinal instrumentation made of SS, while only wear damage was seen on titanium components. Nitinol, one of the prospective materials for the rods in spinal instrumentation for treating scoliosis (Yoshihara, 2013) has good corrosion properties which are better compared with SS (Es-Souni et al., 2005). It is reported not to be susceptible to galvanic corrosion when combined with Ti (Venugopalan & Trepanier, 2000).

However, Nitinol wear debris from articulation against titanium fixtures in sliding spinal devices can be the source of Ni ions. At the same time wear resistance of Nitinol is not completely understood and is reported to be from several to hundreds of times higher compared to Ti and 304 stainless and GGr15 steel (Zhang et al., 2009, Li et al., 2000, Linmao et. al. and Lui & Lee, 2009). However in most experiments Nitinol was predominantly tested against dissimilar materials like tungsten carbide and little is known about its wear behaviour in a body-simulated fluid environment when sliding against Ti which is the predominant material used for fixtures.

Consequently, the purpose of this part of the research and the focus of this Chapter was to investigate wear resistance of Nitinol – Ti6Al4V friction combination in a biological environment using in vitro pin-on-disk wear test and compare this with Ti6Al4V - Ti6Al4V and CoCr – Ti6Al4V combinations which are commonly used for scoliosis instrumentation.

The aims were:

1. **To evaluate volume wear loss of Nitinol, Ti6Al4V and CoCr alloys tested against Ti6Al4V using pin-on-disk in the biological environment;**
2. **To establish the mechanisms of wear damage of Nitinol, Titanium and CoCr during pin-on-disk wear tests;**
3. **To evaluate shape, size and chemical composition of wear debris produced by Nitinol – Ti6Al4V, Ti6Al4V - Ti6Al4V and CoCr – Ti6Al4V friction combinations produced in the pin-on-disk wear tests**

4.2 MATERIALS AND METHODS

4.2.1. Materials

In-vitro wear tests were conducted using a pin-on-disc methodology according to ASTM G99-05 which is often used for analysis of the wear resistance of various combinations of materials used in spinal device made of the optimal combinations of materials.

Pins which were intended to simulate and compare the wear resistance of metal materials used for spinal rods manufacturing were made of Ti-55.8 wt.%Ni (Nitinol), titanium alloy Ti-5.8wt.% Al-3.9wt.%V (Ti6Al4V) and Cobalt Chromium alloy Co-27 wt.% Cr - 5wt.% Mo, 0.03 wt.% C (CoCr). All disks were made of titanium alloy (Ti6Al4V) as this alloy is commonly used for fixtures (Table 4.1). The diameter of pins was 5.5 mm, length 30 mm. Domes on the pins were rounded to 20 mm radius. The diameter of the disks was 40 mm and their height 5 mm. Figure 4.1 shows a photo of a typical pin and disk . Pins and disks made of Ti6Al4V and CoCr alloys were turned from hot rolled and annealed bars. Pins made of Nitinol were annealed in a vacuum at 700^0C for 1 h and subsequently aged at 450^0C to provide optimal fatigue resistance (Chapter 3). The temperature of shape recovery, measured by the free bending method according ASTM F2082, was A_f=37±1^{O}C. The surfaces of the pins and discs were ground and polished to a roughness of Ra= 0.04±0.01μm.

Table 4.1. Combinations of materials in pin-on-disk wear tests

	Pin Counter-part	Disk counter-part
1.	Ti6Al4V	Ti6Al4V
2.	Nitinol	Ti6Al4V
3.	CoCr	Ti6Al4V

Figure 4.1. Photo of disk and pin used in wear test

4.2.2. Methods

4.2.2.1. Scheme and parameters of pin-on-disk wear test

All wear tests were performed in diluted (30g/l of protein) calf serum (Sigma Aldrich), as required by ISO 18192 for the testing of spinal devices (artificial spinal disks) at $37\pm1^{O}C$. The frequency of reciprocation sliding was 1 Hz as recommended in the standards for the prevention of the serum overheating during the tests. During the test, disk counter-parts (fig.4.2) were fixed in containers with lubricant which in turn were mounted on a moving platform. Pins were motionless. This test provided reciprocation/sliding movement of discs against pins thus simulating reciprocation sliding of spinal rods against fixtures in growth-guided devices for scoliosis correction. The load on the pins, calculated from the previous literature data on the in-vivo measurements of bending moments encountered by spinal rods at various functional activities obtained by Rohlmann et.al. (2002), was 10N. The amplitude of reciprocation movement was 6 mm based on the average size of wear scars on the rods from sliding LSZ-4D device retrieved 1 year after the surgery (Chapter II).

Figure 4.2. Photo of pin-on-disk wear test for the in-vitro evaluation of wear resistance of Ti6Al4V – Ti6Al4V, Nitinol- Ti6Al4V and CoCr – Ti6Al4V friction combinations

4.2.2.2. Volume wear loss measurements

Volume wear loss (ΔV) of both counter-parts was determined after 0.2, 0.5 and 0.85 million cycles as $\Delta V=\Delta m/\rho$, where Δm - weight loss gravimetrically measured, grams and ρ – density of the material, g/mm^3. The number of tests for each condition was n=3. Gravimetric measurements and preparation of test specimens for this procedure were carried out according ISO 14242-2.

4.2.2.3. Wear scar analysis

Wear scar analysis was carried out using SEM and EDAX techniques and measurement of wear scars roughness (Ra parameter) as described in Chapter 2.

2.2.2.4. Analysis of wear particles

In order to analyse the size and shape of wear particles, serum was collected after 0.05; 0.2; 0.5 and 0.85 million cycles. After the test, 1 ml from each collection was sampled and mixed. The Procedure for particle isolation from bovine serum proteins and their subsequent preparation for SEM and EDAX analysis is described in Chapter II. The distribution of particle sizes was measured by analysing SEM images using Image Pro3

software (Nexis, Russia). A minimum of 50 particles were analysed for each friction combination as required by ISO 17853:2011.

2.2.2.5. Statistics

Methods of mathematical statistics were used to determine average values and deviations using SPSS 14.0 software.

4.3. RESULTS

4.3.1. Volume wear loss

Figure 4.3A demonstrates volume wear loss of Ti6Al4V (red), Nitinol (blue) and CoCr (yellow) pins tested against titanium disks against the number of cycles. Assuming linear wear, the volumetric loss of Ti6Al4V pins was 33±2mm^3 per 0.5 million cycles which is 100 greater compared to Nitinol and CoCr pins which were measured to be 0.15±0.02 and 0.1±0.01 mm^3 respectively per 0.5 million cycles (results repeated on an expanded scale in fig. 4.3B). Accordingly it can be seen that the wear of Nitinol and CoCr is comparable.

Nevertheless, wear resistance of disk counter-parts (fig. 4.3C) made of Ti6Al4V demonstrated small differences regardless of pin material and was measured to be 37±3, 25±2 and 20±2 mm^3 per 0.5 million cycles when tested against Ti6Al4V, Nitinol and CoCr pins respectively.

Photos of pins and disks after the wear tests (0.85 million cycles) are presented in figure 4.4.

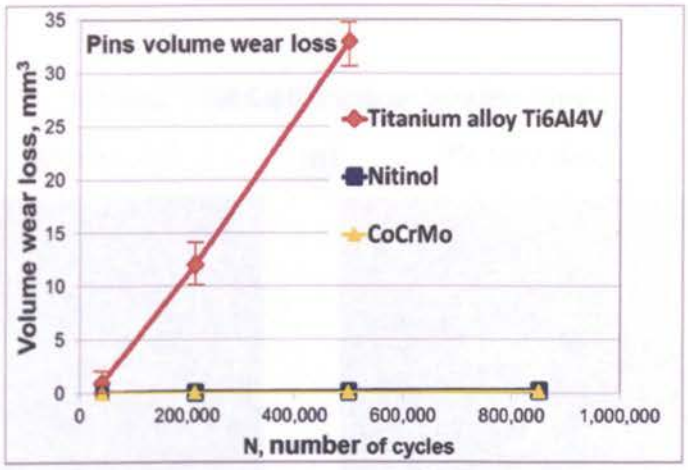

(A)

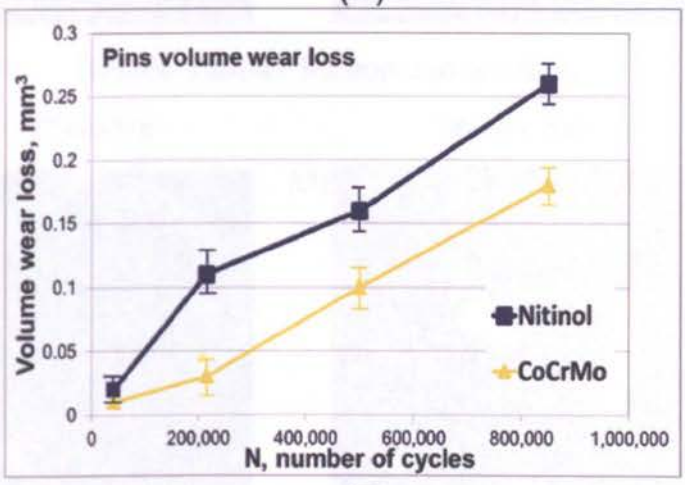

(B)

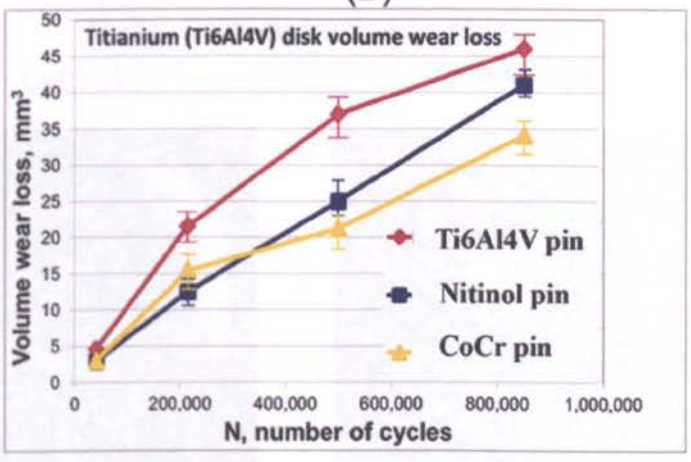

(C)

Figure 4.3. (A) Volume wear loss of Ti6Al4V, Nitinol and CoCr pins tested against Ti6Al4V disks in-vitro pin-on-disk; (B) detailed comparison revealed that volume wear loss of Nitinol pins is comparable to that of CoCr; (C) volume wear loss of titanium disks counter-parts remains high regardless of the pin material.

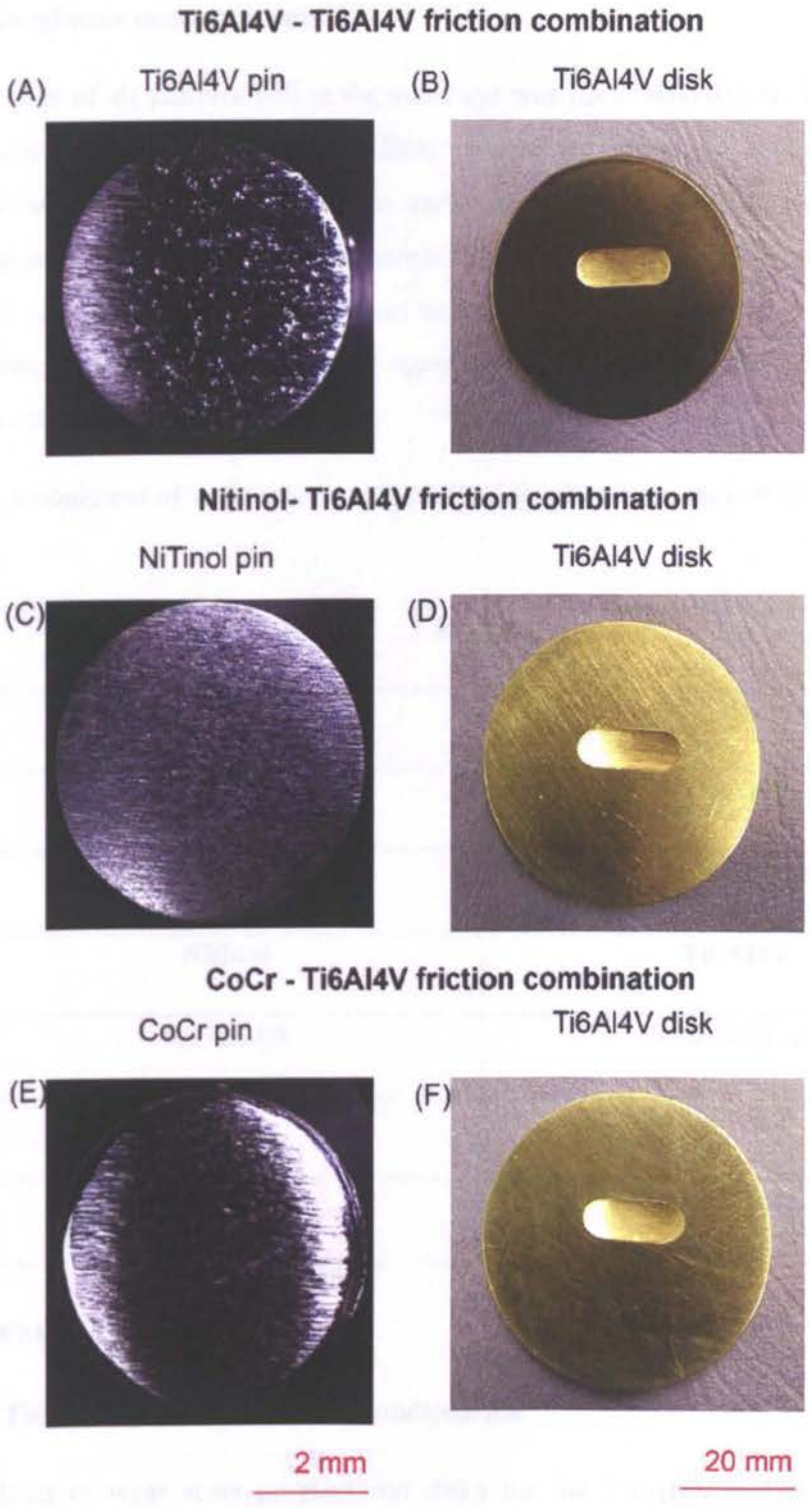

Figure 4.4. Photos of pins and disks after the wear test (0.85 million cycles): (A and B) Ti6Al4V – Ti-6Al4V friction combination; (C and D) Nitinol – Ti6Al4V friction combination; (E and F) CoCr – Ti6Al4V friction combination

4.3.2. Analysis of wear scars

4.3.2.1. Roughness measurements

The roughness of all samples before the wear test was Ra 0.04±0.01μm. The roughness of wear scars after the tests (0.85 million cycles) are presented in Table 4.2. The smoothest surface after the tests was seen on Nitinol pins (0.17±0.05 μm Ra). Roughness of CoCr and titanium pins is two and three times higher respectively. The highest Ra values were observed for disks in Ti6Al4V - Ti6Al4V friction combination. The roughness of titanium disks tested against Nitinol and CoCr are 1.5 and 2 times lower respectively.

Table 4.2. Roughness of wear scars on pins and disks after the wear test (0.85 million cycles)

	Ra, μm	
	Pin	**Disk**
1.	**Ti6Al4V**	**Ti6Al4V**
	0.5±0.07	0.6±0.05 μm
2.	**Nitinol**	**Ti6Al4V**
	0.17±0.05	0.26±0.05 μm
3.	**CoCr**	**Ti6Al4V**
	0.33±0.05	0.38±0.05

4.3.2.2. SEM and EDAX analysis

4.3.2.2.1. Ti6Al4V- Ti6Al4V friction combination

SEM analysis of wear scars on pins and disks for the Ti6Al4V – Ti6Al4V friction combination (fig. 4.5) revealed the presence of severe abrasion grooves and adhesion deposits on both counter-parts, thus indicating both abrasion and adhesion mechanisms of wear damage to the Ti6Al4V alloy.

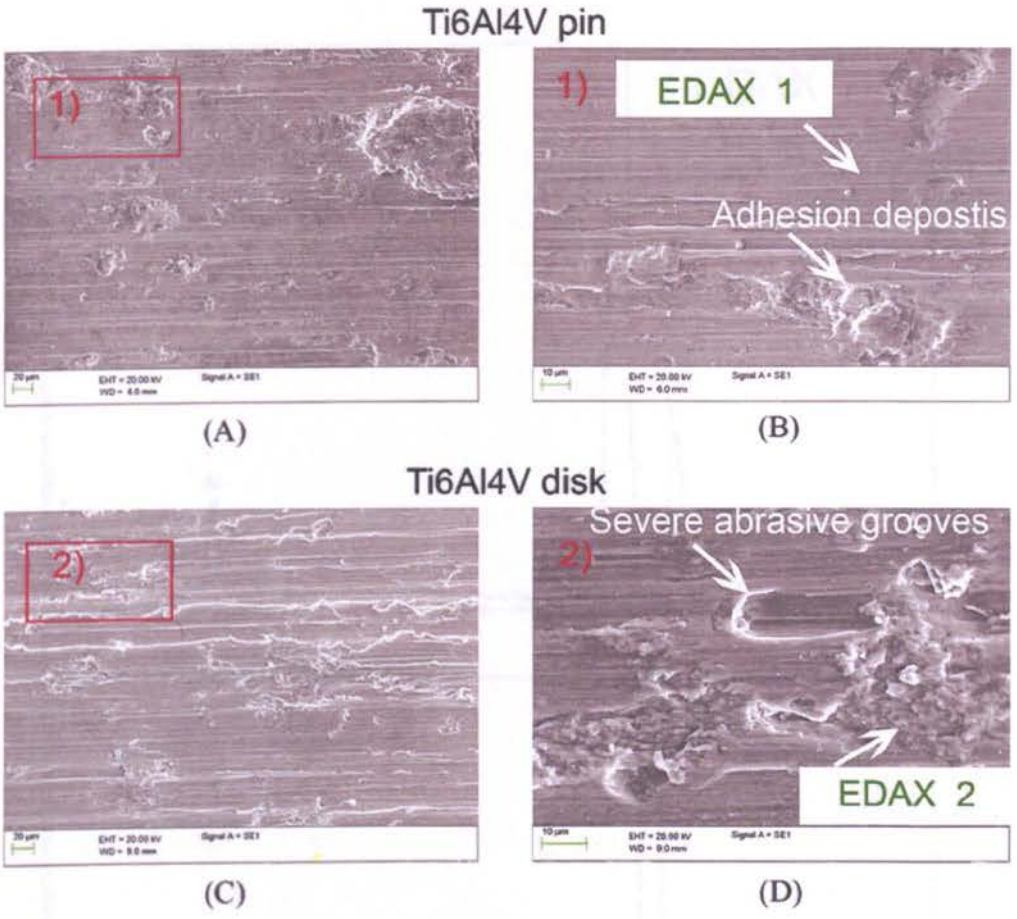

Figure 4.5. SEM of wear scars on titanium pin (A and B) and titanium disk (C and D) in Ti6Al4V - Ti6Al4V friction combination components after 0.1 million cycles of testing

Peaks of Ti, Al and V were typical for the Ti6Al4V alloy and were detected for both wear grooves (EDAX 1) and adhesion deposits (EDAX 2) by EDAX analysis (fig. 4.6).

In contrast to the retrieved components from the LSZ-4D sliding devices, the whole area of wear scars demonstrated an equal level of wear damage with no specific regions showing more pronounced damage.

The wear damage appears to occur mainly in the early stages of sliding contact between the two surfaces. SEM and EDAX analysis of wear scars on pins and disks after 0.5 and 0.85 million cycles did not reveal any difference in wear damage mechanisms compared to that observed after 0.1 million cycles (fig. 4.5 and 4.7).

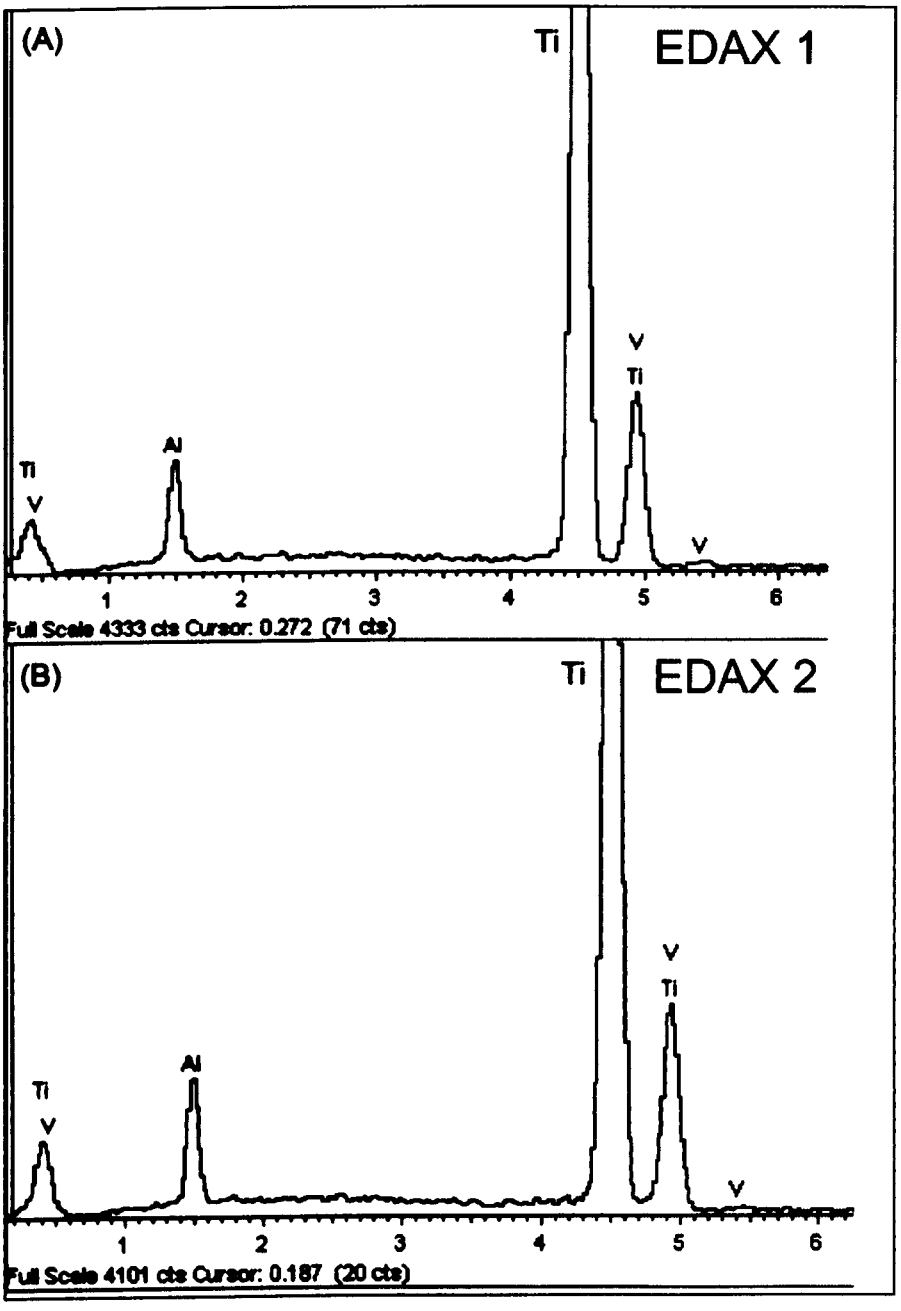

Figure 4.6. EDAX analysis of abrasion grooves (A) and adhesion deposits (B) on wear scars in Ti6Al4V - Ti6Al4V friction combination components after 0.1 million cycles of testing

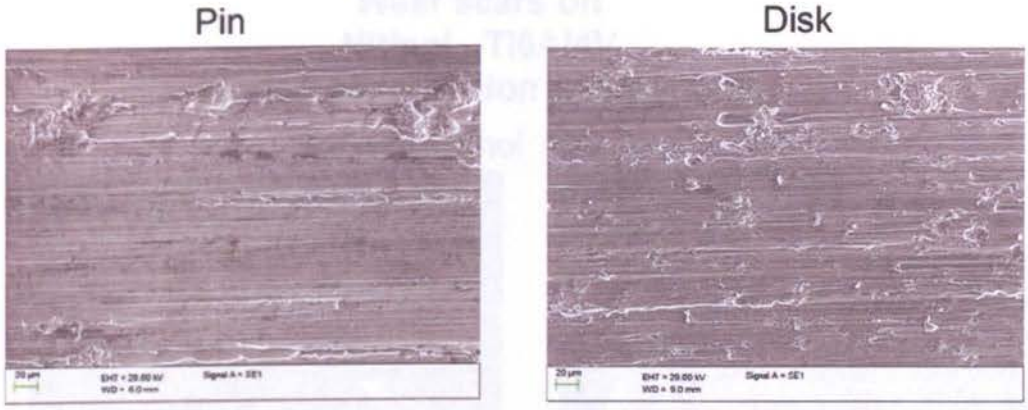

Figure 4.7. SEM of wear scars on pin (A) and disk (B) in Ti6Al4V - Ti6Al4V friction combination after wear test termination at 0.85 million cycles

4.3.2.2.2. Nitinol - Ti6Al4V friction combination

Mild abrasion grooves were observed on the Nitinol pins with approximately 70% of the wear scar surface covered with adhesion deposits (fig. 4.8). The presence of aluminium and increased intensity of Ti peaks in these deposits (fig. 4.9, EDAX 3 and 4) indicates transfer of titanium disk material to the Nitinol counter-part.

Milder wear damage with shallower abrasion grooves and a lower quantity of adhesion deposits was also observed on Ti6Al4V disks when they were tested against Nitinol compared to the Ti6Al4V - Ti6Al4V friction combination (fig. 4.9 and 4.5). No traces of Ni were determined by EDAX analysis on the titanium disks in Nitinol - Ti6Al4V friction combination.

4.3.2.2.3. CoCr - Ti6Al4V friction combination

Abrasion and adhesion mechanisms of wear damage were seen on CoCr pins in CoCr - Ti6Al4V friction combination and predominantly abrasive damage is seen on titanium disks (fig. 4. 10).

EDAX analysis revealed no traces of Co, Cr or Mo on titanium disks, while deposits on CoCr pins had Ti, Al and V in their chemical composition (fig. 4.11) which is similar to Nitinol – Ti6Al4V friction combination.

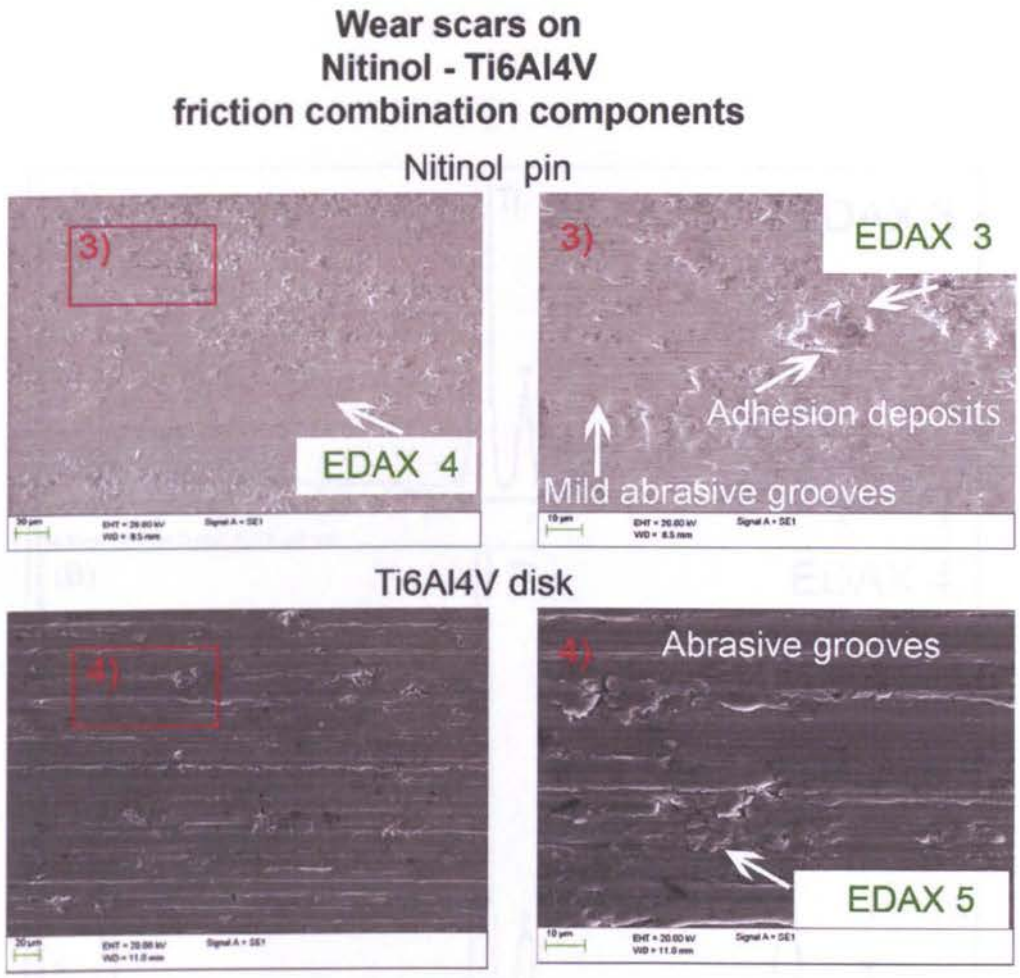

Fig. 4.8. SEM of wear scars on Nitinol pin (A and B) and titanium disk (C and D) in Nitinol - Ti6Al4V friction combination components after 0.1 million cycles of testing

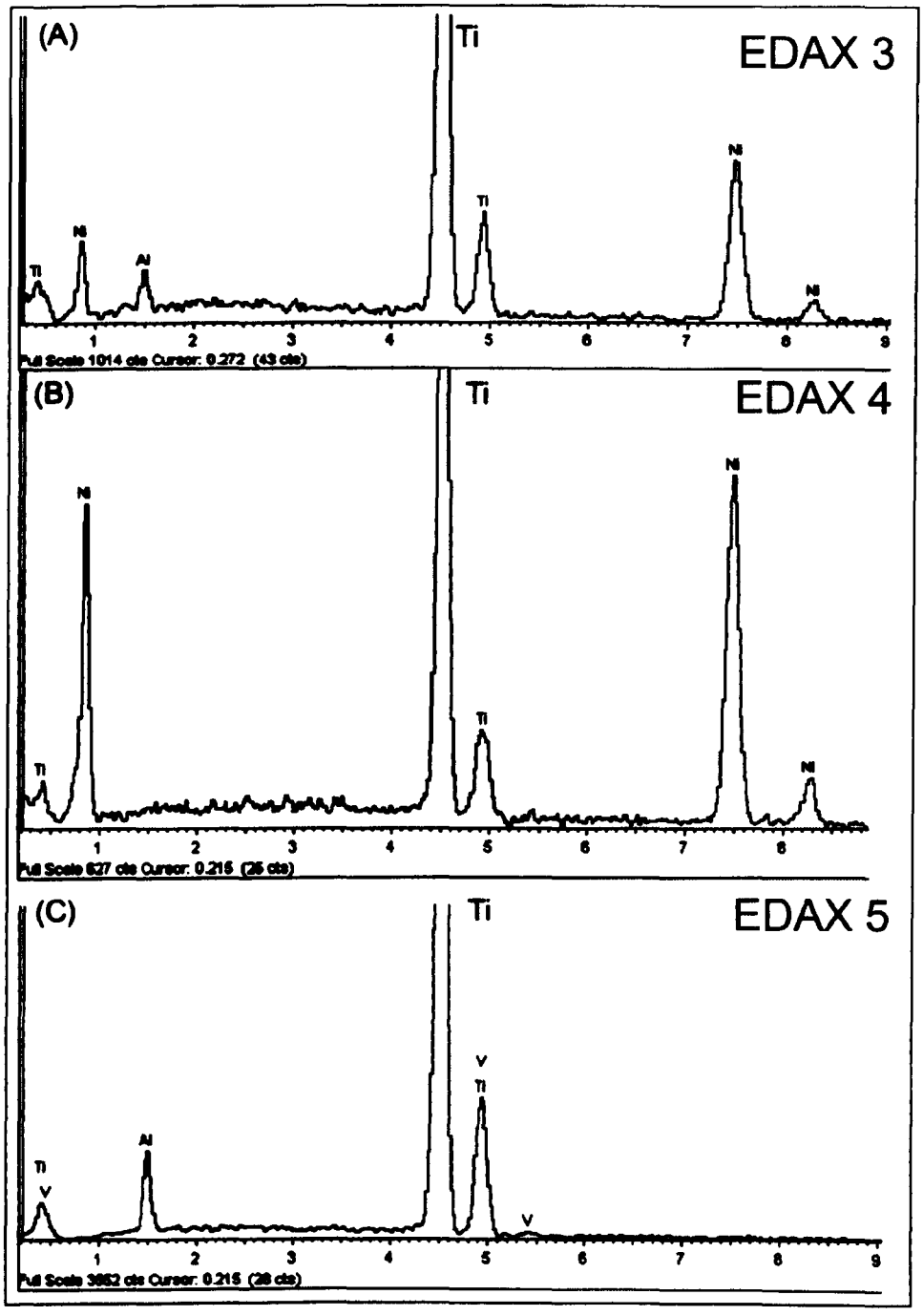

Fig. 4.9 EDAX analysis of wear deposits (A) and grooves (B) on Nitinol pin and adhesion deposits on titanium disk (C) in Nitinol - Ti6Al4V friction combination after 0.1 million cycles of testing

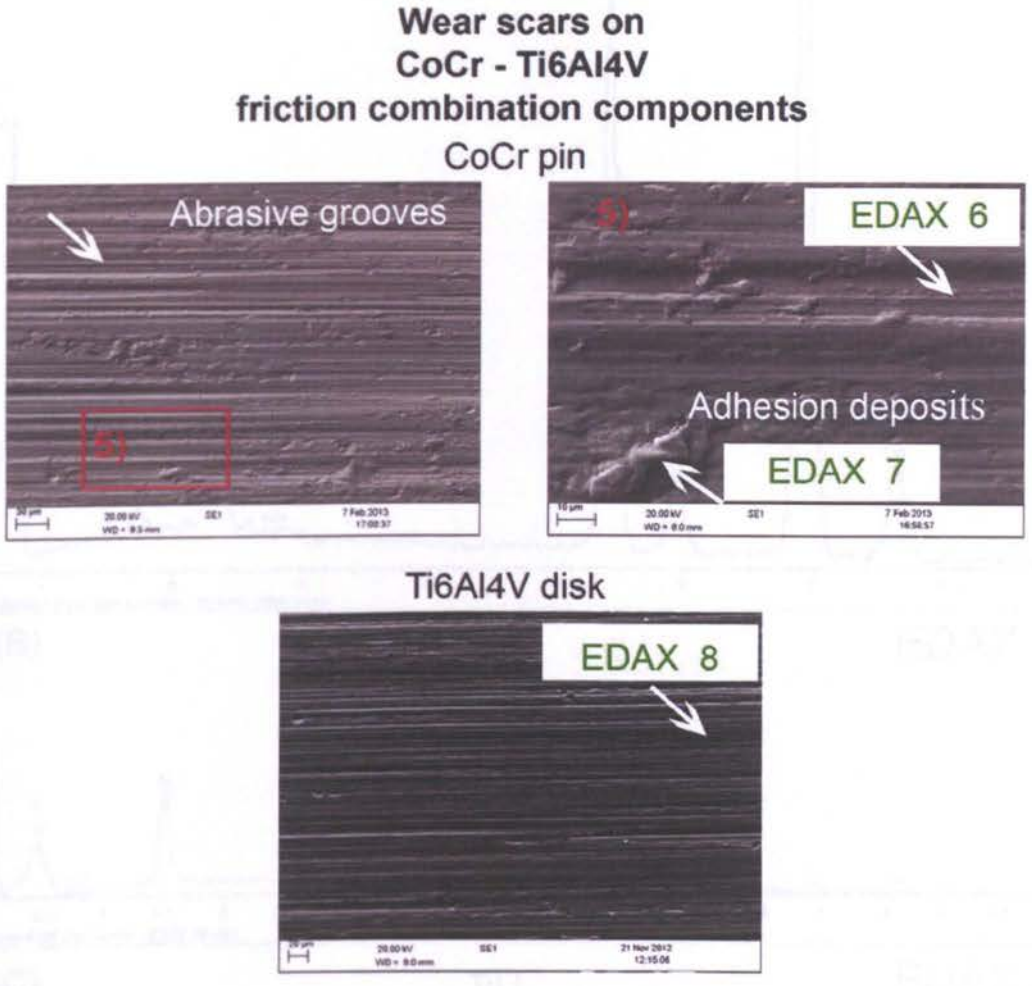

Fig. 4.10 SEM of wear scars on CoCr pins (A and B) and titanium disks (C) in CoCr - Ti6Al4V friction combination components after 0.1 million cycles of testing

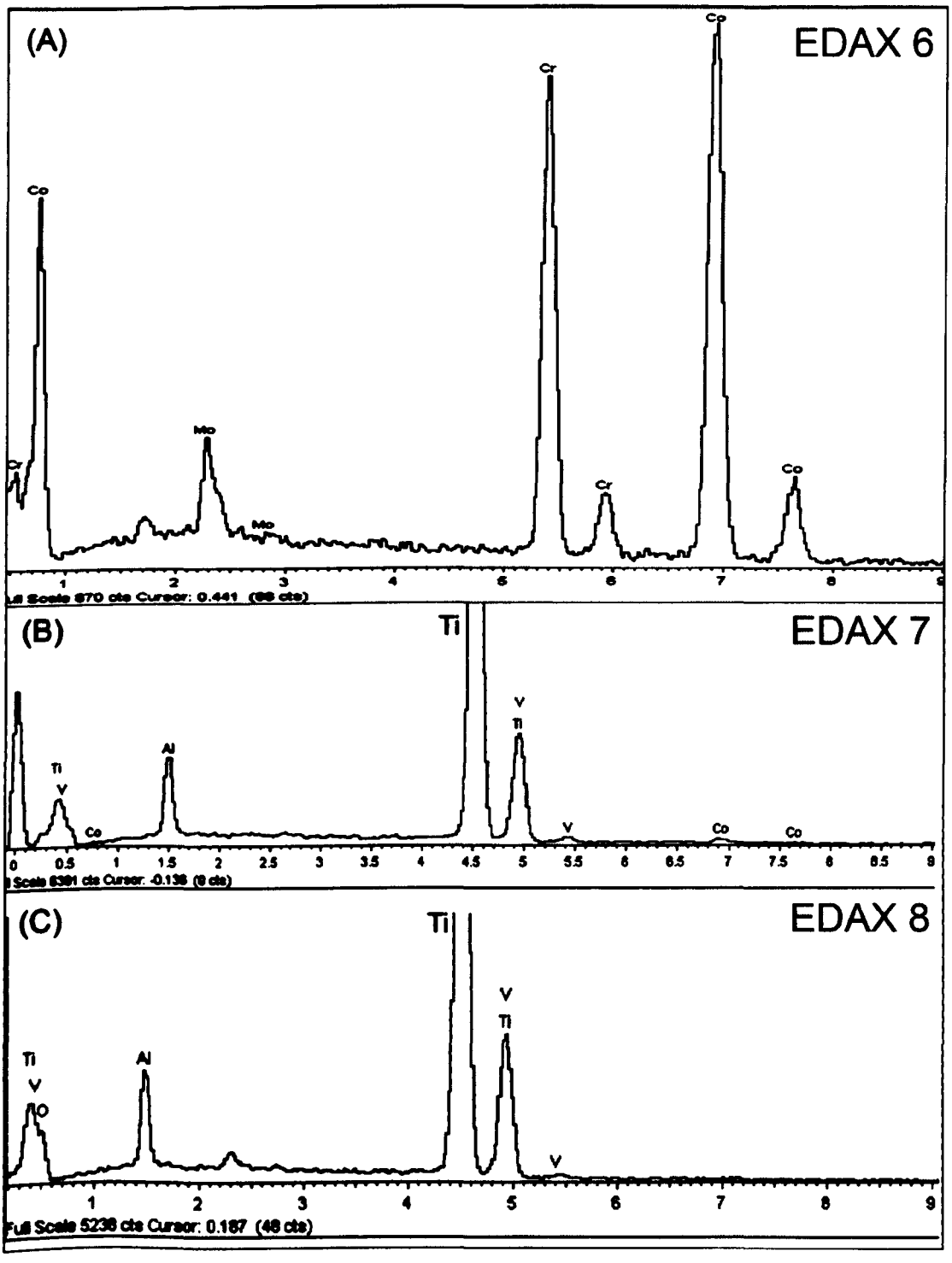

Fig. 4.11 EDAX analysis of wear grooves (A) and adhesion deposits (B) on CoCr pins and wear grooves on titanium disk (C) in CoCr - Ti6Al4V friction combination components after 0.1 million cycles of testing

4.3.3. Analysis of the wear particles

The size distribution and chemical composition of the wear particles was evaluated by SEM EDAX analysis. For the Ti6Al4V-Ti6Al4V friction combination this is shown in figure 4.12. The average aspect ratio of particles was measured to be 1.3-1.6; thus they were classified as round and oval according to ISO 17853:2011. The average particles size was 0.45μm. The minimum size is 0.13, whilst the largest size is 1.6 μm. Size distribution of particles revealed that approximately 68% of particles had sizes less than 0.4 μm. EDAX analysis of the particles shows peaks of titanium, aluminium and vanadium.

The average size of wear particles for the Nitinol - Ti6Al4V friction combination (fig. 4.13) was 0.3 μm (with a range from 0.10 to 1.97 μm). Their shape was round with average aspect ratios being 1.2-1.4. Approximately 70% of particles had sizes less than 0.4 μm. EDAX analysis of particles revealed no traces of Ni.

The average size of wear particles for the CoCr - Ti6Al4V friction combination (fig. 4.14) was 0.4 μm (with a range from 0.03 to 2.1 μm). Their shape was round to oval with average aspect ratios being 1.2-1.6. Approximately 66% of particles had sizes less than 0.4 μm. EDAX analysis of particles revealed no traces of Co, Cr or Mo.

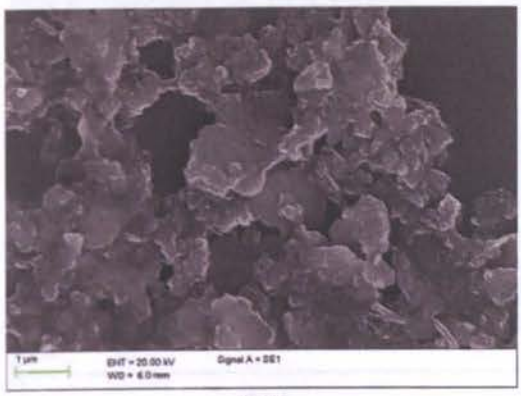

(A)

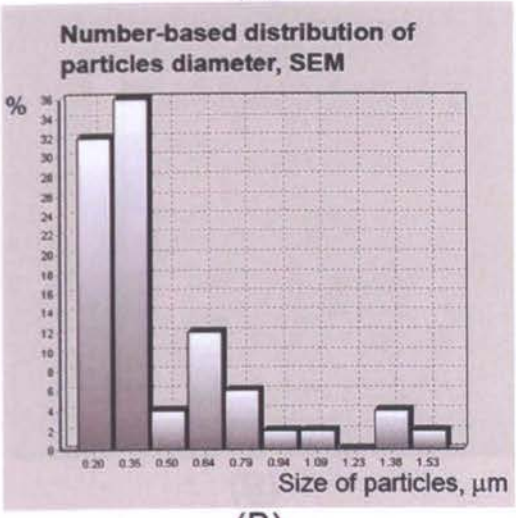

(B)

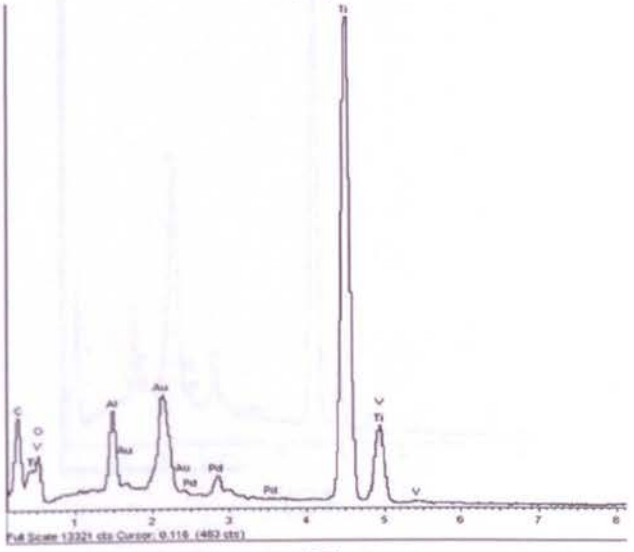

(C)

Figure 4.12. Ti6Al4V - Ti6Al4V friction combination: (A) SEM micrograph of wear particles; (B) particles diameter distribution and (C) chemical composition measured by EDAX analysis

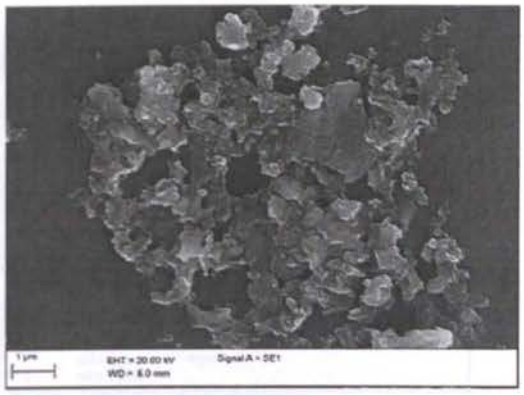

(A)

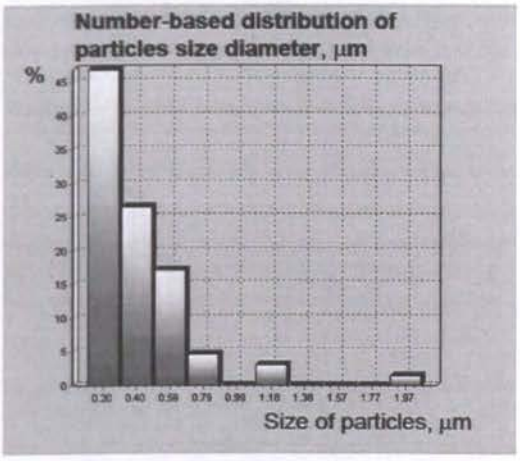

(B)

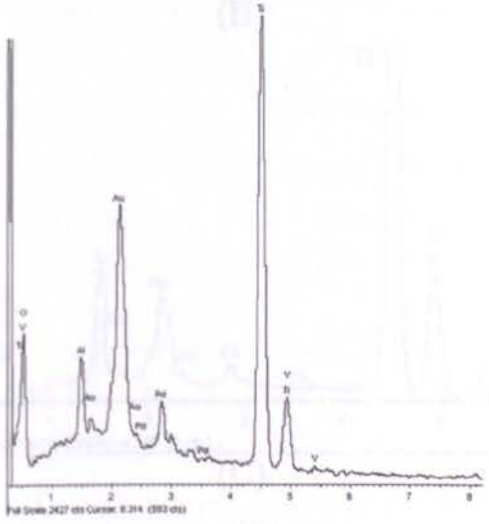

(C)

Figure 4.13. Nitinol - Ti6Al4V friction combination; (A) SEM micrograph of wear particles; (B) particles diameter distribution and (C) chemical composition measured by EDAX analysis

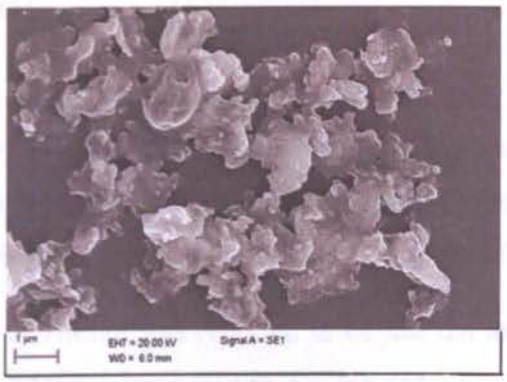

(A)

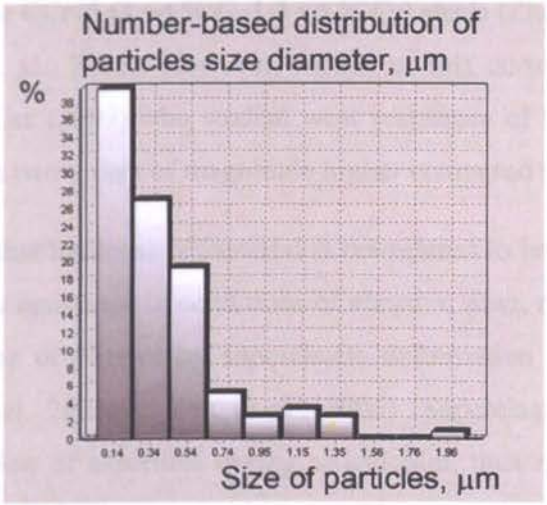

(B)

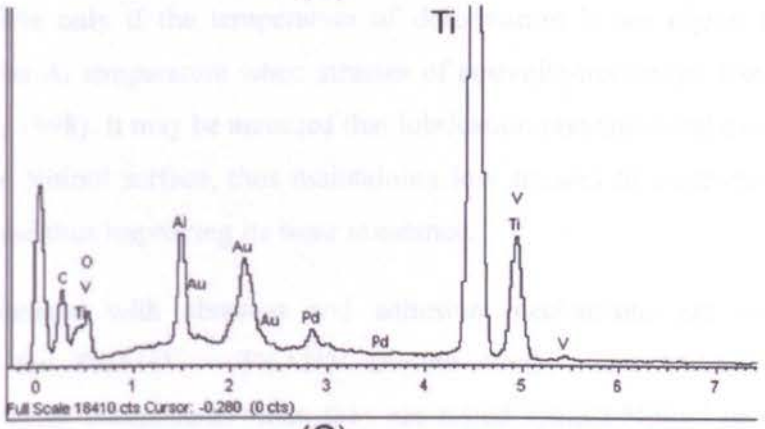

(C)

Figure 4.14. CoCr - Ti6Al4V friction combination: (A) SEM micrograph of wear particles; (B) particles diameter distribution and (C) chemical composition measured by EDAX analysis

4.4. DISCUSSION

The results of the in-vitro wear test study revealed that wear resistance of Nitinol tested against titanium alloy Ti6Al4V in the simulated body environment is comparable to that of CoCr alloy which is known for its good tribological properties. The wear of titanium alloy Ti6Al4V is 100 times greater compared to Nitinol and CoCr.

The wear resistance of Nitinol was reported to be just ten to twenty times better in dry sliding or fretting conditions compared to Ti, 304 (18 wt.% Cr, 10 wt.% Ni, $\leq$ 2 wt.% Mn, Fe – balance) or CCr15 (1 wt.% C, 1.5 wt.% Cr) steels (Zhang et al., 2009, Li et al., 2000 & Linmao et. al., 2005). However, results of this current work agree with the findings of Lui & Lee (2009) who studied wear resistance of Nitinol in oil lubrication and revealed it to be two orders of magnitude higher compared to 304 stainless steel.

In spite of the fact that hardness of material is considered to be one of the main factors which improve wear resistance in conditions of abrasive wear, many authors explain the high wear resistance of Nitinol by superelastic deformation of its surface layers in friction (Quain et al, 2005 & Yan et al., 2006). Superelastic behaviour results in reversible deformation of asperities during articulation, thus reducing contact stresses with a corresponding reduction in asperity wear. However, the superelastic behaviour of Nitinol is possible only if the temperature of deformation is not higher than 20-30 degrees above the A_f temperature when stresses of austenite-martensite transformation are low (Otsuka, 1998). It may be assumed that lubrication prevents local overheating of asperities on the Nitinol surface, thus maintaining low stresses of austenite-martensite transformation and thus improving its wear resistance.

Severe wear damage with abrasion and adhesion mechanisms are revealed for components in the Ti6Al4V – Ti6Al4V friction combination. Milder damage is observed on titanium components when they are tested against Nitinol or CoCr alloy which correlates with reducing Ra roughness values from 0.6±0.05 μm to 0.26±0.05 μm and 0.38± 0.05 μm when titanium is tested against Nitinol and CoCr respectively. The adhesion mechanism of titanium alloys wear damage has been established by other researchers (Taktak & Akbulut, 2007 & Magaziner et al., 2008) and is attributed to removing the protective oxide film from the surface during friction resulting in adhesion of highly chemically active titanium to the counter-body thus causing galling, which is

considered to be the main reason for the poor tribological behaviour of titanium alloys (Williams, 2005). Adhesion transfer of Ti, Al and V from the titanium counter-part along with mild abrasion is also seen on the Nitinol and CoCr components in Nitinol – Ti6Al4V and CoCr – Ti6Al4V friction combinations while no transfer of Ni or Co, which are the main constitutes of Nitinol and CoCr alloys, was detected on their titanium counter-parts.

In the current work the wear particles were round and oval shaped with approximately 70% of them having sizes of less than 0.4 μm across. This analysis was undertaken using SEM images of the particles collected after in-vitro pin-on-disk testing of Ti6Al4V – Ti6Al4V, Nitinol – Ti6Al4V and CoCr – Ni6Al4V friction combinations. This is similar to the size described for metal particles from THR which are reported to be 0.02-0.8 μm for CoCr and from 0.04-0.9 μm for Ti (Doorn et al., 1998). The larger particle size (more than 1 μm) reported by Singh et. al. (2013) for Shilla growth-guidance spinal devices could be explained by the application of laser scattering methodology where particle agglomeration or settlement might influence the calculations.

Comparison of wear scars on retrieved LSZ-4D sling device components (Chapter II) with components of Ti6Al4V –Ti6Al4V friction combination after in-vitro test, reveals both abrasive and adhesive wear damage mechanisms. The size and shape of the wear particles retrieved from tissues surrounding LSZ-4D devices and those digested from bovine serum after in-vitro wear testing are also similar, which helps validate the assumption that the testing methodology simulates in-vivo reciprocation translation movement of rods against fixtures. The wear rate of titanium pins in the Ti6Al4V-Ti6Al4V friction combination is $33\pm2mm^3$ per 0.5 million cycles which corresponds approximately to wear debris produced by two rods of LSZ devices after 6.5 years of implantation (Chapter 2, fig. 2.6). If the observed 0.15 mm^3 volume wear loss of Nitinol pins after 0.5 million cycles were to occur in-vivo as well, which represents relatively low wear, then the biological problems associated with metallosis would not be expected as the release of debris is limited.

Normally (for example ISO 18192 for the testing of spinal disks prostheses) 1 million cycles of in vitro testing is estimated to correspond to 1 year of service. Greater wear values obtained in the current research might be explained by lower amplitude of

motion and contact area in real spinal sliding LSZ-4D devices. Additionally, the roughness and visual depth of abrasive grooves (seen on SEM micrographs) which was observed on titanium pins and disks after in vitro wear test is similar to that measured on severe damaged areas on retrieved LSZ-4D instrumentation (0.5-0.6 and 0.7 μm Ra respectively). Mildly damaged areas on retrieved instrumentation have low roughness (0.1±0.05 μm Ra) and just mild scratches. This might indicate uneven distribution of contact stresses in LSZ-4D instrumentation. It may be assumed that only severely damaged areas in LSZ-4D instrumentation were subjected to stresses applied in my in-vitro wear test.

The low roughness of wear scars after the tests is also beneficial to the corrosion and fatigue resistance of Nitinol due to the lower exposed surface area and the reduction of stress raisers ((Shabalovskaya, 2002, Polinsky et al., 2004 & Patel and Gordon, 2006).

Nevertheless, further wear tests of assembled devices incorporating Nitinol rods are needed in order to evaluate the volume of wear debris generated by specific designs as this, for example, will influence the lubrication and contact stresses. The application of protective wear resistant coatings to Nitinol to further minimise the possibility of Ni leaching from the wear debris would be also beneficial.

High volume wear loss from titanium components, together with the revealed metallosis related complications in patients with implanted LSZ-4D sliding devices, also implies the need for wear resistant coatings on titanium counter-parts. The high wear seen in the current pin-on-disk wear test for Nitinol – Ti6Al4V friction pair, where the loss of material is associated with titanium, also necessitates the application of wear resistant coatings in order to prevent metallosis in patients, who in future, may receive these components.

4.5. CONCLUSIONS

1. The wear resistance of Nitinol tested against titanium alloy Ti6Al4V in the simulated body environment is approximately 100 times higher when compared to titanium alloy (Ti6Al4V) and is comparable to that of CoCr alloy. The wear resistance of titanium counter-parts (discs) did not differ significantly when articulated against Ti6Al4V, Nitinol or CoCr. However when the wear of the pins was analysed, it was

shown that there was a significantly greater wear with titanium than with Nitinol or CoCr.

2. The current research revealed severe wear damage with abrasion and adhesion mechanisms for components in the Ti6Al4V – Ti6Al4V friction combination. Milder damage was observed on titanium components when they were tested against Nitinol or CoCr alloys. Adhesion transfer of titanium and mild abrasion mechanisms of damage were revealed on Nitinol and CoCr components in Nitinol – Ti6Al4V and CoCr – Ni6Al4V friction combinations.

3. Chemical composition of wear particles generated by Ti6Al4V – Ti6Al4V, Nitinol – Ti6Al4V and CoCr – Ni6Al4V friction combinations was associated with Ti, Al and V with no traces of Ni, Co or Cr. The shape of these wear particles was round to oval, with an average size of between 0.3-0.45 μm (minimum 0.03 μm, maximum 2.1 μm).

4. Importantly, the current research shows that equal wear damage mechanisms, as well as shape and size of collected wear particles, were identified for in-vivo LSZ-4D retrievals and in-vitro Ti6Al4V – Ti6Al4V friction combination component tests.

CHAPTER 5

INFLUENCE OF TIN, DLC AND ION IMPLANTATION ON THE WEAR RESISTANCE OF NITINOL AND TITANIUM ALLOY (TI6AL4V)

5.1. INTRODUCTION

Results of the Nitinol – Ti6Al4V friction combination wear tests, aimed to simulate articulation of Nitinol rods in titanium fixtures in spinal implants for early-on-set scoliosis, described in Chapter 4, revealed high wear loss which was associated with the wear of titanium. Since wear debris was shown to cause metallosis related complications such as fistulas and seromas (Chapter 2), it is necessary to reduce the wear of titanium components.

The amount of wear debris generated from Nitinol was found to be small. Nevertheless, further protection of the Nitinol component may also be beneficial since Ni ions are known to be toxic cause allergic reaction (Goyer, 1986 & Lacy et al., 1996). Surface preparation, including electro-polishing and/or etching result in the formation of a titanium based oxide layer on Nitinol surface with a nickel content less than 2-7wt. % (Shabalovskaya, 2008 & Pohl, 2004). However, the chemical composition of Nitinol wear particles generated in-vivo is not well understood.

Surface treatments for improving biocompatibility, wear and corrosion resistance of titanium and Nitinol alloys include thermal oxidation, nitriding, deposition of nitride, carbon, boron and diamond-like carbon coatings as well as ion implantation techniques (Geetha, 2009, Dearnaley & Arps, 2005). The latter being a surface modification rather than a coating. Since the temperature of heat treatment used for ageing required to achieve the appropriate temperature of Nitinol shape recovery starts from 300^0C (Otsuka, 1998), deposition of TiN (titanium nitride), diamond-like carbon (DLC) coatings and implantation with nitrogen ions were chosen due to the low-temperatures used for their deposition.

TiN coatings are well known for increasing the hardness and corrosion resistance of titanium alloys (Shenhar et al., 2000 & Wang et al., 2013). Although during the early history of TiN application delamination from titanium during in-vivo service was reported (Harman et.al., 1997). The adhesion strength of TiN has been improved by introduction of a pure titanium layer adjacent to the surface or the use of pure titanium interlayers (Kim et al, 2002).

DLC is reported to provide a lower friction coefficient compared to TiN when deposited on titanium or Nitinol substrates (Wiklund & Hutchings, 2001& Costa et al., 2010) and that is considered to improve their wear performance. However DLC adhesion to

substrates is still problematic. Ion implantation is a surface treatment and has been shown to have a good adhesion with both titanium and Nitinol due to the implantation of ions inside the substrate and therefore there is an absence of a distinct boundary between the modified layer and substrate. This treatment is known to improve corrosion resistance of Nitinol (Tan et al., 2003 & Oliveira et al., 2012) and its wear performance when tested against soft materials (Alves-Claro et. al., 2008). The improvement of wear performance of metal-on-metal friction pairs for ion implantation is less compared to DLC and TiN (Bowsher et al., 2005). Nevertheless, it was chosen for wear tests in the current research since thin nano-layers are more likely to withstand the high strains encountered by Nitinol during functional loading since residual stresses which stimulate the delaminating of surface layers rise with the increasing of these layers thickness (Takadoum & Bennani, 1997). However, the wear performance of the Nitinol – Ti6Al4V friction combination using TiN and DLC coatings or ion implantation application has not previously been investigated. This is because in most tribological experiments, surface treated metal components were tested against polyethylene, steels or Si_3N_4 or self-matching surfaces as counter-bodies. Since the material of counter bodies might affect wear performance of the whole friction pair, Nitinol – Ti6Al4V friction combination wear performance needs to be investigated for the safe application of this friction pair in sliding conditions in the spine.

The purpose of this part of the research project and the focus of this Chapter was to investigate the influence of titanium nitride, diamond like carbon coatings and ion implantation on the wear resistance of Nitinol – Ti6Al4V friction combination. The aims were:

1. To investigate the influence of TiN coating on the wear resistance, wear scar roughness and damage mechanisms of Nitinol – Ti6Al4V friction combination components with deposition only on titanium or both components;

2. To investigate the influence of DLC coating on wear resistance, wear scar roughness and damage mechanisms of Nitinol – Ti6Al4V friction combination components with deposition only on titanium or both components;

3. To investigate the influence of ion implantation on the wear resistance, wear scar roughness and damage mechanisms of Nitinol – Ti6Al4V friction combination with surface modification only on titanium or both components.

5.2 MATERIALS AND METHODS

5.2.1. Materials

The influence of the deposition of titanium nitride and diamond like carbon coatings as well as ion implantation with nitrogen ions on the wear performance of Nitinol – Ti6Al4V friction combination was investigated in this chapter. These surface treatments were applied either only on titanium components or on both Nitinol and titanium. TiN, DLC and ion implantation were applied only on the titanium component in tests 1, 3 and 5 respectively, while in tests 2, 4 and 6 these treatments were applied to both components (Table 5.1).

Table 5.1. Combinations of materials and coatings in pin-on-disk wear tests

	Pin counter-part	Disk counter-part
	Influence of TiN coating	
1.	Test 1	
	Nitinol	Ti6Al4V+ TiN coating
2.	Test 2	
	Nitinol+ TiN coating	Ti6Al4V+ TiN coating
	Influence of DLC coating	
3.	Test 3	
	Nitinol	Ti6Al4V+ DLC coating
4.	Test 4	
	Nitinol+ DLC coating	Ti6Al4V+ DLC coating
	Influence of Ion implantation	
5.	Test 5	
	Nitinol	Ti6Al4V+ Ion implantation
6.	Test 6	
	Nitinol+ Ion implantation	Ti6Al4V+ Ion implantation

TiN coating was applied by CJSC Implants, Russia, by vacuum arc PVD method. The coating was deposited for 2 hours at 350^{0}C on Nitinol substrates and at 500^{0}C on titanium. To improve the adhesion of the TiN coating a pure titanium layer of 0.2 μm thickness was deposited on both substrates. Interlayer of pure Ti was applied prior to

TiN coating deposition for improving its adhesion to the substrate. Cubic TiN nitride was the main phase of the coating according to the data provided by the company.

DLC was applied by TecVac Ltd., Cambridge, UK by RP radio frequency plasma enhanced chemical vapour deposition method at 200^0C for 1 hour in a methane and ethylene gas mixture. Previously to the deposition of DLC coating, a silicon interlayer was applied to increase adhesion between substrate and coating. Normally, DLC coatings consist of two fractions, which are sp3 type carbon bonding, resembling diamond structure, and sp2 type carbon bonding, resembling graphite structure (Wiklund & Hutchings, 2001& Costa et al., 2010). According to the data provided by the company, the DLC coating had an amorphous structure and the sp3/sp2 ratio was claimed to be 7:3.

Ion implantation was performed by Tech-Ni-Plant Ltd., Birmingham, UK. Implantation of nitrogen ions was performed within a vacuum with acceleration energy 100 keV. The implantation dose was $3.5\text{-}4x10^{17}$ ions cm^{-2}.

Photos of samples with coatings are demonstrated on Figure 5.1.

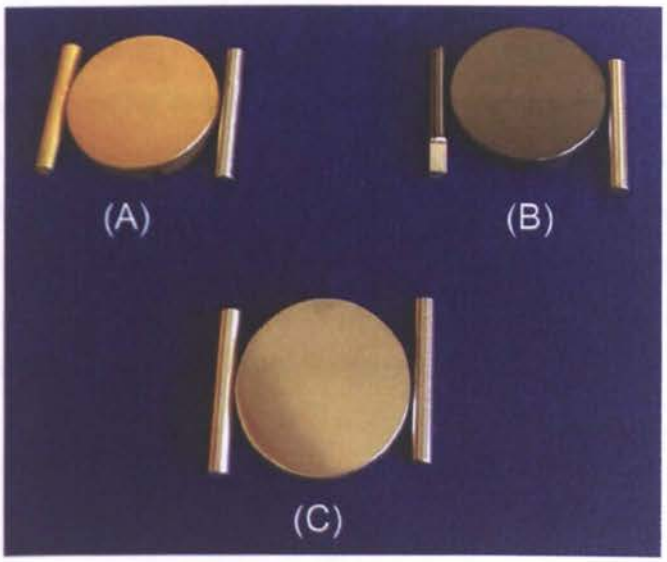

Figure 5.1. Photo of disk and pin used in wear test: A) Nitinol+TiN - Ti6Al4V+TiN friction combination; B) Nitinol+DLC - Ti6Al4V+DLC friction combination; C) Nitinol+Ion implantation - Ti6Al4V+Ion implantation friction combination

5.2.2. METHODS

5.2.2.1. Coatings characterisation

Thickness

In order to measure the thickness of TiN and DLC coatings they were deposited on wire samples (l=30 mm, Ø 0.5 mm) and subjected to fatigue testing as described in Chapter 3. After fatigue failure the thickness of coatings was measured using SEM.

Nano-hardness, elasticity modulus

Nano-hardness and modulus of elasticity were measured using nano-indenter «Nano-Hardness Tester», CSM Instruments (Switzerland) shown on figure 5.2A. The applied load was 5-19 mN in order to ensure that the indentation depth did not exceed 200 nm. Indentation time was 5 seconds. Five measurements were carried out for each coating. Statistical analysis of measured values was carried out using Indentation 3.83 software, CSM Instruments (Switzerland).

Adhesion strength

Adhesion strength of coatings was measured using scratch tests carried out on a REVERTEST scratch testing instrument from CSM Instruments (Switzerland) shown on figure 2B. The initial load was 0.9N while final load was 50N. Loading speed was 49.1 N/min. The scratch length was 5 mm. A diamond 200 μm radius Rockwell C indenter was also used. Three scratches were performed for each coating deposited on the Ti6Al4V substrate. Statistical analysis of measured values was carried out using Scratch 3.10 software, CSM Instruments (Switzerland).

(A) (B)

Figure 5.2. (A) Photo of nano-indenter «Nano-Hardness Tester» and (B) Scratch Tester «REVERTEST», CSM Instruments (Switzerland)

5.2.2.2. Parameters of in-vitro pin-on-disk wear test and volume wear loss measurements

The scheme and parameters of pin-on-disk wear testing and volume wear loss measurements are described in Chapter 4.2.

Mildly damaged components were additionally analysed using a Bruker interferometry microscope. Visualisation images of worn surfaces and profiles were taken for the evaluation of the wear scar depths.

5.2.2.3. Wear scar analysis

The methodology of roughness measurements and SEM and EDAX analysis of wear scar damage is described in Chapter 4.2.

5.2.2.4. Statistics

Methods of mathematical statistics were used to determine average values and deviations using SPSS 14.0 software.

5.3. RESULTS

5.3.1 Characterisation of coatings

5.3.1.1. Thickness

The thickness of TiN and DLC coatings measured using SEM micrographs (fig. 5.3) on fatigue fractured wire samples was 2.8±0.1 and 3.2±0.1 μm for TiN and DLC respectively.

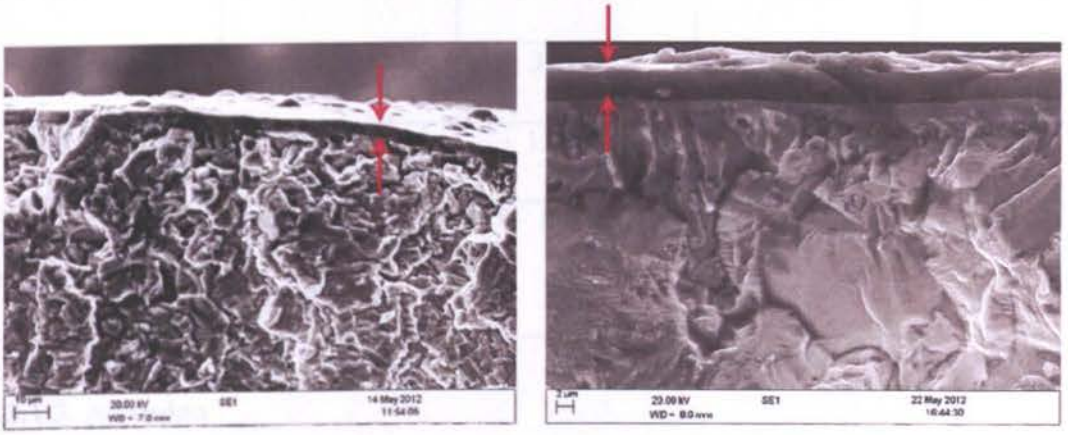

(A) (B)

Figure 5.3. (A) Measuring of TiN and (B) DLC coating thicknesses on fatigue fractured samples using SEM micrographs.

5.3.1.2. Nano-hardness, elastic modulus, roughness

Nano-hardness (HV), elastic modulus (E) and surface roughness for Ti6Al4V and Nitinol substrates and TiN, DLC coatings and ion implantation surfaces are shown in Table 5.2. The applied load was chosen so that the indentation depth (h) be at least 10 fold less compared to TiN and DLC coating thicknesses so that H and E of the coatings can be measured without the influence of the substrate. The highest HV and E were observed for TiN coating (29±1.5 GPa and 370±21 GPa respectively), lower values were revealed for DLC (22±2 GPa and 131±8.5 GPa respectively) whilst a moderate increase of surface hardness was demonstrated after ion implantation (7.2±1 GPa and 135±9 GPa respectively).

Table 5.2. Nano-hardness, elastic modulus, indentation depth and surface roughness after TiN or DLC coating deposition or ion implantation

	HV, GPa	E, GPa	h, nm	Ra, μm
1.Ti6Al4V	5.3±0.08	128±1.6	158±3	0.03±0.01
2. Nitinol	5.5±0.08	38±1	140±8	0.03±0.01
3. TiN coating	29±1.5	370±21	108±4.5	0.04±0.01
4. DLC coating	22±2	131±8.5	50±4	0.02±0.01
5. Ion implantation	7.2±1	135±9	146±13	0.03±0.01

5.3.1.3. Adhesion

Increasing load scratch testing was applied for measuring adhesion strengths of coatings on Ti6Al4V substrate. Testing performed on TiN coating revealed first cracks appearing on the edges of the scratch and an increase of acoustic emission signal at the load f=4,9±0,3 N indicating the onset of failure at this load (Lc_1). This is probably associated with the cohesive strength of the coating. Delamination of TiN coating was detected by further increase of the acoustic emission signal at 26.5±0.8 N, which was found to be the second critical load Lc_2 or adhesion strength of coating (fig. 5.4).

Scratch tests performed on DLC coating revealed first critical load Lc_1 to be 3.3±0.3 N and second critical load Lc_2 to be 12.9±0.5 N (fig. 5.5). It worth noting, that while significant delamination occurred at 12.9±0.5 N, milder delamination of the coating can be seen at f=7N which indicates a lower adhesion strength of DLC compared to the TiN coating.

For comparison, scratch tests were also performed on ion implantation modified surfaces. Since there is no distinct boundary between the substrate and the layer in case of surface modification, and adhesion strength term is thus not applicable. Scratch testing revealed scratching resistance of the modified layer to be 9.1±0.3N, see (fig. 5.6).

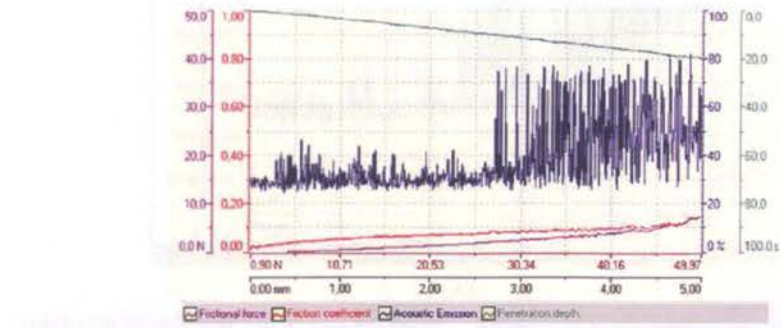

(A)

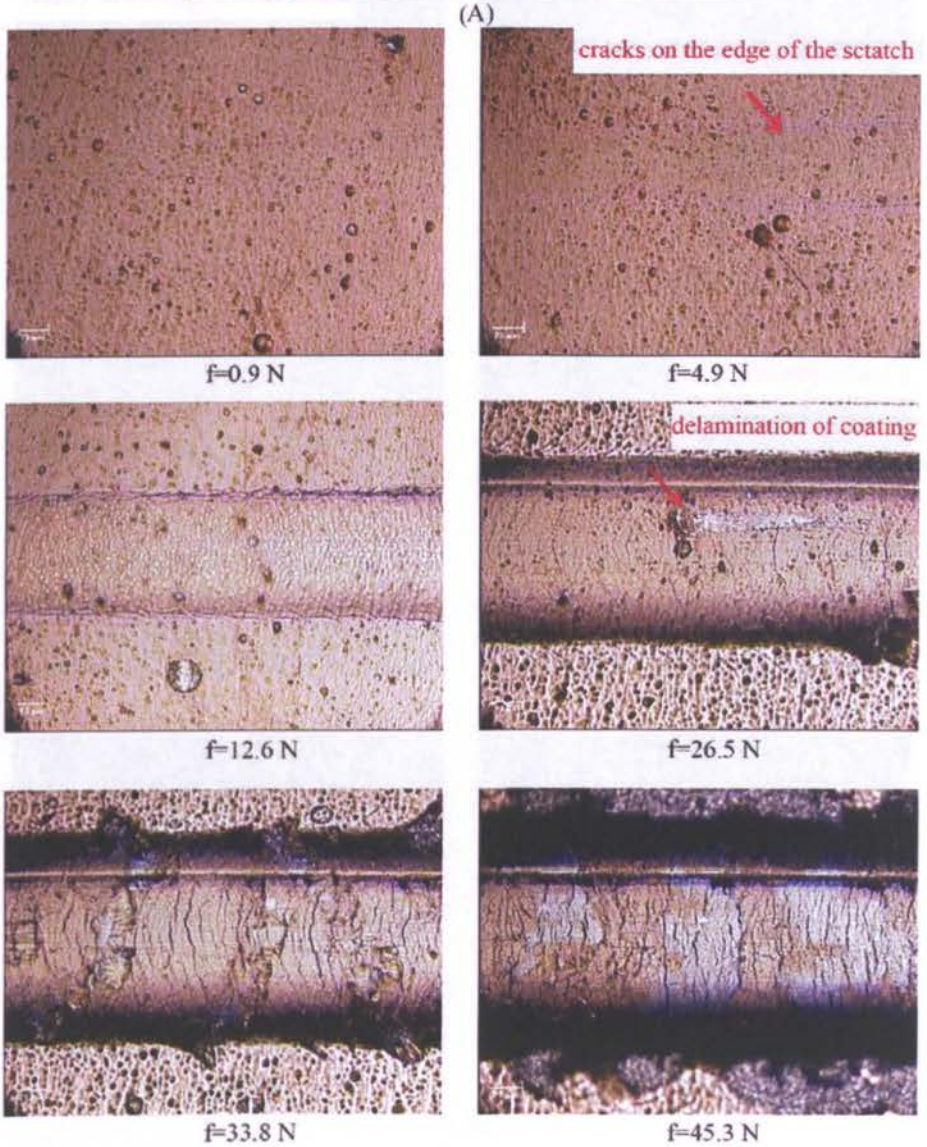

(B)

Figure 5.4. (A) Acoustic emission, frictional force and coefficient and (B) optical micrographs corresponding to different loads (f) in an increased load scratch test performed on TiN coating

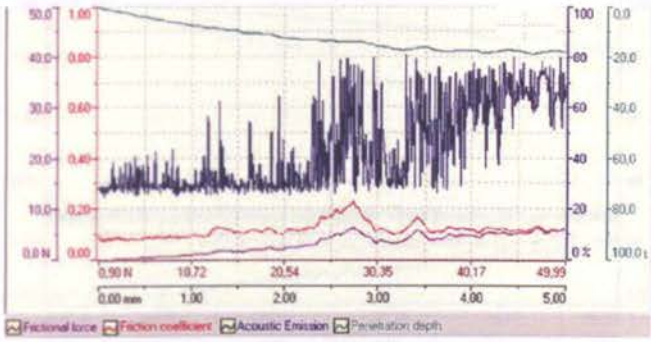

(A)

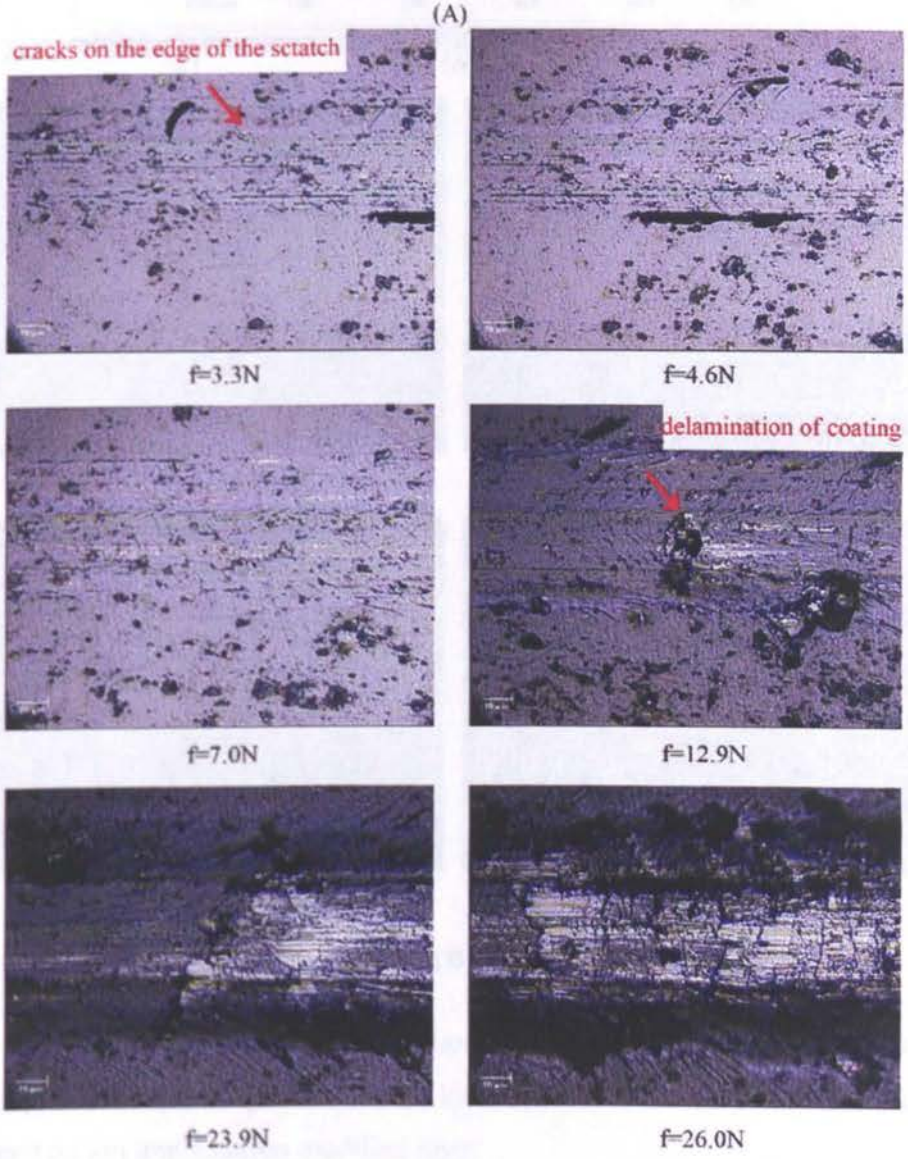

(B)

Figure 5.5. (A) Acoustic emission, frictional force and coefficient and (B) optical micrographs corresponding to different loads (f) in an increased load scratch test performed on DLC coating

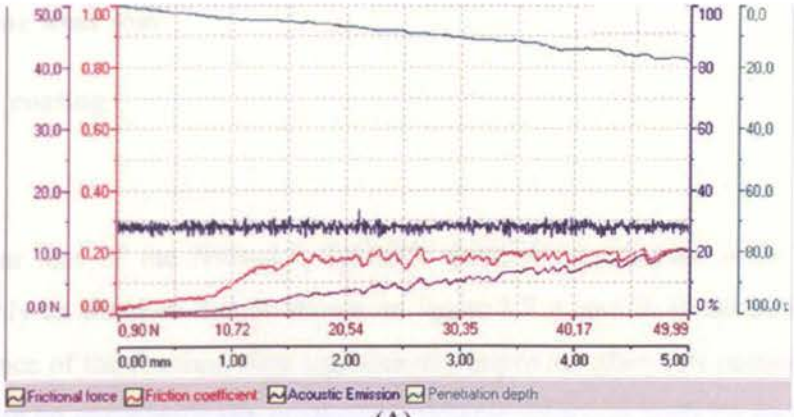

(A)

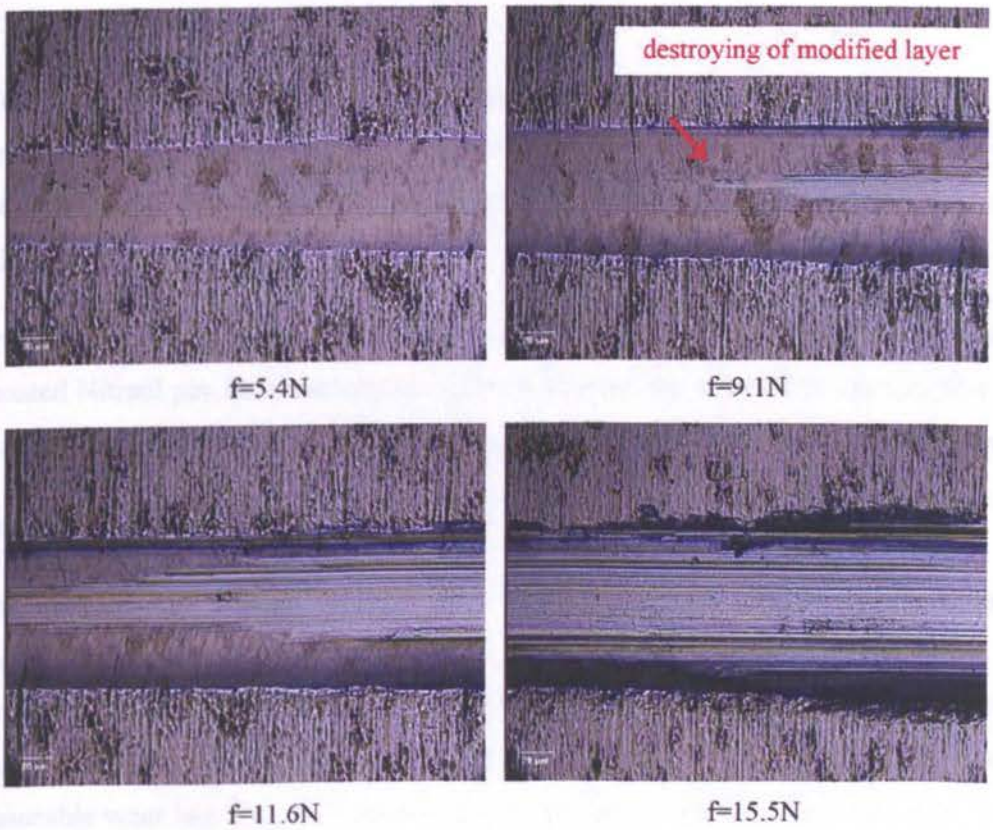

f=5.4N f=9.1N

f=11.6N f=15.5N

(B)

Figure 5.6. (A) Acoustic emission, frictional force and coefficient and (B) optical micrographs corresponding to different loads (f) in an increased load scratch test performed on ion implantation modified layer

5.3.2. Volume wear loss

5.3.2.1. TiN coating

Test 1

Volume wear loss of the Nitinol – Ti6Al4V friction combination with TiN coating deposited only on titanium disk is shown on figure 5.7 A and B. It can be seen that the wear resistance of the titanium disk significantly improved after TiN coating deposition demonstrating no gravimetrically measurable volume wear loss until the end of the wear test at 0.85 million cycles (fig. 5.7).

Mild scratches were observed on these disks after termination of the wear test (fig. 5.8). Interferometry microscopy revealed gradual wearing of the TiN coating on the titanium disk with a depth of wear grooves reaching locally 2±0.1 μm after 0.85 million cycles of testing.

Deposition of TiN coating on the titanium disk did not affect the wear resistance of the uncoated Nitinol pin. Its wear loss was 0.14±0.02 mm^3 per 0.5 million cycles (blue line) which is similar to that when it was tested against uncoated titanium disk (green line).

Test 2

Deposition of TiN coating on both Nitinol pin and titanium disk for the Nitinol – Ti6Al4V friction combination improved wear resistance of both Nitinol pins and titanium disks for up to 0.5 million cycles of testing. No gravimetrically measurable volume wear loss was seen before 0.5 million cycles. However, further testing revealed measurable wear loss (fig. 5.9). Assuming a linear dependence on the number of cycles, the rate of wear loss starting from first 0.5 million cycles was 0.03 and 0.4 mm^3 per 0.5 million cycles for the Nitinol pin and titanium disk respectively. By the end of the wear test prominent wear scars of up to 20±2 μm depth were observed on the titanium disks (fig. 5.10). It should be noted that as the wear increased so did the width of the wear scar indicating that the surfaces were becoming more congruent due to the removal of material. The area of wear damage on the Nitinol pin after TiN coating deposition (Test 2) was smaller but was visually rougher compared to the Test 1 combination where the Nitinol pin was uncoated (fig. 5.10 and 5.8).

Test 1: Nitinol (pin) - Ti6Al4V (disk), TiN coating deposited only on titanium disk

Initial state: Nitinol (pin) - Ti6Al4V (disk), both components uncoated

(A)

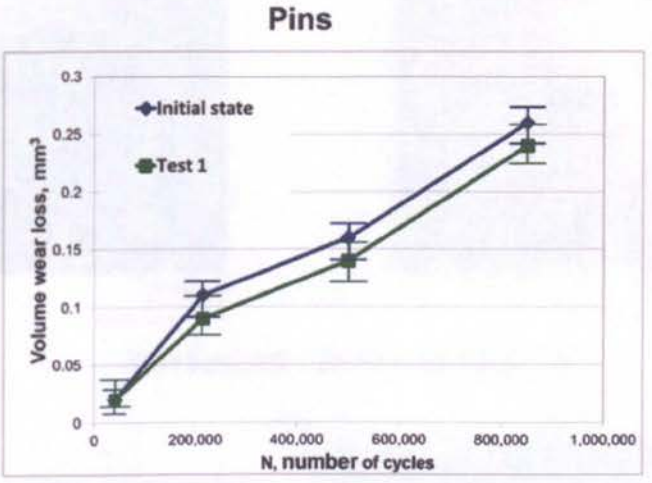

(B)

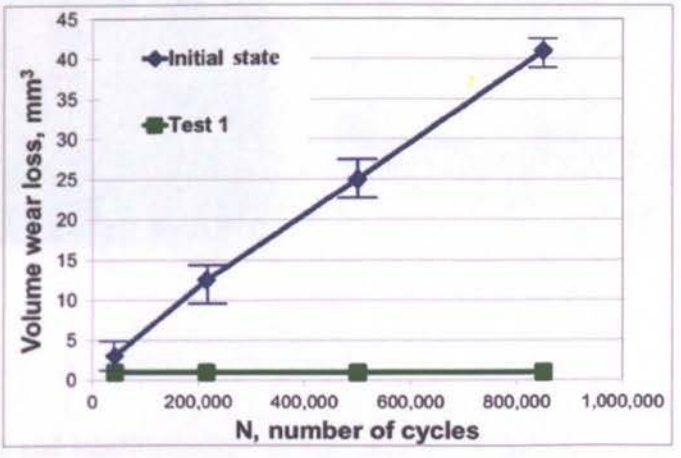

Figure 5.7. (A) Volume wear loss of pins and (B) disks in Nitinol (pin) – Ti6Al4V (disk) friction combination after deposition of TiN coating only on titanium disk (Test 1) compared with initial uncoated state.

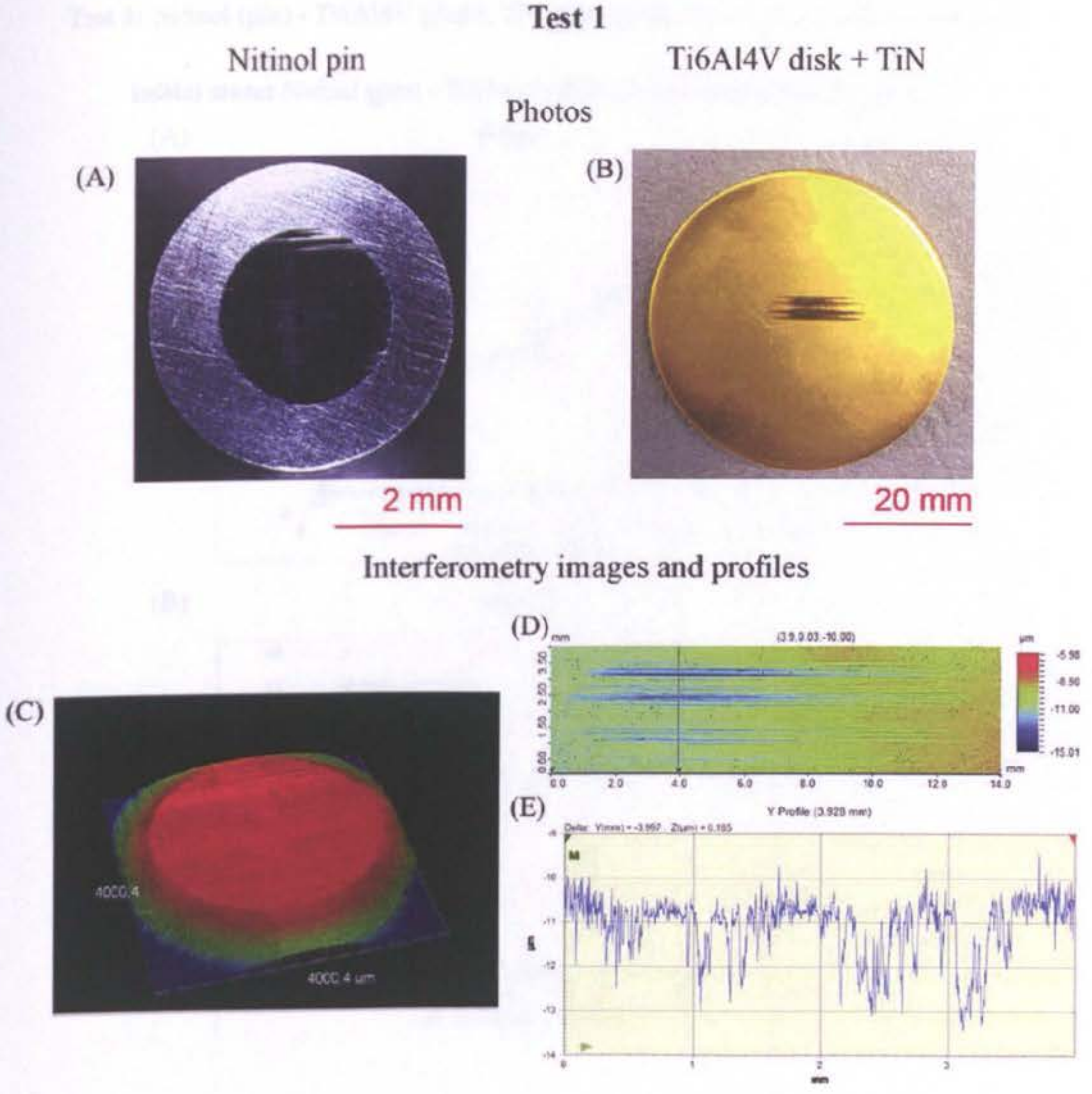

Figure 5.8. Photos and interferometry images of pins (A and C respectively) and disks (B and D respectively) and depth profiles of disks (E) of Nitinol (pin) - Ti6Al4V (disk) friction combination with TiN coating deposited only on disk counter-part (Test 1) after wear test termination at 0.85 million cycles

Test 2: Nitinol (pin) - Ti6Al4V (disk), TiN coating deposited both on both components

Initial state: Nitinol (pin) - Ti6Al4V (disk), both components uncoated

(A) **Pins**

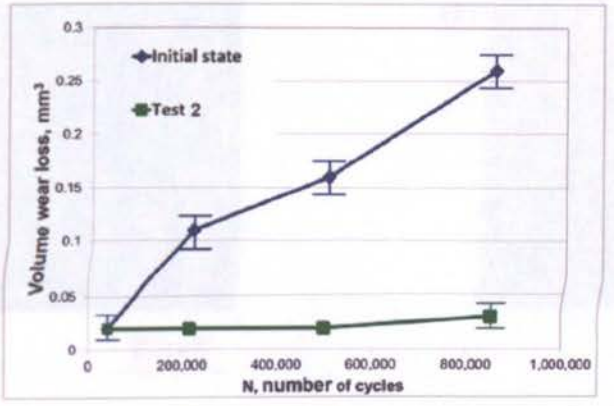

(B) **Disks**

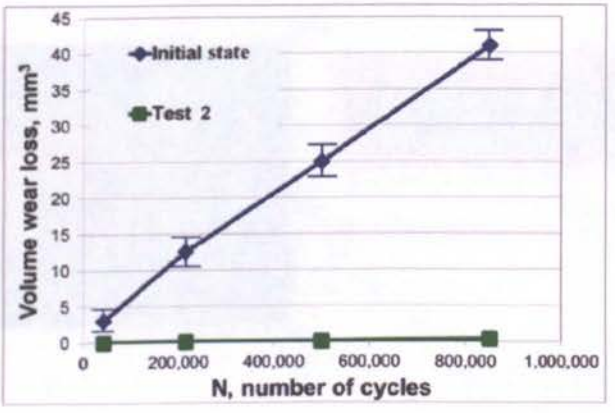

Figure 5.9. Volume wear loss of pins (A) and disks (B) in Nitinol (pin) – Ti6AL4V (disk) friction combination after deposition of TiN coating both on titanium disk and Nitinol pin (Test 2) compared with initial uncoated state.

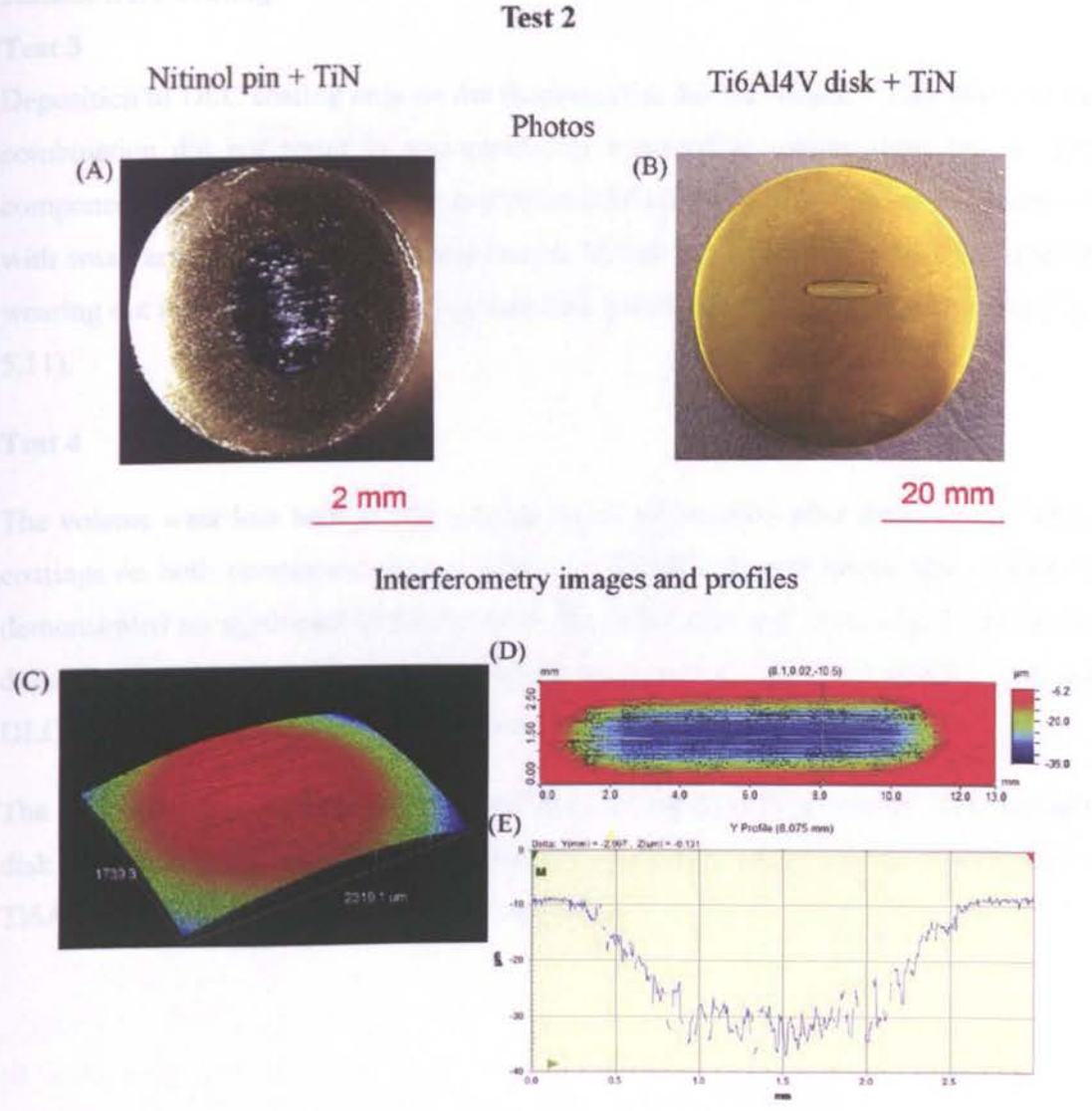

Figure 5.10. Photos and interferometry images of pins (A and C respectively) and disks (B and D respectively) and depth profiles of disks (E) of Nitinol (pin) - Ti6Al4V (disk) friction combination with TiN coating deposited both on disk and pin counter-parts (Test 2) after wear test termination at 0.85 million cycles

5.3.2.2. DLC coating

Test 3

Deposition of DLC coating only on the titanium disk for the Nitinol – Ti6Al4V friction combination did not result in gravimetrically measurable volume wear loss of any components until the wear test termination at 0.85 million cycles. This is in agreement with small area of wear damage observed on Nitinol pin and no signs of DLC coating wearing out or delamination from titanium disk after 0.85 million cycles of testing (fig. 5.11).

Test 4

The volume wear loss both of Nitinol pins and titanium disks after deposition of DLC coatings on both components in the Nitinol – Ti6Al4V friction combination (Test 4) demonstrated no significant difference with the initial uncoated state (fig. 5.12) due to delamination of DLC coating during the first stages of the test. After 10,000 cycles the DLC coating delaminates completely from the disc and pin.

The appearance of wear surface on the Nitinol pin and deep wear scar on the titanium disk after the test was terminated was similar to that observed for the uncoated Nitinol – Ti6Al4V friction combination (fig. 5.13 and 4.4).

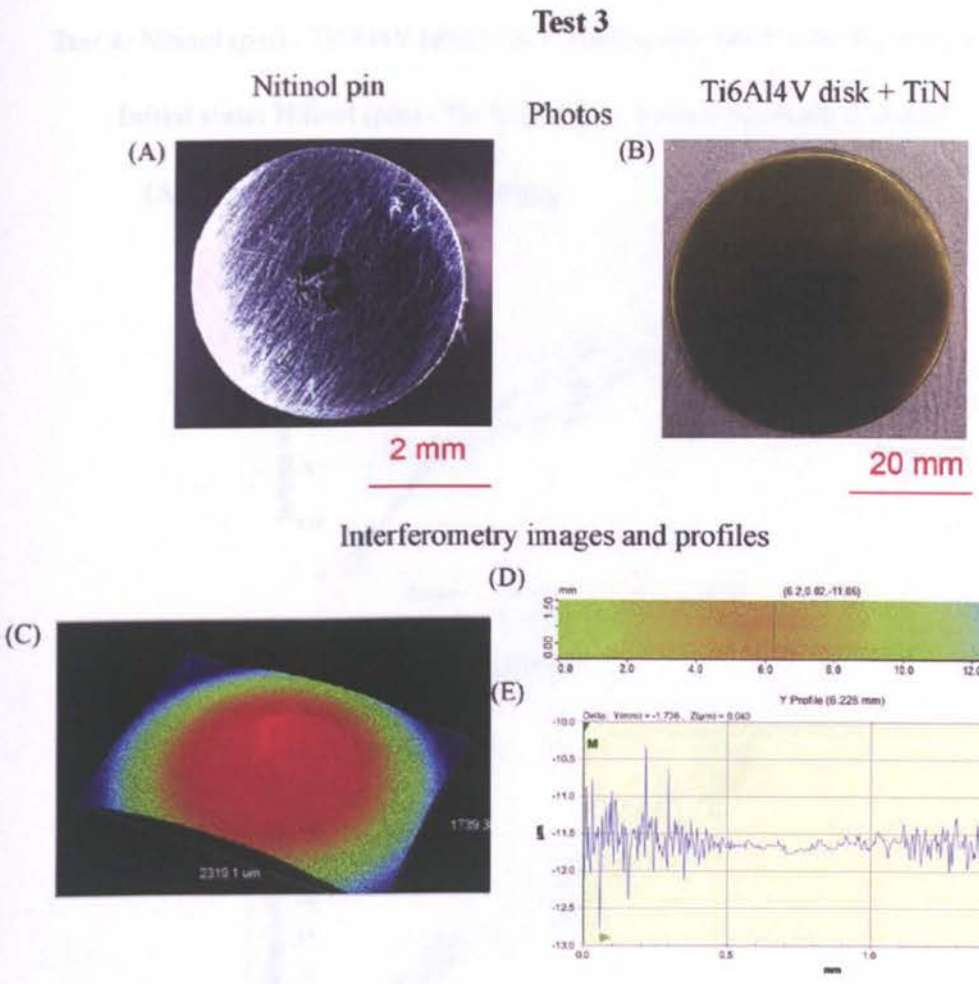

Figure 5.11. Photos and interferometry images of pins (A and C respectively) and disks (B and D respectively) and depth profiles of disks (E) of Nitinol (pin) - Ti6Al4V (disk) friction combination with DLC coating deposited only on titanium disk counter-part (Test 3) after wear test termination at 0.85 million cycles

Test 4: Nitinol (pin) - Ti6Al4V (disk), DLC coating deposited on both components

Initial state: Nitinol (pin) - Ti6Al4V (disk), both components uncoated

(A)

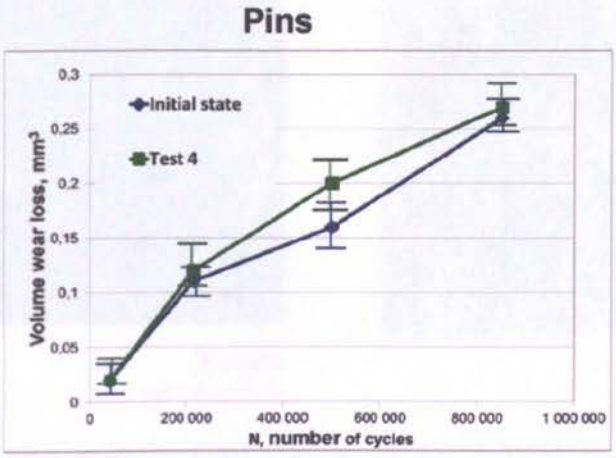

(B)

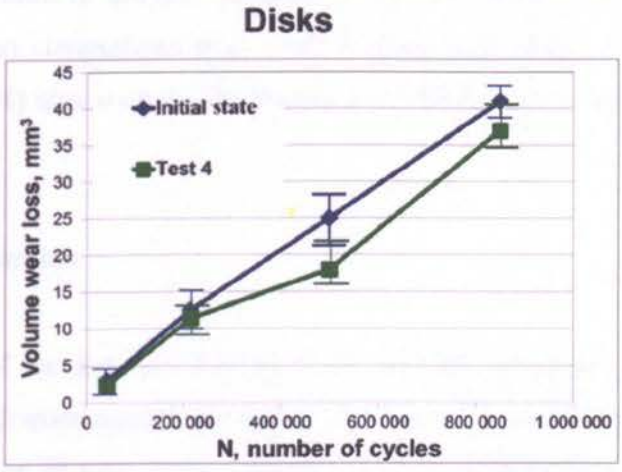

Figure 5.12. (A) Volume wear loss of pins and (B) disks in of the Nitinol (pin) – Ti6AL4V (disk) friction combination after deposition of DLC coating on both titanium disk and Nitinol pin compared with initial uncoated state.

Test 4

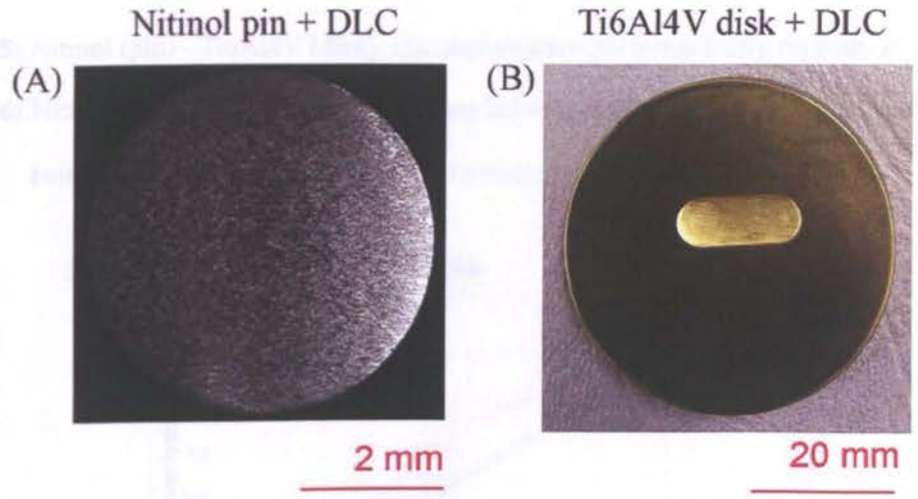

Figure 5.13. (A) Photos of pin and (B) disk of for the Nitinol (pin) - Ti6Al4V (disk) friction combination components with DLC coating deposited on both disk and pin counter-parts (Test 4) after wear test termination at 0.85 million cycles

5.3.2.3. Ion implantation

Test 5 and 6

Ion implantation of the titanium disk (Test 5) or both components (Test 6) for the Nitinol – Ti6Al4V friction combination does not improve wear resistance of the Nitinol pin and the reduction of wear on the titanium disk is minor and does not reduce wear by more than 20% compared to initial uncoated state (fig. 5. 14).

The appearance of a wear surface on the Nitinol pins and wear scars on the titanium disk both for Test 5 and 6 after wear test termination are similar to that observed for the uncoated Nitinol – Ti6Al4V friction combination (fig. 5.15 and 4.4).

Test 5: Nitinol (pin) - Ti6Al4V (disk), ion implantation performed only on titanium disk

Test 6: Nitinol (pin) - Ti6Al4V (disk), ion implantation performed on both components

Initial state: Nitinol (pin) - Ti6Al4V (disk), both components uncoated

(A)

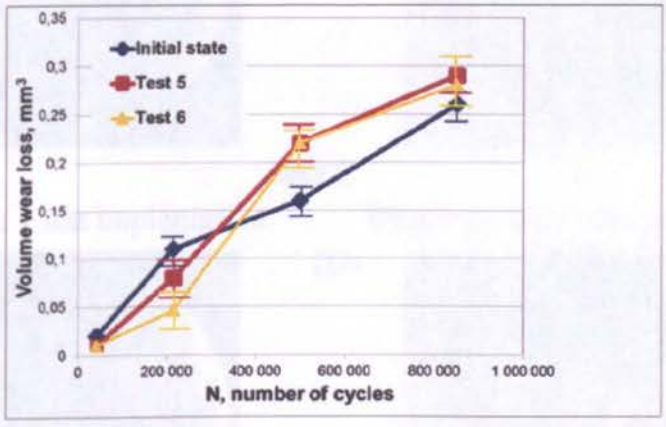

(B)

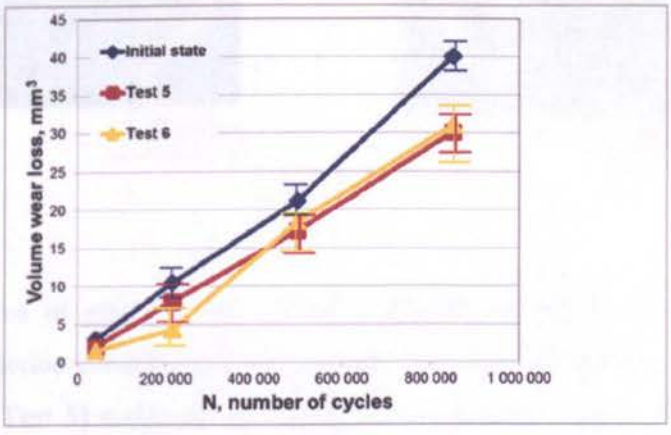

Figure 5.14. (A) Volume wear loss of pins and (B) disks for the Nitinol (pin) – Ti6AL4V (disk) friction combination after ion implantation of titanium disk (Test 5) and both components (Test 6) compared with initial uncoated state.

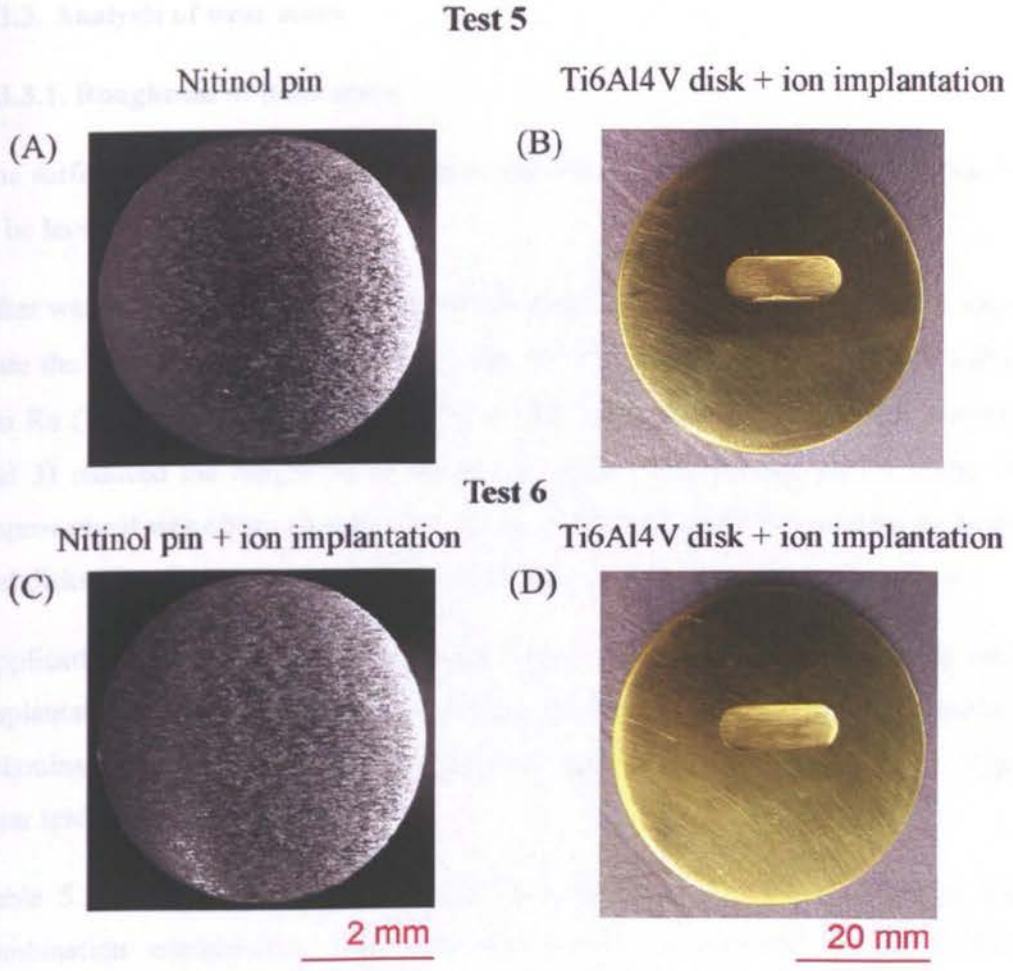

Figure 5.15. Photos of pins (A and C) and disks (B and D) for the Nitinol (pin) - Ti6Al4V (disk) friction combination components with ion implantation performed only on titanium disk (Test 5) and both on disk and pin components (Test 6) after wear test termination at 0.85 million cycles

5.3.3. Analysis of wear scars

5.3.3.1. Roughness of wear scars

The surface roughness of all components was measured before wear test and was found to be less than 0.04 μm Ra.

After wear testing of the Nitinol – Ti6Al4V friction combination in the initial uncoated state the roughness of the Nitinol pin was 0.17±0.05 and the titanium disk 0.26±0.05 μm Ra (Table 5.3). Deposition of DLC or TiN coatings only on titanium disk (Test 1 and 3) reduced the roughness of the surface, after wear testing, by 1.5 times; better improvement was observed with DLC (Test 3). Deposition of TiN coating on both pins and disks (Test 3) resulted in increasing of wear scar roughness on both surfaces.

Application of DLC on both counter-parts (Test 4) and surface modification with ion implantation (Test 5 and 6) did not change wear scar roughness, possibly due to the delamination of coating or wearing of the ion implanted layers during the early stages of wear testing.

Table 5.3 Roughness of wear scars on the Nitinol (pin) – Ti6Al4V (disk) friction combination components after wear test termination at 0.85 million cycles in dependence of surface treatments

	Ra, μm	
	Pin	Disk
Before wear testing		
Initial (uncoated) state	0.17±0.05	0.26±0.05
Test 1 (TiN only on titanium disk)	0.1±0.02	0.1±0.02
Test 2 (TiN on both components)	0.3±0.05	0.9±0.1
Test 3 (DLC only on titanium disk)	0.03±0.01	0.01
Test 4 (DLC on both components)	0.18±0.03	0.32±0.04
Test 5 (Ion implantation only on titanium disk)	0.17±0.05	0.28±0.04
Test 6 (Ion implantation on both components)	0.18±0.04	0.27±0.05

5.3.3.2. SEM and EDAX analysis of wear scars

5.3.3.2.1. TiN coating

Test 1

SEM and EDAX analysis of wear scars on the Nitinol pin in Nitinol – Ti6Al4V friction combination when a TiN coating was deposited only on the titanium disk (Test 1) revealed abrasive wear damage without any adhesion deposits from titanium counter-part (fig. 5.16A). Wear scars on the titanium disks also demonstrate mild abrasion grooves without deposition on the Nitinol counter-body (fig.5.16B). EDAX analysis of the worn area on the disk revealed both nitrogen and titanium peaks and the absence of aluminium or vanadium, indicating the presence of a TiN layer after termination of the wear test (fig. 5.16C).

Test 2

With TiN coating deposited on both the Nitinol pins and titanium disks (Test 2) early delamination of TiN layer from the Nitinol pins was seen at inspection after 5,000 cycles (fig. 5. 17A). This was further confirmed by EDAX analysis which revealed titanium and nitrogen peaks on the TiN coated area of the Nitinol pins with titanium and nickel peaks in the areas where delamination occurred (fig. 5.18). On the other hand, only slight and gradual wearing of the TiN coating on the titanium disk was observed in this friction combination (fig. 5.17B). After 100,000 cycles of testing the TiN coating was observed to completely wear through to the substrate. Upon termination of the test at 0.85 million cycles, wear scars both on the Nitinol pin and the titanium disk demonstrated severe abrasion grooves (fig. 5.17C,D), which correlates with the high roughness of wear scars measured for this friction combination (Table 5.3).

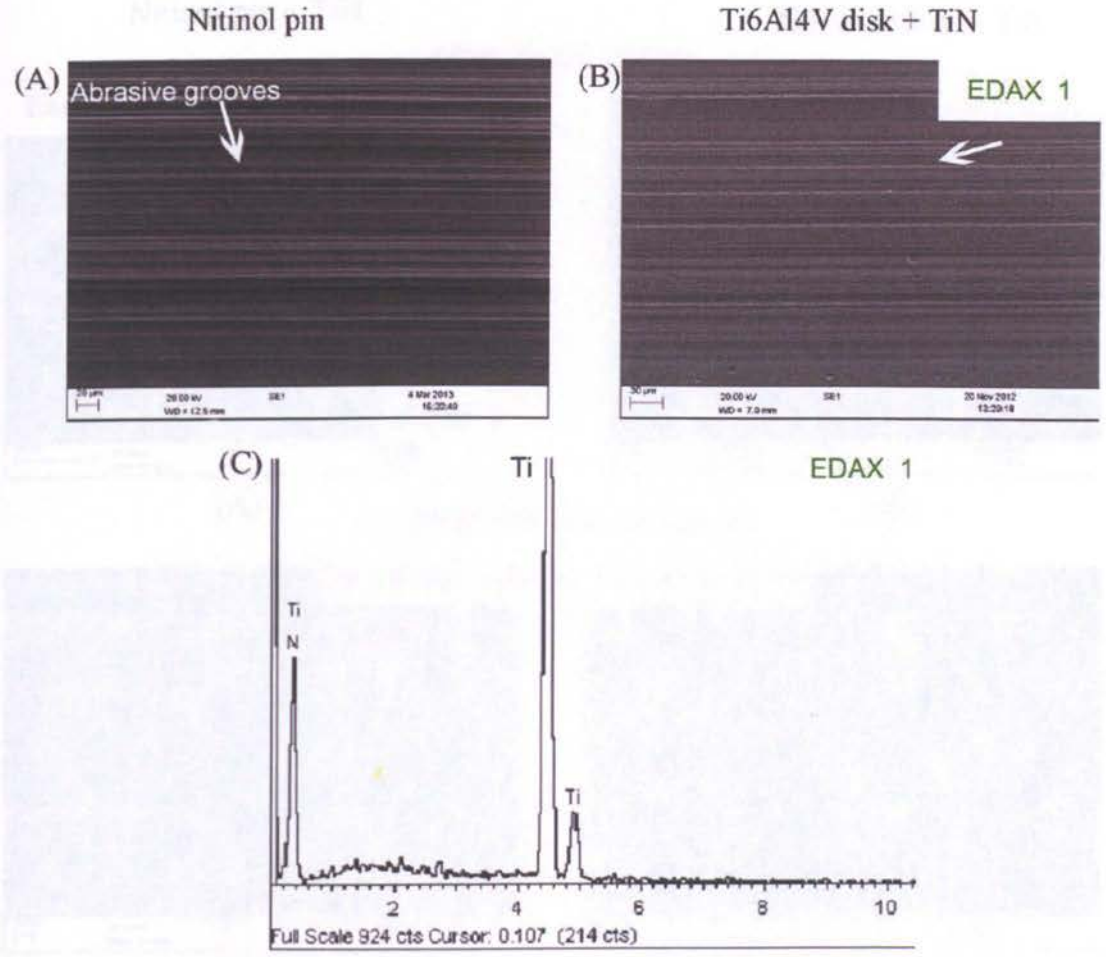

Figure 5.16. (A) SEM micrographs of wear scars on Nitinol pin and (B) titanium disk in Nitinol – Ti6Al4V friction combination in case of TiN coating deposition only on titanium disk counterpart (Test 1) and (C) EDAX analysis of the disk surface after termination of the wear test at 0.85 million cycles.

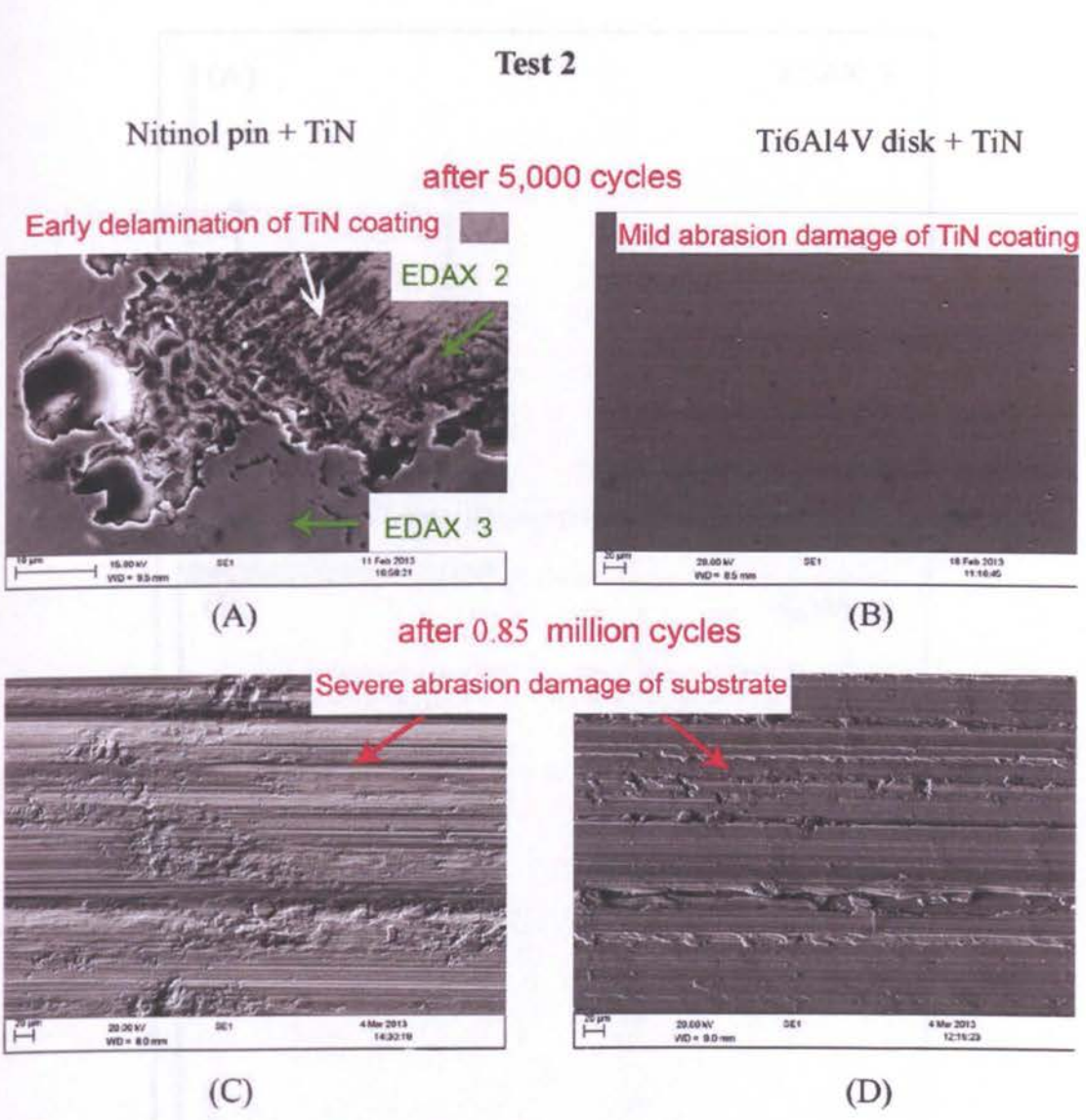

Figure 5.17. (A,C) SEM micrographs of wear scars on Nitinol pin and (B,D) titanium disk for the Nitinol – Ti6Al4V friction combination in the case of deposition of TiN coating on both pin and disk counterparts (Test 2): A and B) after 5,000 cycles; C and D after wear test termination at 0.85 million cycles

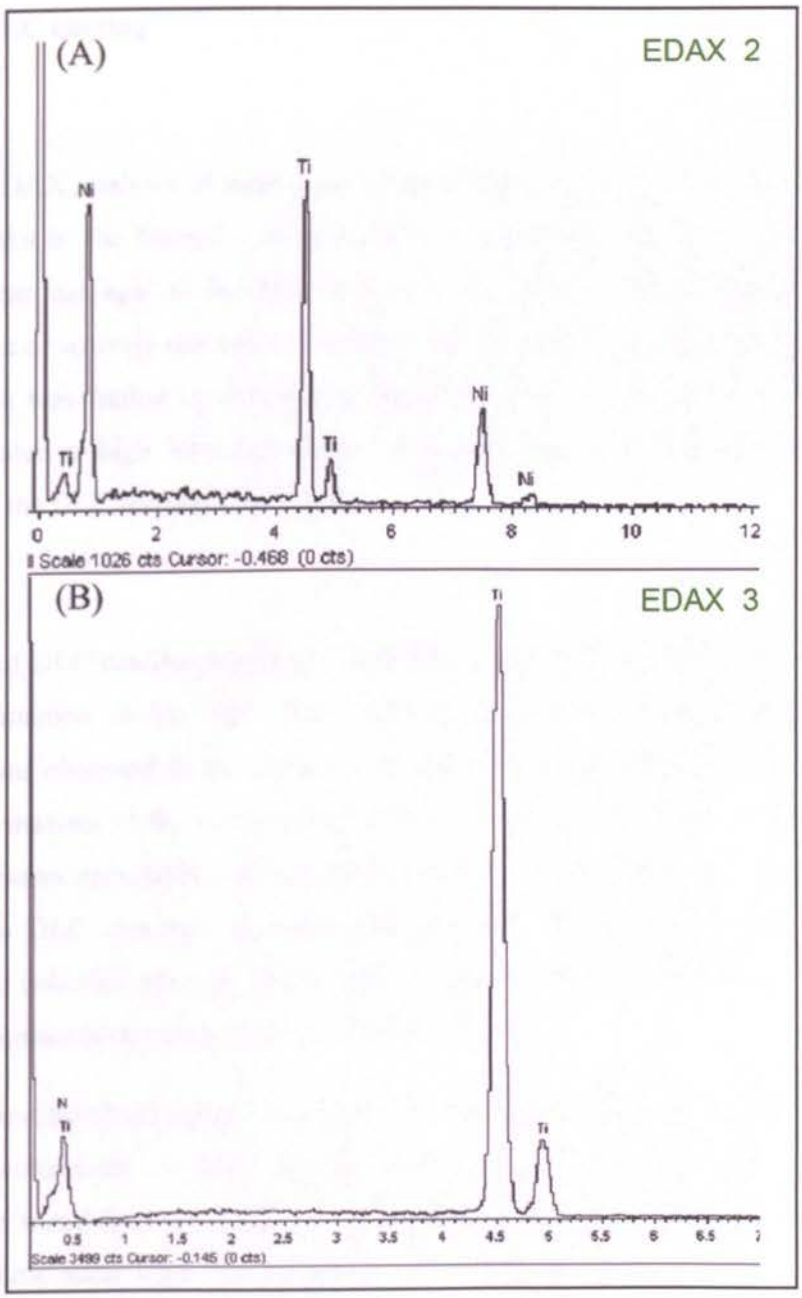

Figure 5.18. EDAX analysis of wear scars on Nitinol pins in Nitinol – Ti6Al4V friction combination after 5,000 cycles of testing in case of deposition of TiN coating on both Nitinol pin and titanium disk counterpart (Test 2): A) area with delaminated TiN coating; B) area with retained TiN coating

5.3.3.2.2. DLC coating

Test 3

SEM and EDAX analysis of wear scars on the Nitinol pins with DLC coating only on titanium disks in the Nitinol – Ti6Al4V friction combination (Test 3) revealed mild abrasive wear damage of the Nitinol pins at the end of the test (fig. 5.19A). No delamination or wearing through of the DLC coating was seen on the titanium disk (fig. 5.19B). This was further confirmed by EDAX analysis of the wear track on the disk which revealed a high intensity signal of carbon and silicon, which are the main elements of the DLC coating (fig. 5.19C).

Test 4

In the case of DLC coating deposition on both the Nitinol pin and titanium disk (Test 4) local delamination of the DLC layer both from the Nitinol pin and titanium disk substrates was observed on the surface at inspection after 5,000 cycles (fig. 5. 20A and B). EDAX analysis of the delaminated areas (fig. 5.21) demonstrated silicon peaks as well as elements associated with the substrate. This might imply that the silicon under layer of the DLC coating has better adhesion with Nitinol and titanium substrates compared to cohesion strength of the DLC coating itself. After 10,000 cycles the DLC coating delaminates completely from the disc and pin.

After wear test termination the Nitinol pin and titanium disk demonstrated adhesion and abrasion mechanisms of wear damage similar to those observed for this friction combination tested in its initial uncoated state (fig. 5. 20 and 4.4) which correlates with similar volume wear loss and roughness of wear scars measured for these friction combinations.

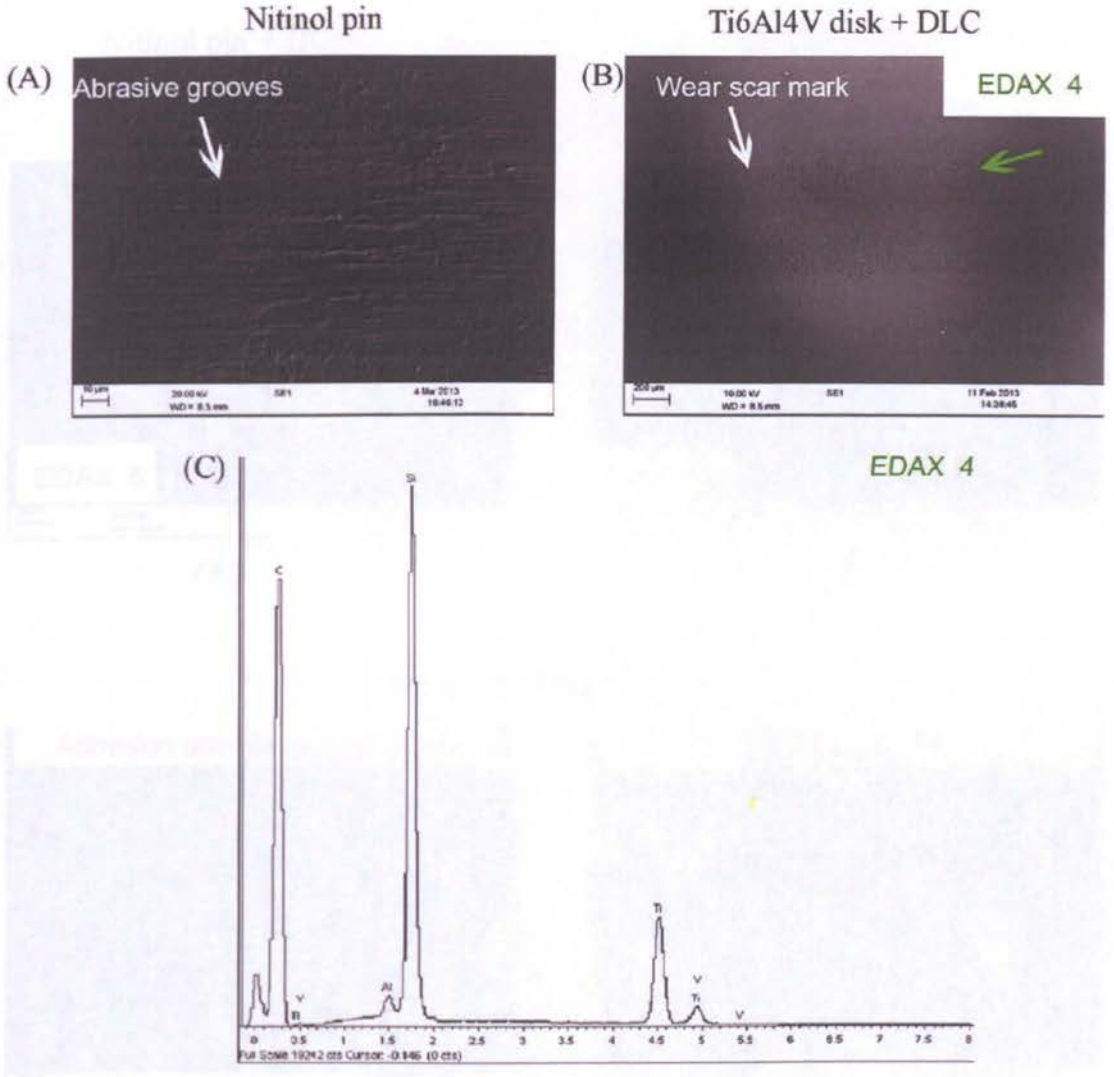

Figure 5.19. (A) SEM micrographs of wear scars on Nitinol pin and (B) titanium disk for the Nitinol – Ti6Al4V friction combination in the case of DLC coating deposition only on the titanium disk counterpart (Test 3) and (C) EDAX analysis of wear track on the disk after termination of the wear test at 0.85 million cycles

Test 4

Nitinol pin + DLC

Ti6Al4V disk + DLC

after 5,000 cycles

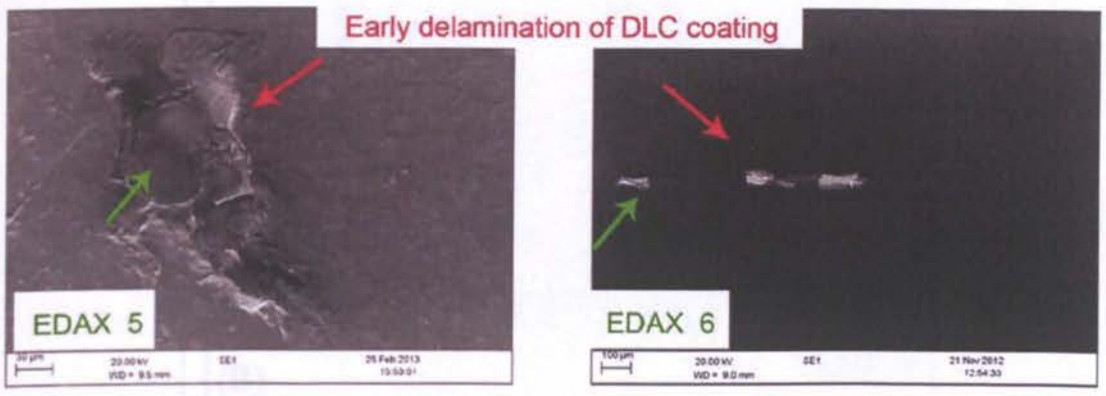

(A) (B)

after 0.85 million cycles

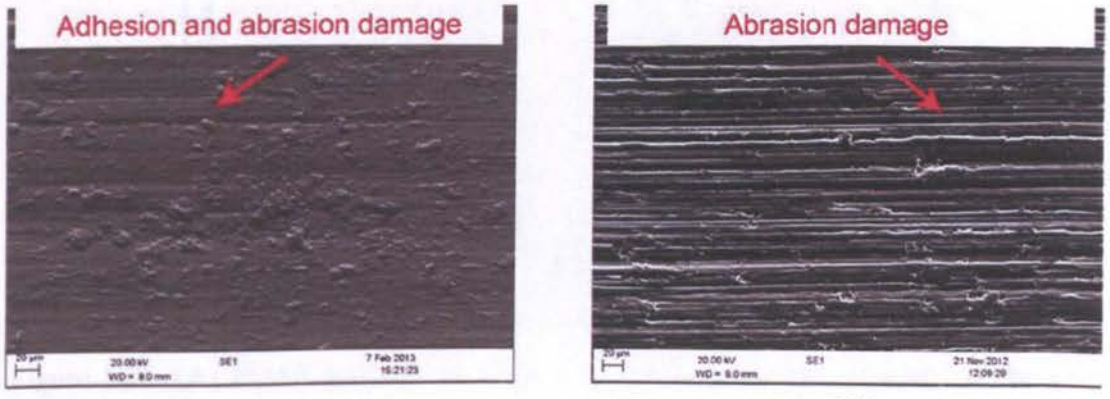

(C) (D)

Figure 5.20. (A,C) SEM micrographs of wear scars on Nitinol pin and (B,D) titanium disk for the Nitinol – Ti6Al4V friction combination in case of deposition of DLC coating on both pin and disk counterparts (Test 4): A) and B) after 5,000 cycles; C and D after wear test termination at 0.85 million cycles

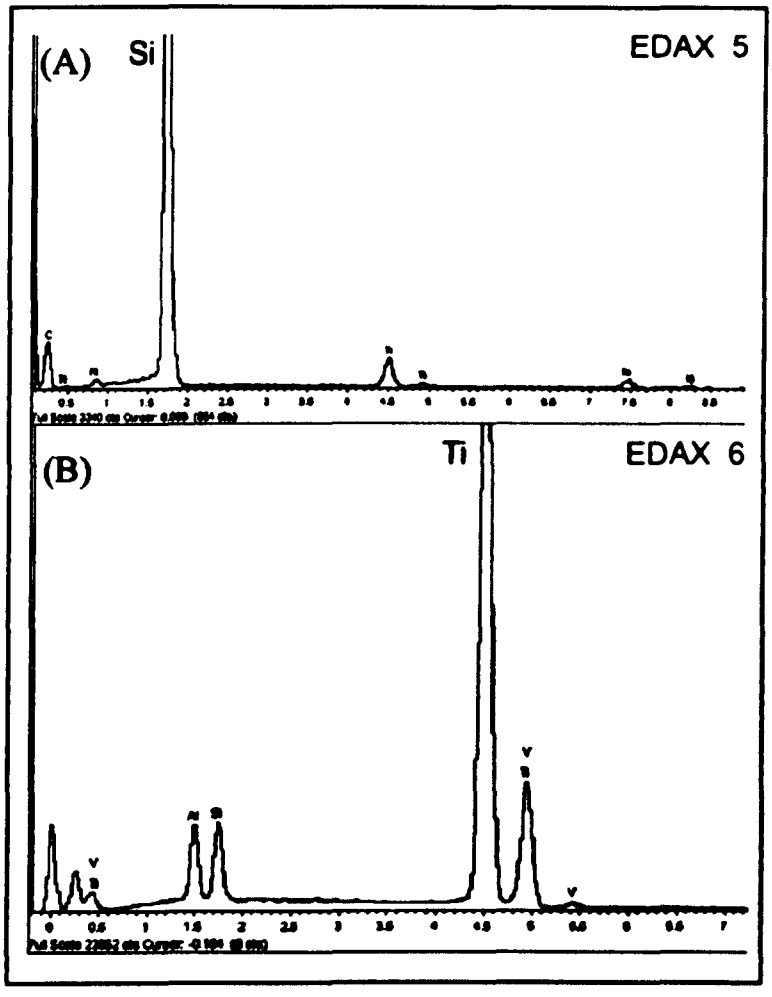

Figure 5.21. (A) EDAX analysis of areas with delaminated DLC coating on the wear scars on Nitinol pins and (B) titanium disk for the Nitinol – Ti6Al4V friction combination (Test 4). After 5,000 cycles of testing silicon peaks in addition to substrates elements can be seen.

5.3.3.2.3. Ion implantation

No difference in the wear scar damage mechanisms was seen when ion implantation with nitrogen ions was performed only on the titanium disks (Test 5) or on both components (Test 6) at the end of wear testing (fig. 5.22, 5.23 and 4.4).

SEM examination of Nitinol pins and titanium disks (Test 6) revealed that the ion implanted layer had worn away after 2,000 cycles of testing (fig. 5.23) from both pin and disk components which is probably the reason why this treatment had limited effect on the wear resistance for the Nitinol – Ti6Al4V friction combination.

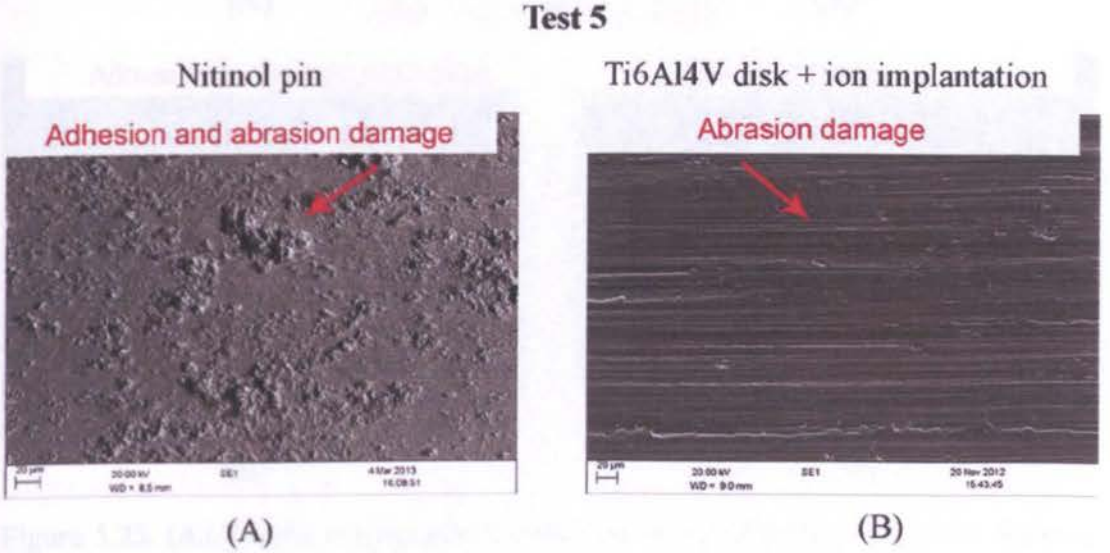

Figure 5.22. (A) SEM micrographs of wear scars on the Nitinol pin and (B) the titanium disk for the Nitinol – Ti6Al4V friction combination components in the case of ion implantation performed only on titanium disk (Test 5) after wear test termination at 0.85 million

Test 6

Nitinol pin + ion implantation Ti6Al4V disk + ion implantation

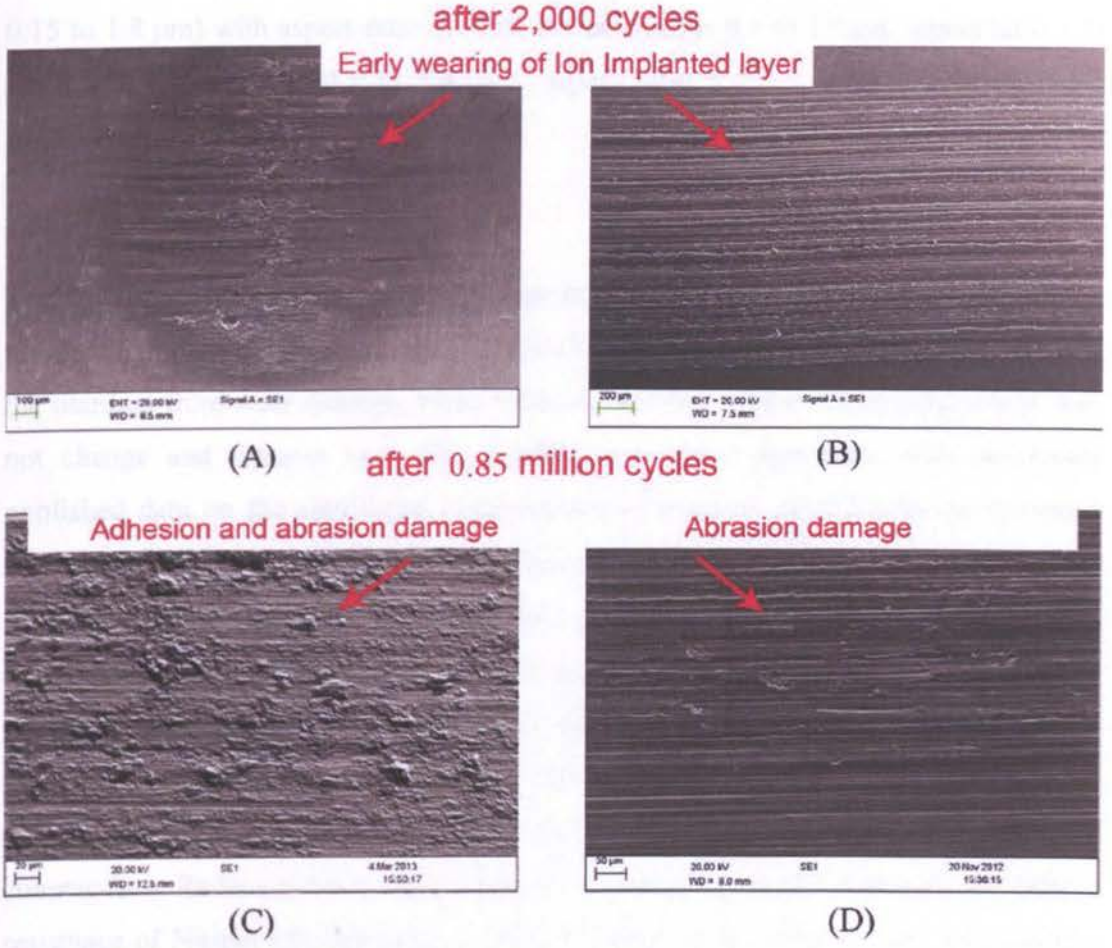

Figure 5.23. (A,C) SEM micrographs of wear scars on Nitinol pin and (B,D) titanium disk in Nitinol – Ti6Al4V friction combination in case of ion implantation performed on both components (Test 6): A) and B) after 2,000 cycles; C and D after wear test termination at 0.85 million cycles (C and D)

5.3.4. Analysis of wear particles

The serum lubricating the articulating components was collected for particle analysis for Tests 1-6. However, after enzymatic digestion (this procedure is described in Chapter II) the wear particles were not seen in the scanning electron microscopy for Test 1, 2 and 3 which had low volumes of wear loss. Wear particles generated by Test 4 (DLC coating deposition on both the Nitinol pin and titanium disk components in the Nitinol – Ti6Al4V friction combination) and by Test 5 and 6 (ion implantation of the

components) had titanium, aluminium and vanadium with no traces of nickel and demonstrated no difference to those collected from Nitinol – Ti6Al4V friction combination in initial uncoated state. The average size of particles was 0.35 μm (range 0.15 to 1.8 μm) with aspect ratio 1.3-1.5; 0.3 μm (range 0.1 to 1.9μm, aspect ratio 1.2-1.4 and 0.3 μm (range 0.1 to 1.9 μm), aspect ratio 1.2 – 1.5 for Test 4, 5 and 6 respectively.

5.4. DISCUSSION

The results of the wear tests revealed that the deposition of TiN coating only on the titanium component for the Nitinol – Ti6Al4V friction combination effectively protects the titanium from wear damage, while volume wear loss of the Nitinol component does not change and remains low. This finding is in good agreement with previously published data on the significant improvement of titanium alloy's wear performance after titanium nitride layer deposition (Shenhar et al., 2000 & Wang et al., 2013). The roughness of the wear scar on the Nitinol component in this friction combination is approximately two fold lower compared to test results for the Nitnol – Ti6Al4V combination in the uncoated state which might be explanted by improving galling resistance of the titanium counter-face after TiN coating deposition (Wiklund & Hutchings, 2001). This results in the elimination of titanium transfer onto the Nitinol counter-face. Reducing the Nitinol roughness is beneficial to the corrosion and fatigue resistance of Nitinol (Shabalovskaya, 2002, Polinsky et al., 2004 & Patel and Gordon, 2006) and should be used for spinal Nitinol rods in humans.

Deposition of TiN on both counter-faces of the Nitinol – Ti6Al4V friction combination reduced the volume wear loss of both components on the first stage of testing. However, early delamination of the TiN coating from the Nitinol pin was observed. This resulted in intensive wear damage of the TiN layer on the titanium component, which might possibly be explained by the abrasive effect of the delaminated titanium nitride wear particles. The high roughness of the wear scars both on Nitinol and titanium counter-faces measured 0.3±0.05 and 0.9±0.1 for Nitinol and Ti6Al4V respectively and suggests that the TiN coating should not be considered further for the Nitinol – Ti6Al4V friction combination in spinal rods in humans.

Deposition of DLC coating only on the titanium components of the Nitinol – Ti6Al4V friction combination improved the wear performance of both titanium and Nitinol. When comparing the effect of DLC and TiN coating, Costa et al. (2010) also reported better performance of DLC coated components. Chakravarthy et al. 2012 reported an improved finish of the uncoated counter-face with DLC coating, which could be explained by the lower roughness and friction coefficient seen for DLC layers compared to TiN (Wiklund & Hutchings, 2001) and possibly a difference in lubrication associated with DLC(Costa et al., 2010).

In the case of deposition of DLC coating on both counter-faces for the Nitinol – Ti6Al4V friction combination, local spallation of the DLC layers from both surfaces was seen after inspection at 5,000 cycles. After 10,000 cycles the coating completely delaminated from the wear track. After this the wear performance of this friction combination did not differ from Nitinol – Ti6Al4V pair in the initial uncoated state. Scratch tests revealed that the adhesion of the DLC coating on the titanium substrate is about two-fold lower compared to that of TiN. Indirectly this is associated with the gradual wearing through of the TiN coating on Ti6Al4V while, catastrophic failure associated with delamination of the DLC was observed. A similar difference in the adhesion strength for TiN and DLC coatings was also reported by Wang & Liu (2011) for Nitinol substrates. The introduction of a silicon interlayer is often reported to improve adhesion of the DLC layers (Sui & Cai, 2006 & Ohgoe et al., 2006). Nevertheless, EDAX analysis of delaminated areas carried out in the current work revealed high intensity silicon peaks, indicating that adhesion between the silicon sub-layer and the substrate is better than that between silicon and carbon layers. Similar findings were reported by Hauert et. al. (2012) who examined failed explanted diamond-like carbon TiAlV coated hip joint balls. Both of these observations imply that further research on the improvement of DLC layers adhesion is required before these coatings are used commercially for spinal growth rods. DLC coating may be restricted to components where edge effects can be eliminated, for example in the case where there is high congruency between opposing surfaces.

Ion implantation was revealed not to affect the wear performance of Nitinol for the Nitinol – Ti6Al4V friction combination, while only a 20% reduction in volumetric wear was found for the titanium counter-part. Similar findings of nitrogen implantation effect were reported by Bowsher et al. (2005) who tested ion implanted metal-on-metal

friction combination for CoCr. Luo & Ge (2009) applied ion implantation in order to improve the fretting wear resistance of Ti6Al4V which showed similar effects. In the current study the wearing out of the ion implanted layer on the Nitinol substrate was seen after only 2,000 cycles, implying that ion implantation may not be effective for Nitinol rods.

5.5. CONCLUSIONS

1. The current research shows that the deposition of TiN (titanium nitride) on only the titanium component of the Nitinol – Ti6Al4V friction combination can significantly improve its wear performance due to protection of the titanium alloy component.
2. It was found that the deposition of DLC (diamond like carbon) on only the titanium component of the Nitinol – Ti6Al4V friction combination can improve wear performance of both titanium and Nitinol in this friction combination. However, the low adhesion strength of commercially applied DLC coatings might restrict its application only to coating components where edge effects can be eliminated, for example in cases where there is high congruency between opposing surfaces. Alternatively, improving the adhesion strength of this coating to the titanium alloy would also be beneficial.
3. Deposition of TiN or DLC coating on both components for the Nitinol – Ti6Al4V friction combination was found not to be effective due to delamination or wearing through of the coatings.
4. It was found out that ion implantation does not improve the wear performance of the Nitinol – Ti6Al4V friction combination due to wearing through of the modified layer during the early stages of sliding contact.

CHAPTER 6

GENERAL DISCUSSION AND CONCLUSIONS

6.1. GENERAL DISCUSSION

Surgery for early onset scoliosis requires the use of instrumentation for the spine where no fusion is permitted and which should also enable the growth of the pediatric spine. The drawback of growing rods (Ellipse Technologies, USA) is the requirement for periodical extension (at least twice a year) (Akbarnia et al., 2013).

However in sliding devices, such as the Shilla (Medtronic, USA) or LSZ-4D (Conmet, Russia) systems this procedure is not necessary since only one or a few fixtures are locked whilst the other fixtures permit the rods to slide and therefore allows spine growth to continue (McCarthy et al., 2014 and Sampiev et al., 2013).

The LSZ-4D sliding device consists of two 6x4 mm rods which are rectangular in cross-section with fixture units consisting of hooks, screws and clips. For the first stage of implantation all the hooks are attached to the vertebrae using screws. Following this the rods are introduced and fixed to the hooks with attaching clips, which are fitted to the screws using nuts. Tightening of the nuts provides the correction of the scoliotic deformation.

Locked clips which stiffly attach the rods to the hooks and thus to the spine are used on one thoracic spine level, while other clips are unlocked (sliding). Unlocked clips have deeper grooves which allow the rods to slide in the longitudinal direction and permits growth of the patient's spine without extension of the implanted device (Sampiev et al., 2013).

One of the main long-term complications after the implantation of spinal devices associated with the instrumentation failure is fatigue fracture of the rods as a result of cyclic loading. (McCarthy et.al., 2013 & Sedra et.al., 2013).

The main activities which impose cyclic loads on spinal implant rods are walking and physical exercise like flexion, extension and lateral bending (Rohlmann et.al., 1997 & Rohlmann et.al., 2002). Walking imposes frequently repeated loads with low amplitude bending moments of 0.5-1 Nm (Rohlmann et.al., 1997), while less frequent flexion or lateral bending moments may be up to 4 Nm (Rohlmann et.al., 2002).

For this reason the fatigue resistance of spinal implant constructs is required to be tested according to the standards ASTM F1717-14 or ISO 12189:2008. For fusion spinal

devices, this test imitates cyclic loading of the rods in spinal constructs during the first two years after surgery, which is the normal time required for the arthrodesis to take place. Since the sliding LSZ-4D device for early onset scoliosis is fusion-less and arthrodesis may not take place for 5-8 years, while the patient's spine is growing, an increase the probability of fatigue fracture is likely and these spinal devices require higher fatigue resistance of the rod material.

In addition, the absence of arthrodesis may result in an increase in the movement of the rods against fixtures during activity. For this reason evaluation of wear scars on the instrumentation is required after the fatigue testing of spinal implant assemblies and this is also required for fusion devices (ASTM F1717-2014). It might also be hypothesized that unlocked (sliding) fixtures in LSZ-4D devices allowing greater movement of the rods against clips and hooks especially due to flexion, extension and lateral bending movements, would result in extensive wear damage of these components resulting in the generation of wear debris and metallosis related complications. However, since growing guidance sliding devices have only recently appeared on the market, there is no information in the literature on their long-term performance. For this reason analysis of long-term complications and examination of retrievals is necessary.

Among traditional metallic materials used for growing guided instrumentation, titanium alloys are the most biocompatible and are now widely used as the material for both fixtures and rods. Nitinol, an alloy with Shape Memory effect could be another promising material for rods in scoliosis instrumentation (Yoshihara, 2013). Nitinol has an ability to return to its preconfigured shape at body temperature and has been used for scoliosis correction. It has the potential benefit of a more gradual and sustained correction (Cheung et al., 2011), while the lower modulus of elasticity may reduce adjacent segment degeneration (Kim et.al., 2007). The strain-controlled fatigue performance of Nitinol is comparable to that of Ti alloys (Kollerov et.al., 2008), however, further optimization of its fatigue performance would still be beneficial for the safe use of rods made of this material in fusion-less spinal instrumentation. On the other hand, wear resistance of Nitinol in a biological environment is poorly understood, especially in combination with Ti counter-body which is the main material used for the fixtures. Nevertheless taking into consideration the poor wear resistance of Ti alloys (Brunette et.al., 2001), it might be hypothesized that improvements in the wear resistance of Ti counter-parts would be needed.

The aim of this thesis was to investigate complications associated with implantation of the growth-guidance sliding LSZ-4D system in pediatric patients and to investigate fatigue and wear resistance of Nitinol and titanium alloys as alternative materials for this application.

The first step of this research thesis was the evaluation of complications associated with the LSZ-4D device and analysis of its retrieved components. Analysis of complications for the 25 patients investigated in my study with implanted growth-guidance LSZ-4D devices revealed that the fatigue fracture of the rods was observed in 4 patients, which is 16% of all patients studied. Such frequency of rod breakage is similar to that reported for other fusion-less instrumentation used for EOS treatment by McCarthy et al. (2013) for Shilla sliding rods made of SS (Medtronik, USA) and by Sedra et al. (2013) for Ti growing rods (Ellipse Tech, USA). On the other hand, frequency of implant failure reported for fusion instrumentation is only up to 3% (Mok et.al., 2009 & Richards, 2014), which is much lower compared with fusion-less devices for EOS. Obviously the absence of fusion in these devices results in a higher range of spine mobility during functional activity and increased fatigue fracture. These observations imply that the material used for rods in fusion-less LSZ-4D devices should have high fatigue resistance. Therefore if Nitinol is going to replace titanium alloy in rods then establishing the optimal structure of Nitinol which provides high fatigue resistance would be beneficial.

Another complication for LSZ-4D devices was found to be metallosis associated with the formation of seromas and fistulas. These complications occurred in 5 out of the 25 patients investigated (20% of patients). There was a statistically significant increase in titanium and vanadium ions in the whole blood of the 25 patients with implanted LSZ-4D devices, which was 2.8 fold for titanium and 4 fold for vanadium.

No statistically significant difference was observed for aluminum content due to wide variation in the levels detected. The concentration of vanadium ions in the blood is higher than that of titanium and does not reflect the ratio of these elements in titanium alloy, which contains 6wt.% of Al and 4wt.% of V.

Similar findings were reported by Cundy et al. (2013) who carried out prospective studies involving pediatric patients treated for scoliosis using fusion instrumentation made of Ti-6wt.%Al-7wt.%Nb implanted on 9 spine levels. These revealed 2.4 and 5.9 fold increases in levels of titanium and niobium respectively and no statistical difference for aluminum content after 1 year follow-up. Kasai et al. (2003) and Richardson at al. (2008) studied adult patients with titanium instrumentation fixed in 2 or 3 levels of the lumbar spine for 5 and 2.2 years respectively and reported a 3.5-4.5 fold and 3.6 fold increases in titanium content in the blood serum. These results are similar to those revealed in my study, revealing that the blood metal content after implantation of growth-guidance sliding LSZ-4D devices are no higher than with traditional fusion instrumentation.

The results of this study indicate that the content of metal ions in the blood of patients with implanted sliding LSZ-4D devices who developed seromas and fistulas were no higher compared with patients who did not develop these complications. This implies that the metal ions content in the blood of patients with spinal instrumentation may not be relevant for predicting the incidence of local complications such as the development of seromas or fistulas.

Histology observations of the tissues revealed high content of metal debris, macrophages and even necrosis in one patient in my series, which has previously been reported to be associated with an adverse inflammatory reaction of tissues to excessive metal debris (Betts et.al., 1992). It might be hypothesized that the accumulation of metal debris in para-spinal tissues is the reason for the local complications. However, further work devoted to the measurement of metal ions in these tissues, compared with that previously reported in literature, is necessary to support this hypothesis.

Analysis of retrieved components of sliding LSZ-4D devices revealed that the volume wear rate of the whole device was 12.5 mm^3 per year from which 5mm^3 per year is derived from the rod and 7.5 mm^3 per year is contributed by fixtures (hooks and clips). These wear rates are similar to values (15-26 mm^3 per year) reported for metal-on-metal THR made of cobalt chromium alloy that failed because of aseptic loosening due to osteolysis, psuedotumour formation and tissue necrosis (Lord et al., 2011, Morlock et al., 2008; Witzleb et al., 2009; McKellop et al., 2008).

No osteolysis or psuedotumour formation was seen in any patients in my study after implantation of sliding spinal LSZ-4D device, which might be explained by the higher biological compatibility of Ti6Al4V titanium debris from spinal implants compared with CoCr alloy debris generated by THR implants (Brunette et.al., 2001). However, high content of metal debris in para-spinal tissues surrounding the LSZ-4D device and the development of seromas or fistulas indicate that the wear resistance of the material used for this instrumentation should be improved.

An investigation of the wear resistance of Nitinol against titanium alloy (Ti6Al4V) in the simulated body is required if a Nitinol rod is to be used in future applications. Additionally, excessive wear debris generated by the fixtures (hooks and clips) may also be reduced using wear-resistant coatings on the titanium components in LSZ-4D spinal instrumentation.

Research carried out in the next phase of this research and reported in Chapter 3 of this thesis was devoted to investigation of the influence of Nitinol structure, including increased dislocation density, size of Ni-rich (Ni_4Ti_3 and Ni_3Ti_2) particles, and volume fraction of Ti-rich ($Ti_4Ni_2O_x$) inclusion on its fatigue behaviour. Analysis of complications after implantation of sliding LSZ-4D devices carried out in Chapter 2 revealed a high rate (16% of patients) of the fatigue failures of titanium (Ti6Al4V) rods similar to other fusion-less spinal instrumentation. For this reason optimization of the bulk structure of Nitinol for improving its fatigue performance was studied in this chapter.

A significant effect of the bulk structure on Nitinol fatigue performance has been indicated by many researchers (Melton & Mercier, 1979, Heckmann & Hornbogen, 2002; Pelton, 2011; Wagner at al., 2010; Wessels et al., 2012). Nevertheless, due to the complex structure of the Nitinol (the phase composition of which may include austenite, martensite, Ti-rich and Ni-rich particles) and difficulties in revealing the influence of each structural parameter separately, predicting its fatigue behaviour is problematic. As a result, adjusting thermo-mechanical treatment is recommended (Pelton, 2011). An attempt to explain the complex influence of various structural parameters was made by Melton and Mercier (1979) and Heckmann & Hornbogen (2002), who assumed that the larger strains in Nitinol are accommodated by stress-induced martensitic transformation leading to better fatigue performance. However until the present time these

considerations have been qualitative. In the current study the author of this thesis used critical strain (ε_{cr}), defined as the maximal strain from which the Nitinol sample can completely recover after unloading and heating to the temperature higher than A_f (Kollerov et al., 2008), as a quantitative value of the strain which Nitinol can accommodate by stress-induced martensitic transformation. This allowed a comparison of critical strains and fatigue resistance of Nitinol samples in different structural states.

Since patient activity may impose both low stain (walking, amplitude of bending moment of 0.5-1 Nm, equivalent to strains up to 0.5% (Rohlmann et.al., 1997) and high stain amplitude (flexion or extension, amplitude of bending moment is up to 4 Nm, equivalent to strains up to 1.5-2%; Rohlmann et.al., 2002) loads on the spine, a comparison of fatigue performance of Nitinol samples was carried out for high and low strains.

The results showed that that the creation of a microstructure which provides high values of critical strain improves high strain amplitude fatigue resistance of Nitinol. A modified Coffin-Manson equation is proposed for describing and predicting the strain-controlled Nitinol fatigue behaviour in the area of high strain amplitudes, where the critical strain serves as one of the coefficients. However, no correlation between Nitinol fatigue resistance and the critical strain was observed for the low amplitude testing conditions. In this case, Nitinol performance may be improved by the precipitation of nanosize Ni-rich particles, creation of increased dislocation density, or by decreasing the $Ti_4Ni_2O_x$ inclusion volume fraction.

The aim of Chapter 4 of this thesis was to investigate the wear resistance of the Nitinol – Ti6Al4V friction combination in a biological environment using in vitro pin-on-disk wear test methodology. Wear performance of this friction combination was compared with that of Ti6Al4V - Ti6Al4V and CoCr – Ti6Al4V combinations which are commonly used for scoliosis instrumentation. Nitinol wear debris from rods articulation against titanium fixtures in sliding spinal devices can be the source of undesirable Ni ions. At the same time wear resistance of Nitinol is not completely understood and is reported to be from several to hundreds folds higher compared to titanium and SS (Zhang et al., 2009, Li et al., 2000, Linmao et. al. and Lui & Lee, 2009). However, in most reported experiments Nitinol was usually tested against dissimilar materials such as tungsten carbide and little is known about its wear

behaviour in body-simulated fluid when sliding against titanium, which is the predominant material used for fixtures in spinal devices.

Diluted bovine serum was used in this work for the in-vitro pin-on-disk wear test as it is normally recommended as a body-simulated fluid for the testing of the articulation for hip and knee prostheses (ISO 14242-1 and ISO 14243-1). The same media was later adopted for the testing of spinal total disk prostheses, with a note in the rationale statement indicating that information on the composition of fluid a spinal device is lacking (ISO 18192:2011).

The wear mechanism and the size and shape of wear particles of titanium against titanium friction pair after in-vitro wear tests was similar to the wear mechanisms identified from retrieved titanium components of LSZ-4D device. The wear debris isolated from tissues adjacent to these implants was similar to that seen in the in vitro, which implies that this test can be used for the comparison of wear resistance of metal materials in spinal instrumentation.

Results of wear tests from the current research showed that the wear resistance of Nitinol tested against titanium alloy (Ti6Al4V) in the simulated body environment is approximately 100 fold greater compared to titanium alloy (Ti6Al4V) and are similar to that of CoCr alloy.

The wear rate of titanium pins in the Ti6Al4V-Ti6Al4V friction combination is $33\pm2mm^3$ per 0.5 million cycles, which corresponds approximately to wear debris produced by two rods of LSZ devices after 6.5 years of implantation revealed in Chapter 2 of my work. If the observed 0.15 mm^3 volume wear loss of Nitinol pins after 0.5 million cycles were to occur in-vivo after 6.5 years, which represents relatively low wear, then the biological problems associated with metallosis would be expected to reduce as the release of debris is limited.

However, results of the current wear testing revealed that the Nitinol – Ti6Al4V combination still generates high volumetric wear associated with debris release from the Ti6Al4V component. It might therefore be concluded that further protection of titanium components with wear resistant coatings would be beneficial.

In the final stage of the current research work reported in Chapter 5, I studied the influence of TiN (titanium nitride), DLC (diamond like carbon) coatings and ion implantation on the wear resistance of Nitinol – Ti6Al4V friction combination.

It was revealed in Chapter 4 of this work that Nitinol – Ti6Al4V friction pair may still generate wear debris associated with the wear damage of titanium component, which means that wear debris may be generated in-vivo by the fixtures (hooks and clips) in LSZ-4D sliding device which are likely to be predominantly made of titanium alloy. For this reason different wear resistant coatings and surface treatments were used to improve the overall performance of Nitinol – Ti6Al4V friction pair.

TiN coatings are well known for increasing the hardness and corrosion resistance of titanium alloys (Shenhar et al., 2000 & Wang et al., 2013). DLC is reported to provide a lower friction coefficient compared to TiN when deposited on titanium or Nitinol substrates (Wiklund & Hutchings, 2001 & Costa et al., 2010) and that is considered to improve their wear performance. However DLC adhesion to substrates is still problematic. Ion implantation is a surface treatment and has good bonding with both titanium and Nitinol due to the implantation of ions inside the substrate and an absence of a distinct boundary between the modified layer. Improvement of wear of metal-on-metal friction pairs for ion implantation was less compared to DLC and TiN (Bowsher et al., 2005), nevertheless, it was also used for wear tests in the current research since thin nano-layers are more likely to withstand the high strains encountered by Nitinol during functional loading. However, the wear performance of the Nitinol – Ti6Al4V friction combination using TiN and DLC coatings or ion implantation application has not previously been investigated.

Tests carried out in the current research have revealed that the deposition of TiN (titanium nitride) only on the titanium component in the Nitinol – Ti6Al4V combination significantly improved the wear performance and this was associated with the protection of titanium whereas DLC improved the wear performance of both titanium and Nitinol. Scratch tests revealed that adhesion of the DLC coating on the titanium substrate is about two fold lower compared to that of TiN. Indirectly, this correlates with the gradual wearing through of the TiN coating on Ti6Al4V while, catastrophic failure associated with delamination of DLC was observed. A similar difference in the adhesion strength for TiN and DLC coatings was also reported by Wang & Liu (2011)

for Nitinol substrates. Introduction of a silicon interlayer is often reported to improve adhesion of DLC layers (Sui & Cai, 2006 & Ohgoe et al., 2006). Nevertheless EDAX analysis of delaminated areas carried out in the current work revealed a high intensity of silicon peaks, indicating that adhesion between silicon sub-layer and substrate is better that between silicon and carbon layers. Similar findings were reported by Hauert et. al. (2012) who examined failed explanted diamond-like carbon TiAlV coated hip joint balls. Both of these observations imply that further research for the improvement of DLC layers adhesion is required before commercially available DLC coatings can be used for spinal grow rods. DLC coating may be restricted to components where edge effects can be eliminated, for example in cases where there is high congruency between opposing surfaces.

The effect of ion implantation or deposition of TiN or DLC coatings on both counter parts was found to be less effective in protecting the Nitinol – Ti6Al4V friction combination components.

The results of the current study demonstrated that the implantation of sliding LSZ-4D devices for EOS results in metallosis which is some cases led to the development of complications including seromas and fistulas formation observed in 5 out of 25 patients investigated. The volume wear rate measured for the retrieved components of the LSZ-4D devices was found to be 12.5 mm^3 per year. Fatigue fracture of rods was observed in 4 patients. A statistically significant increase in titanium and vanadium ions in the whole blood of all 25 patients with implanted LSZ-4D devices was revealed. With a view to replacing titanium alloy rods with Nitinol, an investigation on the fatigue behaviour and wear resistance of Nitinol was carried out. It revealed that creating a microstructure which increased deformation due to a martensitic phase transformation improved high strain amplitude fatigue resistance of Nitinol, whereas precipitation of nanosize Ni-rich particles and reduction of $Ti_4Ni_2O_x$ inclusions resulted in an increase in low strain fatigue resistance. Wear resistance of Nitinol tested against titanium alloy (Ti6Al4V) in the simulated body environment is approximately 100 fold greater compared to titanium alloy (Ti6Al4V) and is similar to that of CoCr alloy. Nevertheless, the Nitinol – Ti6Al4V combination still generates high volumetric wear associated with debris release form the Ti6Al4V component. It was found that the deposition of TiN (titanium nitride) only on the titanium component in the Nitinol – Ti6Al4V combination significantly improved the wear performance and this was associated with the protection

of titanium component whereas DLC can improve wear performance of both titanium and Nitinol.

6.2. GENERAL CONCLUSIONS

1. Analysis of retrieved components of LSZ growth-guidance sliding devices (LSZ-4D) made from titanium alloy (Ti6Al4V) implanted in paediatric patients together with associated tissues showed metallosis which is in some cases led to the development of complications including seromas and fistulas formation. These complications occurred in 5 out of the 25 patients investigated. The volume wear rate measured for the retrieved components of LSZ-4D devices was found to be 12.5 mm^3 per year from which 5mm^3 per year is derived from the rod and 7.5 mm^3 per year is contributed by fixtures. Fatigue fracture of rods was observed in 4 patients. A statistically significant increase in titanium and vanadium ions in the whole blood of all 25 patients with implanted LSZ-4D devices was revealed. A statistically significant content of titanium was also revealed in patients who developed seroma and fistulas complications ($p=0.035$).

2. An investigation on the fatigue behaviour of Nitinol revealed that creating a microstructure which increased deformation due to a martensitic phase transformation improved high strain amplitude fatigue resistance of Nitinol, whereas, precipitation of nanosize Ni-rich particles and decreasing$Ti_4Ni_2O_x$inclusions resulted in an increase in low strain fatigue resistance.

3. The wear behaviour of Nitinol in comparison to titanium alloy was investigated and showed that the wear resistance of Nitinol tested against titanium alloy (Ti6Al4V), in the simulated body environment is approximately 100 fold greater compared to titanium alloy (Ti6Al4V) and is similar to that of CoCr alloy. Nevertheless, Nitinol – Ti6Al4V combination still generates high volumetric wear with debris release from the Ti6Al4V component.

4. Coating and treating the surface with TiN (titanium nitride), DLC (diamond like carbon) coatings and ion implantation of nitrogen ions in some instances reduced the wear. The deposition of TiN (titanium nitride) only on titanium component in Nitinol – Ti6Al4V combination significantly improved the wear performance. This was associated with the protection of the titanium component whereas the application of DLC improved wear performance of both titanium and Nitinol. Ion implantation or deposition of TiN or DLC coatings on both counter parts was found to be less effective

6.3. RECOMMENDATIONS FOR FUTURE WORK

The current study demonstrated that metallosis and blood ion levels increased when titanium growing rods LSZ-4D were used. One of the recommendations resulting from the current work is that once patients have stopped growing, these rods be replaced by rods with locked fixtures to prevent wear and metallosis. The author further suggests that patients with growing spinal rods be evaluated for metal ion levels and that depending on these the titanium rods could be replaced by Nitinol.

One of the limitations of the current work was the replication of the in-vivo loads by pin-on-disk wear test. It would be necessary in the future to test the Nitinol rods attached to titanium fixtures with coatings in a more realistic in-vivo environment using spine simulator that imposed moments and loads associated with a typical walking/movement cycle. This test could also investigate the fatigue resistance of the material, as well as its wear performance. Resistance to corrosion is important and the current research did not measure this. Future work in this area is considered to be highly beneficial. The effect of Nitinol rods on strains developed in adjacent vertebra would also be an important future study as the author suggests that this may reduce adjacent segment problems due to the reduced stiffness of rods made from Nitinol.

Bibliography

Adler, P. (2007) Martensite transformation and fatigue behaviour of nitinol. In: Jerina, K., Mitchell, M., Woods, T. & Berg, B. (edt.), *Fatigue and Fracture of Medical Metallic Materials and Devices: 2nd Volume.* West Conshohocken: ASTM International. P. 150

Akbarnia, B., Kabirian, N., Pawelek, J., Thompson, G., Emans, J., Sponseller, P. & Skaggs, D. (2013a) *Long-term results of growing rod treatment in 201 patients: is there a difference between etiologies?* 50th anniversary International Phillip Zorab Symposium. June 20-21, 2013. London:BSRF.

Akbarnia, B. A., Cheung, K., Noordeen, H., Elsebaie, H., Yazici, M., Dannawi, Z., & Kabirian, N. (2013b) *Next generation of growth-sparing techniques: preliminary clinical results of a magnetically controlled growing rod in 14 patients with early-onset scoliosis.* Spine. Vol.38 No.8, pp.665-670.

Alves-Claro, A. P. R., Claro, F. A. E., & Uzumaki, E. T. (2008) *Wear resistance of nickel–titanium endodontic files after surface treatment.* Journal of Materials Science: Materials in Medicine. Vol. 19 No.10, pp.3273-3277.

ASTM G99-05 (2010) *Standard Test Method for Wear Testing with a Pin-on-Disk Apparatus.* Section Three – Corrosion of metals; Wear and Erosion. West Conshohocken, PA: ASTM International.

ASTM F2082-06 (2006) *Standard Test Method for Determination of Transformation Temperature of Nickel-Titanium Shape Memory Alloys by Bend and Free Recovery.* Section 13.01 Medical and Surgical Materials and Devices- West Conshohocken, PA: ASTM International.

ASTM F1717-2014 (2014) *Standard Test Methods for Spinal Implant Constructs in a Vertebrectomy Model.* Section 13.01 Medical and Surgical Materials and Devices- West Conshohocken, PA: ASTM International.

Benzel, C (2001) *Biomechanics of spine stabilization.* New York: Thieme.

Betts, F., Wright, T., Salvati, E. A., Boskey, A., & Bansal, M. (1992). *Cobalt-alloy metal debris in periarticular tissues from total hip revision arthroplasties: metal contents and associated histologic findings.* Clinical orthopedics and related research, Vol. 276, pp. 75-82.

Betz, R., Kim, J., D'Andrea L. (2003) *An innovative technique of vertebral body stapling for the treatment of patients with adosolent idiopathic scoliosis: a feasibility, safety and utility study.* Spine. Vol. 28, pp. 255-65.

Betz, R. R., Ranade, A., Samdani, A. F., Chafetz, R., D'Andrea, L. P., Gaughan, J. P., ... & Mulcahey, M. J. (2010). *Vertebral body stapling: a fusionless treatment option for a growing child with moderate idiopathic scoliosis.* Spine. Vol. 35 No. 2, pp. 169-176.

Bondy, K., Williams, C. & Luedemann R. (1991) *Stress-enhanced ion release – the effect of static loading.* Biomaterials, Vol. 12, pp. 627–639.

Bowsher, J. G., Hussain, A., Williams, P., Nevelos, J., & Shelton, J. C. (2004) *Effect of ion implantation on the tribology of metal-on-metal hip prostheses.* The Journal of arthroplasty. Vol. 19 No.8, pp.107-111.

Brunette, D., Tengvall, P., Textor, M. & Thomsen, P. (2001) *Titanium in medicine.* Berlin: Springer-Verlag Berlin Heidelberg.

Burton, C. (2010) *The infamous transitional syndrome* [Internet], Minnesota. Available at: www.burtonreport.com/infspine/SurgStabilTransitionalSynd.htm (Accessed 10 October 2011).

Campbell, J. & Estey, M. (2013) *Metal ion release from hip prostheses: cobalt and chromium toxicity and the role of the clinical laboratory.* ClinChem Lab Med. Vol. 51 No. 1, pp.213-220

Chandran, M., Bhattacharya, S. S., Rao, M. S., & Kamaraj, M. (2012) *A comparative study on wear behavior of TiN and diamond coated WC–Co substrates against hypereutectic Al–Si alloys.* Applied Surface Science. Vol. 261, pp.520-527.

Cheung, K., Kuong, E., Samartzis, D. & Yeung, K. (2011). *Assessing the Safety and Efficacy of a Novel Superelastic Rod in Comparison to Conventional Titanium Rod for Scoliosis Curve Correction.* 18th International Meeting on advanced spinal techniques. July 13-16, 2011. Copenhagen: SRS.

Chuprina, V. G., & Shalya, I. M. (2002) *Reactions of TiNi with oxygen.* Powder Metallurgy and Metal Ceramics. Vol. 41 No.1-2, pp.85-89.

Cluett, J. (2012) Arthrodesis – *Fusion of a Joint* [Internet], Available at: http://orthopedics.about.com/od/arthritistreatment/g/arthrodesis.htm (Accessed 5 August 2014).

Coffin, L. & Tavernelli, J. (1959) Trans. Am. Inst. Min. Eng. Vol. 215, pp.794–807.

Costa, M. Y. P., Cioffi, M. O. H., Voorwald, H. J. C., & Guimaraes, V. A. (2010) *An investigation on sliding wear behavior of PVD coatings.* Tribology International. Vol. 43 No. 11, pp.2196-2202.

Cox, A., Baxevanis, T., Lagoudas, D., Rahim, M. & Eggeler,G. (2013) *Finite element analysis on the driving force for fatigue crack formation near particle/viod assemblies in NiTi.* International Conference on Shape Memory and Superelastic Technologies. May 20-24, 2013. Prague, Czech Republic, ASM International.

Cundy, T., Antoniou, G. , Sutherland, L. & Cundy, P. (2013) *Serum Titanium, Niobium, and Aluminum Levels After Instrumented Spinal Arthrodesis in Children.* Spine. Vol. 38 No.7, pp.564-570.

Cunningham, B., Orbegoso, C. & Dmitriev, A. (2003) *The effect of spinal instrumentation particulate wear debris: an in vivo rabbit model and applied clinical study of retrieved instrumentation cases.* Spine J. Vol.3, pp.19–32.

Davis, J.R. (2003) *Handbook of materials for medical devices.* Materials Park, OH: ASTM International. 341p.

Dearnaley, G., & Arps, J. H. (2005) *Biomedical applications of diamond-like carbon (DLC) coatings: A review.* Surface and Coatings Technology. Vol. 200 No.7, pp.2518-2524.

Doorn, P., Campbell, P. & Worrall, J. (1998) *Metal wear particle characterization from metal on metal total hip replacements: transmission electron microscopy study of periprosthetic tissues and isolated particles.* J Biomed Mat Res. Vol. 42 No. 1, pp.103-111.

Duerig, T., Pelton, A. & Stöckel, D. (1999) *An overview of nitinol medical applications.* Materials Science and Engineering: A. Vol. 273, pp.149-160.

Eggeler, G., Hornbogen, E., Yawny, A., Heckmann, A., & Wagner, M. (2004) *Structural and functional fatigue of NiTi shape memory alloys.* Materials Science and Engineering: A. Vol. 378 No.1, pp.24-33.

Es-Souni, M., Es-Souni, M., & Fischer-Brandies, H. (2005) *Assessing the biocompatibility of NiTi shape memory alloys used for medical applications.* Analytical and bioanalytical chemistry. Vol. 381 No.3, pp.557-567.

Filip, P., Lausmaa, J., Musialek, J. & Mazanec, K. (2001) *Structure and surface of TiNi human implants.* Biomaterials. Vol. 22, pp. 2131 – 2138.

Fredriksson, W., Malmgren, S., Gustafsson, T., Gorgoi, M., & Edström, K. (2012) *Full depth profile of passive films on 316L stainless steel based on high resolution HAXPES in combination with ARXPS,* Applied Surface Science. Vol. 258 No. 15, pp.5790-5797.

Gall, K., Tyber, J., Wilkesanders, G. & Robertson, S. (2008) *Effect of microstructure on the fatigue of hot-rolled and cold-drawn NiTi shape memory alloys.* Materials Science and Engineering A Vol. 486, pp. 389–403.

Gall, K., & Maier, H. J. (2002) *Cyclic deformation mechanisms in precipitated NiTi shape memory alloys.* Acta Materialia. Vol. 50 No. 18, pp.4643-4657.

Geetha, M., Singh, A. K., Asokamani, R., & Gogia, A. K. (2009) *Ti based biomaterials, the ultimate choice for orthopaedic implants–a review.* Progress in Materials Science. Vol. 54 No. 3, pp.397-425.

Gorinin, I. & Chechylin, B. (1990) *Titanium in industry.* Moscow: Industry Publisher. 399p.

Goyer, R. A., & Clarkson, T. W. (1996) Toxic effects of metals. In: *Klaassen, C. (eds.), Casarett & Doull's Toxicology. The Basic Science of Poisons.* McGraw-Hill Health Professions Division, pp. 811-868.

Granchi, D., Ciapetti, G., Savarino, L., Caledagna, D., Donati, M. & Pizzoferatto,A. (1996) *Assessment of metal extract toxity on human lymphocytes cultured in vitro.* J. Biomed. Mater. Res. Vol. 31, pp.183-191.

Guille, J., D'Andrea, L. and Berz, R. (2007) *Fusionless treatment of scoliosis.* Clinics of North America. Vol. 38, pp. 541-545.

Hallab, N., Cunningham, B. & Jacobs, J. (2003) *Spinal implant debris-induced osteolysis.* Spine Vol. 28(suppl), pp.125–38.

Harman, M. K., Banks, S. A., & Hodge, W. A. (1997) *Wear analysis of a retrieved hip implant with titanium nitride coating.* The Journal of arthroplasty. Vol. 12 No. 8, pp.938-945.

Hart, A., Sabah, S., Bandi, A., Maggiore, P., Tarassoli, P., Sampson, B., & A Skinner, J. (2011) *Sensitivity and specificity of blood cobalt and chromium metal ions for predicting failure of*

metal-on-metal hip replacement. Journal of Bone & Joint Surgery, British Volume. Vol. 93 No. 10, pp.1308-1313.

Hauert, R., Falub, C. V., Thorwarth, G., Thorwarth, K., Affolter, C., Stiefel, M. & Taeger, G. (2012) *Retrospective lifetime estimation of failed and explanted diamond-like carbon coated hip joint balls.* Acta biomaterialia, Vol. 8 No. 8, pp.3170-3176.

Heckmann, A. & Hornbogen, E. (2002) *Effects of thermomechanical pre-treatment on pseudo-elastic fatigue of a NiTi alloy.* Materials Science Forum. Vol. 394-5, pp. 325-328.

Herkowitz, H. N., Garfin, S. R., Eismont, F. J., Bell, G. R., & Balderston, R. A. (2011). *Rothman-Simeone The Spine: Expert Consult.* Elsevier Health Sciences.

ISO12189:2008 *Implants for surgery. Mechanical testing of implantable spinal devices. Fatigue test method for spinal implant assemblies using an anterior support.* Part 11.040.40: Implants for surgery, Prosthetics and Orthotics. Geneva, Switzerland: International Organization for Standardization.

ISO 14242 (2000) *Wear of total hip-joint prostheses - Implants for surgery, Prosthetics and Orthotics.* Geneva, Switzerland: International Organization for Standardization.

ISO 14243 (2006) *Wear of total knee-joint prostheses - Implants for surgery, Prosthetics and Orthotics.* Geneva, Switzerland: International Organization for Standardization.

ISO 4287 (1997) *Geometrical Product Specifications (GPS) -- Surface texture: Profile method -- Terms, definitions and surface texture parameters. Properties of surfaces.*Geneva, Switzerland: International Organization for Standardization.

ISO 4288 (1996) *Geometrical Product Specifications (GPS) -- Surface texture: Profile method -- Rules and procedures for the assessment of surface texture Properties of surfaces.*Geneva, Switzerland: International Organization for Standardization.

ISO 17853 (2011) *Wear of implant materials – Polymer and metal wear particles – Isolation and characterization.* Part 11.040.40: Implants for surgery, Prosthetics and Orthotics. Geneva, Switzerland: International Organization for Standardization.

ISO 18192-1 (2011) *Implants for surgery -- Wear of total intervertebral spinal disc prostheses* -- Part 1: Loading and displacement parameters for wear testing and corresponding environmental

conditions for test. Implants for surgery, Prosthetics and Orthotics. Geneva, Switzerland: International Organization for Standardization.

Karimi, S., Nickchi, T., & Alfantazi, A. M. (2012) *Long-term corrosion investigation of AISI 316L, Co–28Cr–6Mo, and Ti–6Al–4V alloys in simulated body solutions.* Applied Surface Science, Vol. 258 No.16, pp.6087-6096.

Karol, L., Johnston, C. & Mladenov, K. (2008) *Pulmonary function following early thoracic fusion in non-neuromuscular scoliosis.* The Journal of Bone & Joint Surgery. Vol. 90 No. 6, pp.1272-1281.

Kasai, Y., Iida, R., & Uchida, A. (2003) *Metal concentrations in the serum and hair of patients with titanium alloy spinal implants.* Spine. Vol. 28 No.12, pp.1320-1326.

Kollerov, M., Il'in, A., Radnaeyv, E., Sergeyv, S., Zagorodnyj, N. & Nevzorov, A. (2002) *Biologically and mechanically compatible implants from titanium nickelide in the treatment of damaged dorsal and lumbar spine.* The Bulletin of traumatology and Orthopedics, Vol. 2, pp. 19-26 (in Russian).

Kollerov, M., Il'in, A., Gusev, D. & Lamzin, D (2008) *Effect of Deformation Mechanisms on the Fatigue Properties of Metallic Materials.* Metally. Vol. 2008 No. 5, pp. 72-79.

Kim, Y., Zhang, H., Moon, B., Park, K., Ji, K., Lee, W., Oh, K., Ryu, G. & Kim, H. (2007) *Nitinol spring rod dynamic stabilization system and Nitinol memory loops in surgical treatment for lumbar disc disorders: short-term follow up.* Neurosurg Focus, Vol. 22(1), pp. 1-9.

Kim, G. S., Lee, S. Y., Hahn, J. H., Lee, B. Y., Han, J. G., Lee, J. H., & Lee, S. Y. (2002) *Effects of the thickness of Ti buffer layer on the mechanical properties of TiN coatings.* Surface and Coatings Technology. Vol. 171 No.1, pp.83-90.

Kumar, P. & Lagoudas, D. (2008) Introduction to Shape memory alloys. In: Lagoudas, D. (edt.), *Shape memory alloys: Modelling and engineering applications.* Texas: Springer, pp. 1-52. 435p.

Lacy, S. A., Merritt, K., Brown, S. A., & Puryear, A. (1996). *Distribution of nickel and cobalt following dermal and systemic administration with in vitro and in vivo studies.* Journal of biomedical materials research. Vol. 32 No. 2, pp.279-283.

Laka, A., Zagorodni, N., Sampiev M. & Abakirov, M. (2008) *Surgical treatment of various forms of scoliosis by the lamellar endocorrector «LSZ».* SICOT/SIROT 2008. XXIV Triennial World Congress. Hong Kong: Elsevier

Laka, A. (2011) Personal communication. 15 June 2011.

Laskovski, A. (2011) *Biomedical Engineering, Trends in Materials Science.* Intech. P. 564.

Lee, J., Billi, F. & Sangiorgio, S. (2008) *Wear of an experimental metal-on-metal artificial disc for the lumbar spine.* Spine. Vol. 3, pp.597-606.

Lenke, L. (2005) *Cotrel-Dubousset Horizon spinal instrumentation.* In: Kim, D., Vaccaro, A. & Fessler, R. (edt.), Spinal instrumentation: surgical techniques. New York: Thieme.

Li, D. (2000) *Development of novel wear-resistant materials: TiNi-based pseudoelastic tribomaterials.* Materials and Design. Vol. 2, pp. 551-555.

Lin, H. & Bumgardner, J. (2004) *Changes in the surface oxide composition of Co–Cr–Mo implant alloy by macrophage cells and their released reactive chemical species.* Biomaterials, Vol. 25 No. 7, pp. 1233-1238.

Long, M. & Rack, H (1998) *Titanium alloys in total joint replacement – a material science perspective.* Biomaterials. Vol. 19, pp. 1621-1629.

Lord, J., Langton, D. & Nargol, A. (2011) *Volumetric wear assessment of failed metal-on-metal hip resurfacing prostheses.* Wear Vol. 272, pp.79-87.

Lowery, P., & Roll, D. (1998) *Comparing the characteristics of surface-passivated and electropolished 316L stainless steel* [Internet], Available at: www.astropak.com/images/technical-papers/pdf-11.pdf (Accessed 12 October 2012)

Luo, Y., & Ge, S. (2009) *Fretting wear behavior of nitrogen ion implanted titanium alloys in bovine serum lubrication.* Tribology International. Vol. 42 No.9, pp.1373-1379.

Magaziner, R. S., Jain, V. K., & Mall, S. (2008) *Wear characterization of Ti–6Al–4V under fretting–reciprocating sliding conditions.* Wear. Vol. 264 No.11, pp.1002-1014.

Maletta, C., Sgambitterra, E., Furgiuele, F., Casati, R., & Tuissi, A. (2012) *Fatigue of pseudoelastic NiTi within the stress-induced transformation regime: a modified Coffin–Manson approach.* Smart Materials and Structures. Vol. 21 No. 11, 112001.

Manson, S. (1966) *Thermal stress and low cycle fatigue*. McGraw-Hill: New York

McCarthy, R., Johnson, C. & Armstrong, R. (2010) *Systems, devices and methods for stabilization of the spinal column*. Patent US7708762.

McCarthy, R. & McCullough, F. (2013) *Implant Revisions with Shilla Patients at Five Year Follow-Up: Lessons Learned*. 48th SRS Annual Meeting & Course in Lyon, France. P.229.

McCarthy, R., Luhmann ,S. & Lenke, L. (2014) *The Shilla Growth Guidance Technique for Early-Onset Spinal Deformities at 2-Year Follow-Up: A Preliminary Report*. J. Pediatr Orthop. Vol. 34, pp.1-7.

McKellop, H., Rostlund, R.& Ebramzadeh, E. (2001) Wear of titanium 6-4 alloy in laboratory tests and in retrieved human joint replacements. In: Brunette, D. (eds). *Titanium in medicine: material science, surface science, engineering*. Berlin: Springer;: 747-770.

Melton, K.N. & Mercier, O. (1979) *Fatigue of NiTi Thermoelastic Martinsites*. Acta Metallurgica. Vol.27, pp. 137-144.

Miao, W., Mi, X., Wang, X., Li, H. & Qi, B. (2007) *Effect of different surface treatments on fatigue life of NiTi wires*. Materials Science Forum. Vol. 561-5, 2265-68.

Mochida, Y., Bauer, T. & Nitto, H. (2000) *Influence of stability and mechanical properties of a spinal fixation device on production of wear debris particles in vivo*. J Biomed Mater Res .Vol. 53, pp.193–8.

Mok, J. M., Cloyd, J. M., Bradford, D. S., Hu, S. S., Deviren, V., Smith, J. A. & Berven, S. H. (2009). *Reoperation after primary fusion for adult spinal deformity: rate, reason, and timing*. Spine, Vol. 34 No.8, pp. 832-839.

Morlock, M., Bishop, N. & Zustin, J. (2008) *Modes of implant failure after hip resurfacing: morphological and wear analysis of 267 retrieval specimens*. J. Bone Joint Surg. Am. Vol. 90, suppl. 3, pp.89–95.

Morgan, N., Painter, J. & Moffat, A. (2003) *Mean Strain Effects and Microstructural Observations During In Vitro Fatigue Testing of NiTi*. International Conference on Shape Memory and Superelastic Technologies. May 5-8, 2003. Pacific Grove, ASM International.

Morgan, N., Wick, A., DiCello, J. & Graham, R.. (2006) *Carbon and oxygen levels in nitinol alloys and the implications for medical device manufacture and durability.* International Conference on Shape Memory and Superelastic Technologies. May 2006. Pacific Grove, ASM International.

Movshovich, I. (1964) *Scoliosis.Surgical anatomy and pathogenesis*. Moscow: Medicina.

Moumni, Z., Van Herpen, A., & Riberty, P. (2005) *Fatigue analysis of shape memory alloys: energy approach.* Smart materials and structures. Vol. 14 No. 5, S287.

Noordeen, H, Shah, S, Elsebaie, H., Garrido, E., Farooq, N., & Mukhtar, M. (2011) *In vivo distraction force and length measurements of growing rods: Which factors influence on the ability to lengthen?* Spine. Vol. *36 No.* 26, pp. 2299-2303.

Ohgoe, Y., Kobayashi, S., Ozeki, K., Aoki, H., Nakamori, H., Hirakuri, K. K., & Miyashita, O. (2006) *Reduction effect of nickel ion release on a diamond-like carbon film coated onto an orthodontic archwire*. Thin Solid Films. Vol. 497 No.1, pp.218-222.

O'Leary, P. T., Sturm, P. F., Hammerberg, K. W., Lubicky, J. P., & Mardjetko, S. M. (2011). *Convex hemiepiphysiodesis: the limits of vertebral stapling.* Spine. Vol. 36 No. 19, pp.1579-1583.

Oliveira, R. M., Fernandes, B. B., Carreri, F. C., Gonçalves, J. A. N., Ueda, M., Silva, M. M. N. F. & Otubo, J. (2012) *Surface modification of NiTi by plasma based ion implantation for application in harsh environments.* Applied Surface Science. Vol. 263, pp.763-768.

Otsuka, K. & and Wayman, C. (1998) *Shape Memory Materials*. Cambridge: Cambridge University Press.

Park, J. (2003) Metallic biomaterials. In: Park, J. & Bronzino, J. (eds.) *Biomaterials. Principles and applications.* Boca Raton: CRC Press, pp. 1-20.

Patel, M., Plumley, D. & Bouthot, R. (2006) *The significance of melt practice on fatigue properties of superelastic TiNi fine diameter wire*. International Conference on Shape Memory and Superelastic Technologies. May 7-11, 2006. Pacific Grove, ASM International.

Pelton, A. (2011) Nitinol Fatigue: A Review of microstructures and Mechanisms. *Journal of Materials Engineering and Performance*. Vol. 20, pp. 613-617.

Pelton, A. R., Schroeder, V., Mitchell, M. R., Gong, X. Y., Barney, M., & Robertson, S. W. (2008) *Fatigue and durability of Nitinol stents*. Journal of the mechanical behavior of biomedical materials. Vol. 1 No. 2, pp.153-164.

Pohl, M., Heßing, C., & Frenzel, J. (2004) *Electrolytic processing of NiTi shape memory alloys*. Materials Science and Engineering: A. Vol. 378 No. 1, pp.191-199.

Polinsky, M. A., Norwich, D. W., & Wu, M. H. (2000) *A study of the effects of surface modifications and processing on the fatigue properties of NiTi wire*. International Conference on Shape Memory and Superelastic Technologies. April 30 – May 4, 2000. Pacific Grove, ASM International.

Quain, L. (2005) *The role of phase transaction in the fretting behavior of NiTi shape memory alloy*. Wear. Vol. 259, pp.309-318.

Radin, E., Blaha, D., Rose, R. & Litsky, A. (1992) *Practical biomechanics of the orthopaedic surgeon*. 2nd edition. New York: Churchill Livingstone.

Reinoehl, M., Bradley, D., Bouthot, R. & Proft, J. (2000) *The influence of melt practice on final fatigue properties of superelasticNiTi wires*. International Conference on Shape Memory and Superelastic Technologies. 30 April – 4 May 2000. Pacific Grove, ASM International.

Richards, M. (2014) Unanticipated Revision Surgery in Adult Spinal Deformity: An Experience With 815 Cases at One Institution. *Spine*, Article in Press

Richardson, T. D., Pineda, S. J., Strenge, K. B., Van Fleet, T. A., MacGregor, M., Milbrandt, J. C.& Freitag, P. (2008) *Serum titanium levels after instrumented spinal arthrodesis*. Spine. Vol. 33 No.7, pp.792-796.

Rohlmann, A., Bergmann, G., & Graichen, F. (1997) *Loads on an internal spinal fixation device during walking*. Journal of biomechanics. Vol. 30 No. 1, pp.41-47.

Rohlmann A, Graichen F, Bergmann G. (2002) *Loads on an Internal spinal fixation device during physical therapy*. J Bone Joint Surg Am. Vol. 82, pp. 44-52.

Rohmiller, M. & Akbarnia, B. (2006) Infantile scoliosis. In: Heary, R. & Albert, T. (edt.), *Spinal deformities: the essentials*. New York: Thieme.

Rondelli, G. & Vicentini, B. (2000) Evaluation by electrochemical tests of the passive film stability of equiatomic Ni-Ti alloy also in presence of stress-induced martensite. *J. Biomed. Mater. Res.*, Vol. 51, pp. 47–54.

Runciman, A., Xu, D., Pelton, A. R., & Ritchie, R. O. (2011). *An equivalent strain/Coffin–Manson approach to multiaxial fatigue and life prediction in superelastic Nitinol medical devices.* Biomaterials. Vol. 32 No. 22, pp.4987-4993.

Ryhänen, J., Niemi, E. U. O. O., Serlo, W., Niemelä, E., Sandvik, P., Pernu, H., & Salo, T. (1997) *Biocompatibility of nickel - titanium shape memory metal and its corrosion behavior in human cell cultures.* Journal of biomedical materials research. Vol.35 No. 4, pp.451-457.

Ryhänen, J., Kallioinen, M., Serlo, S., Peramaki, P., Junila, J., Sandvik, P., Niemelä, E. & Tuukkanen, J. (1999) Bone healing and mineralization, implant corrosion and trace metals after nickel-titanium shape memory metal intramedullary fixation. *J. Biomed. Mater. Res.* Vo. 47, pp. 472–480.

Sampiev, M., Laka, A. & Zagorodniy, N. (2013) *The application of growth-guidance LSZ device for infantile and adolescent scoliosis treatment.* Russian Medical Journal. Vol. 5, pp.24-28.

Sanders, J., Sanders, A., More, E. & Ashman, R. (1993). A preliminary investigation of shape memory alloys in the surgical correction of scoliosis. *Spine*, Vol. 18 No. 12, pp. 1640–1646

Shabalovskaya, S. (2002) Surface, corrosion and biocompatibility aspects of Nitinol as an implant material. *Bio-Medical Materials and Engineering.* Vol. 12, pp. 69 – 109.

Shabalovskaya, S., Anderegg, J. & Humbeeck, J. (2008) Critical overview of Nitinol surfaces and their modifications for medical applications. *Acta Biomaterialia*, Vol. 4, pp. 447 – 467.

Sedra, F., Yoon, W., Shaw, M. & Noordeen, H. *Treatment of early-onset scoliosis with magnetically driven growth rods: preliminary results with a 1-year follow-up.* 50th anniversary International Phillip Zorab Symposium. June 20-21, 2013. London:BSRF.

Shenhar, A., Gotman, I., Radin, S., & Ducheyne, P. (2000) *Microstructure and fretting behavior of hard TiN-based coatings on surgical titanium alloys.* Ceramics international. Vol. 26 No. 7, pp.709-713.

Singh, V., Simpson, J.& Rawlinson, J. (2013) *Growth Guidance system for early-onset scoliosis.* Spine Vol. 38 pp.1546-1553.

Sui, J. H., & Cai, W. (2006) *Effect of diamond-like carbon (DLC) on the properties of the NiTi alloys.* Diamond and related materials. Vol. 15 No.10, pp.1720-1726.

Tabanli, R., Simha, N. & Berg, B. (2001) *Mean Strain Effects on the Fatigue Properties of Superelastic NiTi.* Metall. Mater. Trans. A, Vol. 32A, pp. 1866–1869.

Takadoum, J., & Bennani, H. H. (1997). *Influence of substrate roughness and coating thickness on adhesion, friction and wear of TiN films.* Surface and Coatings Technology. Vol. 96 No.2, pp. 272-282.

Taktak, S., & Akbulut, H. (2007) *Dry wear and friction behaviour of plasma nitrided Ti–6Al–4V alloy after explosive shock treatment.* Tribology international. Vol. 40 No.3, pp. 423-432.

Tan, L., Dodd, R. A., & Crone, W. C. (2003) *Corrosion and wear-corrosion behavior of NiTi modified by plasma source ion implantation.* Biomaterials. Vol. 24 No. 22, pp.3931-3939.

Theologis, A. A., Cahill, P., Auriemma, M., Betz, R., & Diab, M. (2013). *Vertebral Body Stapling in Children Younger Than 10 Years With Idiopathic Scoliosis With Curve Magnitude of 30° to 39°.* Spine. Vol. 38 No. 25, E1583-E1588.

Tolomeo, D., Davidson, S. & M. Santinoranout, M. (2000) *Cyclic Properties of Superelastic Nitinol: Design Implications.* International Conference on Shape Memory and Superelastic Technologies. 30 April – 4May, 2000. Pacific Grove, ASM International.

Trepllnier, C. (1999). *J. Biomed. Mater. Res.* Vol., p. 165.

Venugolapan R. & Trepanier C. (2000) *Assessing the corrosion behaviour of Nitinol for minimally – invasive device design.* Minimally Invasive Therapy & Allied Technologies, Vol. 9, pp. 67–75.

Villarraga, M., Cripton, P. & Teti, S. (2006) *Wear and corrosion in retrieved thoracolumbar posterior fixation.* Spine. Vol. 31,pp.2454-2462.

Wagner, M. X., Dey, S. R., Gugel, H., Frenzel, J., Somsen, C., & Eggeler, G. (2010). *Effect of low-temperature precipitation on the transformation characteristics of Ni-rich NiTi shape memory alloys during thermal cycling.* Intermetallics. Vol. 18 No.6, pp.1172-1179.

Wang, J., Warren, D. & Harvinder, S. (1999) *Metal debris from titanium spinal implants.* Spine. Vol.24, pp.899-903.

Wang, C. T., Gao, N., Gee, M. G., Wood, R. J., & Langdon, T. G. (2013) *Processing of an ultrafine-grained titanium by high-pressure torsion: an evaluation of the wear properties with and without a TiN coating.* Journal of the mechanical behavior of biomedical materials. Vol. 17, pp.166-175.

Wang, Y., Zheng, G., Zhang X. (2011) Temporary *use of shape memory spinal rod in the treatment of scoliosis.* Eur Spine J. Vol. 20(1), pp. 118-22.

Wang, J., & Liu, M. (2011) *Study on the tribological properties of hard films deposited on biomedical NiTi alloy.* Materials Chemistry and Physics, Vol. 129 No. 1, pp. 40-45.

Watanabe, K., Matsumoto, M., Suzuki, T., Kawakami, N., Tsuji, T. & Yamamoto, T. *Risk factors for proximal junction kyphosis associated with growing-rod surgery for early-onset scoliosis.* 50th anniversary International Phillip Zorab Symposium. June 20-21, 2013. London:BSRF.

Wessels, M., Hekman, E. & Verkerke, B.(2012) *Influence of prestrain, heat treatment and surface treatment on bending fatigue of NiTi rods.* Journal of Biomechanics S1, 45.

Wever, D. J., Veldhuizen, A. G., De Vries, J., Busscher, H. J., Uges, D. R. A., & Van Horn, J. R. (1998) *Electrochemical and surface characterization of a nickel–titanium alloy* Biomaterials. Vol. 19 No. 7-9, pp.761-769.

Wever, D., Elstrodt, J., Veldhuizen, A. & Horn, J. (2002) *Scoliosis correction with shape-memory metal: results of an experimental study.* European Spine Journal, Vol. 11 No. 2, pp. 100–106.

Wiklund, U., & Hutchings, I. M. (2001) *Investigation of surface treatments for galling protection of titanium alloys.* Wear. Vol. 251 No. 1, pp.1034-1041.

Williams, J. A. (2005) *Wear and wear particles—some fundamentals.* Tribology International. Vol. 38 No.10, pp.863-870.

Witzleb, W., Hanisch, U. & Ziegler, J. (2009) *In vivo wear rate of the Birmingham hip resurfacing arthroplasty: a review of 10 retrieved components.* J.Arthroplasty. Vol. 24 No.6, pp.951–956.

Wurzel, D. & Hornbogen, E. (2000) *The influence of thermomechanical treatments on fatigue behaviour of NiTi alloys.* International Conference on Shape Memory and Superelastic Technologies. 30 April – 4May, 2000. Pacific Grove, ASM International.

Yan, W. (2006) *Theoretical investigation of wear-resistance mechanism of superelastic shape memory alloy NiTi.* Materials Science and Engineering A. Vol. 427, pp.348-355.

Yoon, W., Panagiotidou, A., H Noordeen, H. & Blunn, G. (2013) *Cobalt Chrome and titanium corrosion in scoliosis correction. Is there a problem?* British Scoliosis Society Meeting 2013. September 11-13, 2013. Stoke-on-Trent, UK.

Yoshihara, H. (2013). *Rods in spinal surgery: a review of the literature.* The Spine Journal. Vol. 13 No.10, pp.1350-1358.

APPENDIX

CONFERENCE PRESENTATIONS:

"Metallosis is a Complication of Growth-Guidance and Sliding Devices for Early-on-set Scoliosis" Lukina, E.; Laka, A.; Kollerov M.; Sampiev M.; Mason, P.; Wagstaff. P.; Yoon, W.; Noordeen, H.; Blunn,G. Presented at 21st International Meeting on Advanced Spine Techniques (IMAST), July 16-19, 2014, in Valencia, Spain.

"In vitro investigation of Titanium and Superelastic Nitinol wear resistance for guided-growth devices for early on-set scoliosis (EOS) treatment" Lukina, E., Blunn, G., Kollerov, M., Meswania, J., Mason, P., Wagstaff, P., Laka, A., Noordeen, H., Yoon, W. Presented at British Scoliosis Society Meeting. September 11-13, 2013. Stoke on Trend, UK

"The investigation of NiTi tribological behaviour in the body simulated environment" Lukina, E., Kollerov, M., Mason, P., Wagstaff, P., Blunn, G. Presented at International Conference of Shape Memory and Superelastic Technologies. May 20-24, 2013. Prague, Czech Republic.

"Influence of the Structure on the Strain-Controlled Fatigue of Nitinol" Kollerov, M., Lukina, E., Gusev, D., Mason, P., Wagstaff, P. Presented at European Symposium on Martensitic Transformations, September, 9-15, 2012. Saint-Petersburg, Russia

PUBLICATIONS IN JOURNAL:

"Impact of material structure on the fatigue behaviour of NiTi leading to a modified Coffin-Manson equation" Kollerov, M., Lukina, E., Gusev, D., Mason, P., Wagstaff, P. Published in Materials Science and Engineering A. Elsevier. Vol. 585, (2013) pp. 356-362.